ÓBUDAI EGYETEM
ÓBUDA UNIVERSITY

# Optimization of ball end milling tool path in case of free form milling

Ph.D. Dissertation

By
Abdul Whab Mgherony
M.Sc. in Mechatronical Engineering

Supervisor
Dr.habil MIKÓ Balázs

Óbuda University, Doctoral School of Materials Sciences and Technologies
Budapest, Hungary

2024

## Complex exam committee

President

|Prof. Dr. Réger Mihály, ÓE

Members:

Dr. Drégely-Kiss Ágota, ÓE

Dr. Andó Mátyás, ELTE

## Public Defense Committee:

President

Endre Ruszinkó DSc university professor, ÓE

Secretary

Péter Varga PhD assistant professor, ÓE

Members

Csaba Felhő PhD associate Professor, ME

Árpád Cziffra PhD associate Professor, ÓE

Viktor Gonda PhD university associate professor, ÓE

Opponents

Ildiko Mankova DSc associate professor, Kassai University of Technology

Gábor Ferenc Erdős, PhD, associate professor, BME, SZTAKI

**Declaration**

The research presented in this thesis has been conducted under the guidance and supervision of Dr. habil MIKÓ Balázs, who is a member of the Obuda Doctoral School Committee. I hereby confirm that the content of this thesis is entirely original and has not been submitted, either in whole or in part, for any degree or diploma at this institution or any other higher education institution.

Abdul Whab Mgherony

Budapest, August 8th, 2024

**Abstract**

In the ever-evolving landscape of advanced industries, free-form surfaces have become ubiquitous, finding applications in aerospace, automobile, consumer products, and die and mould manufacturing. The versatility of ball-end mills in machining these complex surfaces is unquestionable. However, a persistent challenge arises when machining with such tools: the dynamic change in working diameter due to variations in surface inclination.

When utilizing a ball-end tool, the machining process deviates from using the entire tool diameter, giving rise to what is termed the "effective diameter." This occurrence is a consequence of the varying radius from one cutting edge to another in relation to the tool's axis of rotation. The fluctuation in the effective diameter leads to alterations in cutting parameters.

The effective diameter is intricately linked to the depth of cut (ap), the nominal diameter of the tool, and the surface slope. It exhibits an increase as the depth of cut grows. When the depth of cut equals the radius of the tool, the effective diameter aligns with the nominal diameter. Nevertheless, in certain finishing operations where the depth of cut typically falls within the range of 0.1mm to 0.3mm, the effective diameter remains smaller than the nominal diameter. While this challenge can be addressed through simultaneous five-axis milling, the associated costs and complexity of this technology may present significant hurdles.

This thesis aims to address the challenges of machining free-form surfaces using ball-end tools in 3-axis milling machine. Free-form surfaces exhibit varying inclinations, leading to fluctuations in the tool's working diameter, which results in inconsistent cutting speeds and milling parameters despite a constant spindle speed. Consequently, the machined surface lacks uniformity.

Two approaches to solve this problem are discussed in this work. One approach introduced here relies on the maintenance of a consistent cutting speed by continuously computing the working diameter and subsequently adjusting both spindle speed and feed rates accordingly. The algorithm employed for this purpose recalibrates the necessary spindle speed and feed rates based on the real-time working diameter of the ball-end milling cutter, utilizing the STL file which represents the machined surface's geometry and the APT format for the tool path.

The other method to overcome the change in the effective diameter is by optimizing the tool path planning. Unlike conventional tool path planning techniques, the proposed method calculates the working diameter at each adjacent point and guides the tool's movement toward points where the smallest change in working diameter is expected. This approach effectively reduces fluctuations in cutting speed, resulting in the generation of more homogeneous surfaces.

**Acknowledgements**

I take this moment with immense joy to express my heartfelt appreciation to Dr. Mikó Balázs, my supervisor, for his unwavering guidance, invaluable counsel, encouragement, and substantial support throughout my academic and research journey. Dr. Mikó Balázs's approach greatly influenced and enriched my experience, fostering moments of laughter and constructive discourse. I am eternally grateful for the immense value he added to my learning journey.

Special gratitude is extended to Dr. Gabriella Farkas for her support, especially during my first year, and her assistance in utilizing measurement tools. I would also like to thank Mr. Nagy János for providing laboratory facilities; without his help, this work would never have been possible. Additionally, my thanks go to Prof. Judit Borsa, the Director of the PhD School, and Prof. Réger Mihály for their helpful tips, advice, motivation, and support during my PhD process.

I appreciate Mrs. Hersics Katalin and the entire Óbuda University staff.

In addition, I wish to pay a special tribute to my late father, Shawkat, who departed when I was a child. Despite the brevity of our time together, his enduring love left an indelible mark, providing a foundation of strength and resilience. His spirit continues to inspire me, complementing the unwavering support of my beloved mother, Aasya Abou Aljadaiel, and my sisters, Manar and Nour. Together, their collective encouragement, sacrifices, well-wishes, and love have played pivotal roles in propelling me to this significant point in my journey.

Lastly, words fail to capture my appreciation for my wonderful wife, Zhanara, whose love, motivation, support, tolerance, patience, and enthusiasm were instrumental during my research. Her constant encouragement has been the driving force behind the completion of this work.

## Nomenclature

| | |
|---|---|
| $a_e$ | Width of cut [mm] |
| $A_f$ | Feed direction [°] |
| $A_{N1}$<br>$A_{N2}$ | Surface inclination angles [°] |
| $a_p$ | Depth of cut [mm] |
| $D_c$ | Tool diameter [mm] |
| $D_{eff}$ | working diameter [mm] |
| $f_z$ | Feed per tooth [mm] |
| n | Spindle speed [rpm] |
| Ra | The average roughness of a surface |
| Rq | Standard deviation of the height distribution |
| Rz | The difference between the tallest “peak” and the deepest “valley” in the surface. |
| $v_c$ | Cutting speed [m/min] |
| $v_f$ | Feed speed [mm/min] |
| z | Number of teeth of milling cutter [-] |

# 1 Contents

# 1. Introduction

## 1.1 Introduction to CNC machining and milling

CNC machining is a precise cutting process that employs a rotating cutter to remove a predetermined amount of material from a workpiece. There are fundamental milling operations, including facing and peripheral milling. In peripheral milling, the generated surface is parallel to the axis of rotation, while face milling results in a surface perpendicular to the axis [1].

Beyond these operations, specific techniques such as profile milling, sculpture milling using ball end tools, slot milling for part cutting, and pocket milling for creating rectangular or circular pockets are employed [2].

Milling operations can be classified as down (climbing) or up (conventional) milling. In up milling, the cutter rotation opposes the feed direction when the cutter axis and workpiece do not intersect. Conversely, in down milling, the cutter rotation and feed direction align [1].

Milling machines are categorized based on spindle orientation into horizontal and vertical types. Vertical mills, where the spindle is oriented vertically, are more common and are used for machining flat parts. Horizontal mills, with a horizontally oriented spindle, are preferable for machining heavy box-shaped parts, such as gear housings [3][4].

Various types of milling machines exist in the industry. The knee and column milling machine, available in both horizontal and vertical configurations, is the most common. Additionally, the universal mill allows the spindle head to rotate at a 90◦ angle to the longitudinal axis of the table, enabling both vertical and horizontal spindle orientations [1].

## 1.2 End mill cutters

End mill cutters stand out as the go-to tools in CNC milling, widely employed in both horizontal and vertical milling machines to perform a variety of operations such as slotting, profiling, and facing. Available in diverse materials and styles, including ball end mills, flat mills, and fillet mills, end mills offer versatility to meet specific machining requirements [5].

The use of ball end mills has become pervasive in manufacturing, particularly in high-speed machining processes. This tool's distinctive cutting edge, featuring configurations such as helix-type or S-type, plays a pivotal role in sculpting surfaces, commonly referred to as free-form surfaces [6].

Free-form surfaces find widespread applications across industries, including aerospace, automobile manufacturing, consumer products, and the die/mold industry. The ball end mill takes center stage in machining these complex surfaces due to its extended product life, high machining precision, cost-effectiveness in the manufacturing process, and its capability to feed axially, making it an indispensable tool in various industrial applications [6].

The ball end mill typically exhibits a cylindrical shape with a helix angle ranging from 20° to 45° in the former and a spherical shape in the latter. This unique geometry along the cutting-edge results in variable helix angles but a constant lead. During the milling process, a special generation occurs by projecting the helix angle perpendicular to the tool's axis onto a sphere. This variability in helix angles is a distinguishing feature of the ball end mill, contributing to its versatility in machining applications [2].

Ball end mills are available in both single and double-ended configurations, with diameters ranging from 1/32 to 2 1/2 inches, providing a broad spectrum of options to cater to different machining needs [7].

## 1.3 Importance of tool path optimization

CNC machining has revolutionized manufacturing processes by providing unparalleled precision and efficiency. Within this realm, tool path optimization stands out as a critical aspect that significantly influences the overall performance of milling operations, especially in tasks like ball end milling of free-form surfaces.

Tool path optimization ensures that the cutting tool follows an optimized trajectory, minimizing unnecessary movements and optimizing the sequence of cuts. This not only reduces machining time but also enhances overall process efficiency. In free-form surface milling, where intricate shapes demand precision, every movement of the cutting tool contributes to the final product's quality [8].

On the other hand, the selection of an optimal tool path directly impacts the surface finish of the machined component. By strategically planning the tool path, the milling process can minimize tool marks, vibrations, and other imperfections on the free-form surface. This is crucial in industries such as aerospace and medical manufacturing, where smooth and flawless surfaces are non-negotiable requirements [9].

Optimized tool paths help manage the wear and tear of cutting tools more effectively. By avoiding unnecessary stress on the tool, the lifespan of the cutting tool can be extended. This not only reduces the frequency of tool changes but also contributes to cost savings and uninterrupted manufacturing processes [10].

Free-form surfaces often present intricate geometries that require meticulous attention during machining. Tool path optimization algorithms can adapt to the complexities of these surfaces, ensuring that the cutting tool navigates smoothly without compromising precision. This adaptability is crucial for meeting the increasingly sophisticated design requirements across various industries [11].

In essence, tool path optimization is not merely a technicality within CNC machining; it is a strategic approach that impacts the core aspects of manufacturing, from efficiency and surface finish to tool longevity and material utilization. As we delve into the specific challenges of ball end milling for free-form surfaces, the role of optimized tool paths will become even more apparent in achieving superior results.

## 1.4 Challenges in 3-axis ball end milling of free-form surfaces

Ball end milling is a versatile machining process widely used for its ability to produce complex shapes and contours. However, when applied to free-form surfaces, unique challenges arise that necessitate careful consideration and specialized approaches.

Free-form surfaces inherently exhibit irregularities and complex geometries. Achieving a smooth and precise surface finish during ball end milling becomes challenging due to the varying curvatures and intricacies of the workpiece. Tool path optimization must account for these irregularities to minimize deviations and ensure a high-quality final product.

On the other hand, the nature of free-form surfaces often leads to regions where standard tools struggle to engage effectively. These accessibility issues can result in incomplete machining or compromise the structural integrity of the cutting tool. Addressing tool engagement challenges requires innovative tool path planning to navigate intricate features without sacrificing efficiency [12].

Beside that free-form surfaces typically require intricate tool paths that may extend the overall machining time. Balancing the need for precision with the desire for efficient production becomes a critical challenge. Tool path optimization strategies must find the right

compromise, minimizing machining time without compromising the quality of the machined surface [13].

Ball end milling relies on spherical cutting tools, and selecting the appropriate tool for a specific free-form surface can be a complex decision. Moreover, due to the often-intricate tool paths, the cutting tools may experience accelerated wear. Managing tool selection and wear is crucial for maintaining the desired surface quality throughout the milling process [14].

Programming CNC machines for ball end milling of free-form surfaces demands advanced algorithms and computational methods. The complexity of generating tool paths that accurately represent the desired surface, while also optimizing for efficiency and tool life, requires a comprehensive understanding of both machining principles and software capabilities.

Free-form surfaces may be composed of a variety of materials, each with its own machining characteristics. The challenges in ball end milling extend to adapting the milling process to different materials, considering factors such as hardness, brittleness, and thermal conductivity. Tool path optimization should be versatile enough to accommodate these material variations.

Addressing these challenges requires a holistic approach that combines advanced tool path optimization algorithms, an understanding of material properties, and a keen awareness of the intricacies of free-form surfaces. The subsequent sections of this thesis will explore methodologies and strategies to overcome these challenges and enhance the effectiveness of ball end milling for free-form surfaces. It is worth noting that a primary focus of this study is the optimization of the milling process, with particular emphasis on the crucial factor of the effective diameter.

### 1.4.1 Effective diameter

When utilizing a ball end tool, the machining process involves the effective diameter rather than the entire diameter. This concept arises due to the variation in radius from one cutting edge to another concerning the rotation axis of the tool. This change in effective diameter introduces modifications in cutting parameters, impacting the overall machining process [2].

The effective diameter is intricately linked to the depth of cut ($a_p$), nominal diameter, and surface slope. Notably, it increases proportionally with the depth of cut. At the critical point where the depth of cut equals the radius of the tool, the effective diameter aligns with the nominal diameter. However, in certain finishing operations where the depth of cut ranges from 0.1 to 0.3mm, the effective diameter will be less than the nominal diameter [2].

When engaging in milling operations on inclined surfaces using a ball end tool, three distinct types of milling operations come into play: downward milling, upward milling, and horizontal milling at a constant Z-level. These operations follow one another in sequence, contributing to variations in actual cutting speed during the machining of free-form surfaces. The selection of an appropriate toolpath becomes crucial in minimizing the differences in cutting speed and optimizing the machining process.

## 1.5 Surface roughness

Surfaces are defined as material boundaries, possessing intrinsic properties like color and measured attributes such as hardness [15]. Conversely, surface texture pertains to the geometrical form of a surface, encompassing waviness, roughness, and form. The surface wavelength distinguishes these characteristics. Roughness typically arises from the manufacturing process, exhibiting periodicity and often manifesting as tool and grit marks. Waviness, meanwhile, is linked to machine factors such as irregularities in tool feed or chatter

vibrations. Form errors can stem from factors like inadequate workpiece rigidity during manufacturing, high residual stress on the surface, or material strains [16].

Regarding surface roughness, multiple perspectives emerge. Firstly, there's the matter of defining it, followed by determining methods for its measurement. In the design phase of a machine, numerous factors must be weighed to establish the appropriate surface roughness value, including functionality, tribology, fitting, lubrication, and aesthetic considerations. Subsequently, consideration shifts to how the surface can be manufactured to meet these requirements, culminating in an inquiry into estimating surface roughness based on production process parameters.

Many parameters are used to describe the surface roughness based on standards (like ISO 21920), such as Rt which represents the maximum depth of the roughness Figure 1-1 (a), this parameter is sometimes replaced with Rp and Rv which represent respectively, the height of the highest peak and the depth of the lowest valley with respect to the mean Figure 1-1 (b). Rz is another parameter of surface roughness, which can be defined as the sum of the average of the five lowest valleys and the average of the five highest peaks Figure 1-1 (c). The parameter that has a significant mathematical influence is the root mean squared Rq. Ra, on the other hand, represents the arithmetic average Figure 1-1 (d) [15][17].

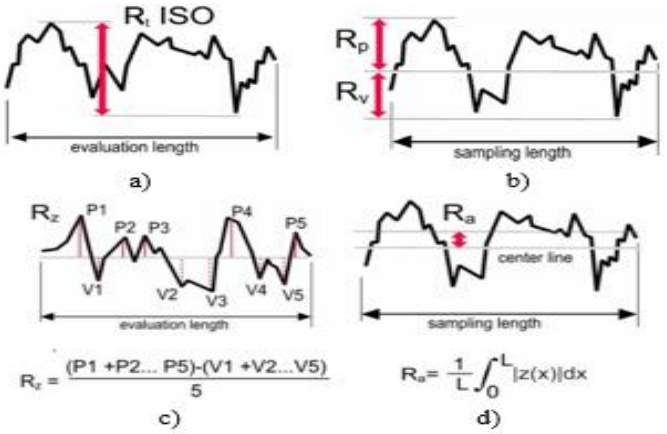


*Figure 1-1: Cusp height in case of a longitudinal turning and Z-level milling*

The stylus stands out as one of the most prevalent tools for measuring surface 2D profiles or 3D surfaces. Renowned for its reliability, versatility, and ease of construction, the three-dimensional stylus remains a favored choice [18]. Its fundamental principle involves converting the vertical movement of the stylus into electrical signals via a transducer. Equipped with a pickup, the stylus traverses the surface at a consistent speed. Subsequently, the transducer signal undergoes amplification, and the device duly records the signal [19].

The vertical range of a stylus is determined by the dynamic range of its transducer, while the horizontal range relies on the length of the pickup traverse. Horizontal resolution, in turn, is governed by the dimensions of the stylus. One of the primary advantages of the stylus lies in its electrical signal output. However, this versatile tool is not without its drawbacks. Complexity and fragility are among its notable disadvantages, along with its reputation for being relatively costly [15].

In industrial settings, the quality of produced surfaces is a pivotal factor, influenced by various parameters such as cutting conditions, workpiece material, cutting tool characteristics, and the chosen cutting strategy [20]. Specifically, in ball end milling operations, cutting conditions wield a profound impact on the machining process and directly influence surface

roughness. For instance, the axial depth of cut plays a crucial role in determining surface roughness parameters such as Ra and Rt, particularly in the milling of hardened steels [21].

Furthermore, the width of cut and feed rate significantly affect surface roughness when the milled part is perpendicular to the machined surface [22]. In Z-level milling of S355 steel, the parameter Rz increases with the augmentation of feed and depth of cut [23].

Surface inclination angle also emerges as a key determinant of surface texture, with the selection of an appropriate angle capable of reducing roughness [24]. Conversely, horizontal surfaces may exhibit poor roughness due to suboptimal cutting conditions [23]. Additionally, the chosen milling strategy has a notable impact on the final surface quality, with up-milling at high tool feed and cutting width resulting in reduced surface roughness [22]. These factors collectively underscore the intricate relationship between cutting conditions, milling parameters, and the resulting surface characteristics in the ball end milling process.

Approaches for predicting surface roughness can be classified into three main categories as follows:

### 1.5.1 Experimental approach

In this method, multiple factors are selected, and corresponding experiments are conducted. Subsequently, the results are meticulously analyzed to discern the impact of each factor and its influence on the observed characteristics. Typically, the gathered data is utilized to construct a model employing regression analysis. Such an approach proves invaluable when cause-and-effect relationships among the factors lack an analytical formulation. [19].

Kovač et al. [25] developed a power function-based model specifically for turning stainless steel. The model considered parameters such as cutting speed, feed rate, and depth of cut. Notably, feed rate exerted the most significant influence on surface roughness, while the effects of cutting speed and depth of cut were comparatively minor.

The Taguchi method for Design of Experiments (DoE) and Response Surface Methodology (RSM) stand out as the most commonly employed approaches for defining factors and levels and predicting surface roughness.

The Taguchi method encompasses a predefined set of standard arrays, which dictate the number of experiments to be conducted based on the factors and their respective levels. This method offers the capability to explore both the linear effects of factors and certain interactions among them[19] . Tlhabadira et al. [26] employed this approach to optimize surface roughness during milling operations. They utilized linear regression to analyze the Ra surface roughness, considering factors such as feed rate, spindle speed, depth of cut, and cutting speed. Similarly, Sharma and Dwivendi [27] investigated the impact of specific cutting parameters on surface roughness during slot milling using the Taguchi method. Their findings revealed that feed rate exerted the most significant effect, followed by spindle speed and depth of cut.

Response Surface Methodology (RSM) seamlessly combines statistical and mathematical techniques to develop, refine, and optimize processes. This methodology is instrumental in both process design and formulation. Typically, first and second-order models are employed in RSM to effectively capture and analyze process behavior [28].

### 1.5.2 Artificial intelligence approach

Advancements in genetic algorithms (GAs), artificial neural networks (ANN), expert systems, and fuzzy logic have facilitated the integration of artificial intelligence into surface roughness prediction. Notably, among researchers, artificial neural networks (ANNs) and genetic algorithms (GAs) emerge as the primary methods employed for this purpose. [19].

Artificial neural networks (ANNs) serve as mathematical modeling tools that mimic biological neural networks. With their capacity to establish relationships between inputs and outputs, ANNs have found widespread application in engineering for tasks such as optimization, prediction, and classification. Typically composed of multiple layers of neurons [29]. ANNs have been adopted by numerous researchers for various applications.

For instance, Deshpande et al. [30] utilized artificial neural networks to forecast the surface roughness of Inconel 718 during turning, considering parameters such as cutting speed, feed rate, and depth of cut. Similarly, Vasanth et al. [31] employed ANN to predict the surface roughness of SS410 steel during hard turning.

The Genetic Algorithm (GA), rooted in evolutionary theory, synthesizes principles of natural selection and genetics to solve optimization problems and achieve optimal solutions with high probability. This mechanism, characterized by its simplicity, initiates by forming a set of chromosomes. In the reproduction phase, favorable strings are selected. Subsequently, each chromosome undergoes splitting, followed by recombination with halves from different chromosomes. Mutation, involving the flipping of chromosomes, introduces variation. GA generates offspring from selected parents, progressively evolving the population towards the optimal solution. The process culminates when a chromosome with the best fitness criteria is reached [32].

Li et al. [33] utilized the Genetic Algorithm to predict the surface roughness of GH4169 during turning. Specifically, the GA was employed to determine the parameters of the power function of $R_a$, enhancing predictive accuracy.

Zhou et al. [34] conducted an investigation into the turning process, varying parameters such as cutting speed, feed rate, and depth of cut. They developed a surface roughness prediction model using the genetic-gradient boosting regression tree method, based on measured data.

In a similar vein, Savkovic et al. [35] proposed a neural network-based model to predict surface roughness in face milling. They considered input parameters including cutting speed, feed per tooth, and depth of cut, each explored across five levels. Utilizing measured data, they compared the efficacy of fuzzy logic and power function models against the neural network-based approach, which demonstrated superior performance.

### 1.5.3 Machining theory-based approach

In this approach, emphasis is placed on various aspects of machining theory, including cutting tool properties, process kinematics, and chip formation. Utilizing computer-aided design (CAD) methods, models are constructed to simulate the formation of machined surface profiles. This process typically yields a geometric model based on rigorous mathematical equations. Subsequently, computer algorithms are employed to implement these models and manage complex calculations. However, due to inherent limitations, these models may lack accuracy, necessitating the introduction and examination of additional parameters in many cases. [19].

Kundrák and Felhő [36] introduce a geometric modeling approach for face milled surfaces using CAD systems. This method enables the consideration of geometric errors, such as runout, associated with the milling cutter [37]. The theoretical Ra parameter can then be calculated based on the CAD model of the machined surface, factoring in the number of teeth and potential errors.

In a similar way, Meijer et al. [38] present an analytical geometric model for face milled surfaces. Their model incorporates the contour of the cutting edge and is compared against a simulation-based model that accounts for the entire path of the cutting edge.

## 1.6 Objective of the thesis:

The principal objective of this thesis was to optimize the tool path for end ball milling of free-form surfaces. The specific goals were pursued through two distinct strategies:

1. Dynamic Spindle Speed Control:

    i. Investigated the impact of dynamically changing the spindle speed during the milling process, taking into account the milling diameter at each point.

    ii. Assessed how varying the spindle speed influenced the cutting speed, with the aim of ensuring minimal changes in the working diameter throughout the machining operation.

    iii. Developed and implemented a methodology, utilizing a Python program, to dynamically adjust the spindle speed along the tool path for optimal milling performance.

2. CAM System Tool Path Optimization:

    i. Explored the utilization of a Computer-Aided Manufacturing (CAM) system to generate a tool path that minimizes the change in the tool's effective diameter.

    ii. Investigated the selection of appropriate milling directions from point to point on the path to achieve a smoother and more consistent machining process.

    iii. Developed a systematic approach, possibly through the enhancement of a Python program, to integrate CAM-generated tool paths that prioritize minimal changes in the tool's effective diameter.

To visually illustrate the concepts of these two strategies, Figure 1-2 presents a schematic representation of the dynamic spindle speed control and CAM system tool path optimization methods. As shown in the figure, a key step in both strategies involves calculating the working diameter for each point. In the context of spindle speed control, this calculation aids in determining the spindle speed required to maintain a constant cutting speed. Conversely, in tool path planning, this calculation assists in selecting the next point on the path, ensuring minimal changes in the working diameter and, consequently, minimizing variations in cutting speed.

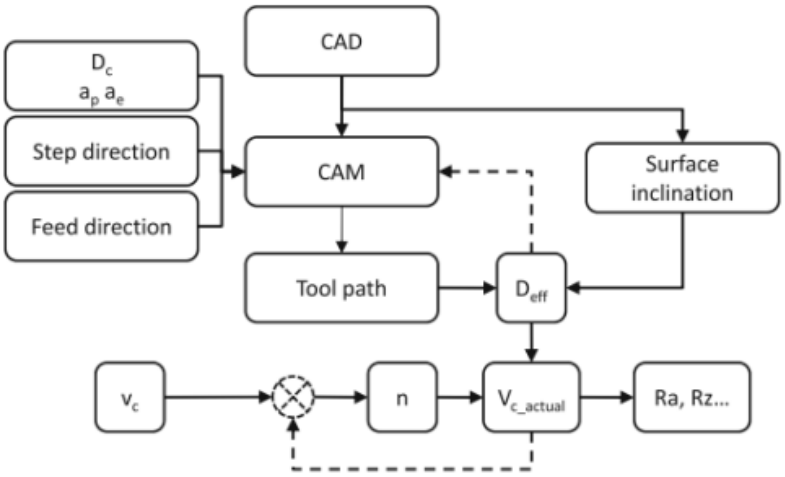


*Figure 1-2:Illustrating the Concept of Tool Path Optimization Strategies.*

By addressing these objectives, the thesis aimed to contribute to advancements in tool path optimization for free-form surface milling. While the dynamic spindle speed control strategy was fully implemented and analyzed, the CAM system tool path optimization, although explored conceptually, did not undergo experimental validation.

The result of the project signifies a step forward in understanding and implementing advanced tool path optimization strategies for ball-end milling. Future work may involve further experimentation and refinement of the CAM system tool path optimization, building upon the groundwork laid in this thesis.

## 1.7 Scope and limitation

### 1.7.1 Scope

The scope of this thesis encompasses the optimization of tool paths for end ball milling of free-form surfaces, focusing on two primary strategies: dynamic spindle speed control and CAM system tool path optimization. The research aims to advance understanding and implementation in these specific areas, contributing insights and methodologies for improving machining efficiency and surface quality.

### 1.7.2 Limitations:

1. Experimental Validation: While the dynamic spindle speed control strategy has been fully implemented and analyzed, the CAM system tool path optimization is conceptual, lacking experimental validation in the current study.
2. Specific Milling Context: The findings and recommendations are tailored to the context of end ball milling for free-form surfaces, and their direct applicability to other milling processes or machining contexts may require further investigation.
3. Software and Hardware Constraints: The effectiveness of the proposed methodologies is influenced by the capabilities and limitations of the software tools and CNC hardware used in the study. Generalization to different platforms may necessitate adjustments.
4. Material Specificity: The research primarily considers the milling of free-form surfaces in various materials. The applicability of the proposed strategies may vary based on specific material properties and cutting tool considerations.

5. Single-Tool Focus: The study predominantly concentrates on optimizing tool paths for end ball milling using a specific type of cutting tool. The extension of findings to other tool types may require additional exploration.

By acknowledging these limitations, the study ensures a focused and realistic approach while providing valuable insights within the defined scope.

## 1.8 Revised research gap:

1. Sparse Attention to Dynamic Spindle Speed Control: While various tool path optimization methods have been discussed, there is a scarcity of research specifically addressing dynamic spindle speed control in the context of end ball milling. This study aims to fill this gap by investigating the implications and benefits of adjusting spindle speed dynamically during the milling process.
2. Limited Insight into Working Diameter Calculation and Its Impact: Existing literature lacks in-depth exploration of the working diameter calculation and its direct impact on tool path optimization. This research addresses this gap by delving into the intricacies of working diameter calculations, emphasizing their role in determining optimal spindle speeds and influencing overall machining efficiency.

By identifying and addressing these research gaps, this thesis aims to contribute a more nuanced understanding of tool path optimization for end ball milling of free-form surfaces, with specific emphasis on dynamic spindle speed control, CAM system tool path optimization, and the intricate effects of working diameter calculations on machining outcomes.

To provide a visual overview of the comprehensive work done, Figure 1-3 represents a roadmap outlining key milestones throughout my research. Each node represents a pivotal step, interconnected to trace the path of my contributions. As we delve deeper into the following chapters, this graphical representation will guide the reader through the dynamic landscape of my work.

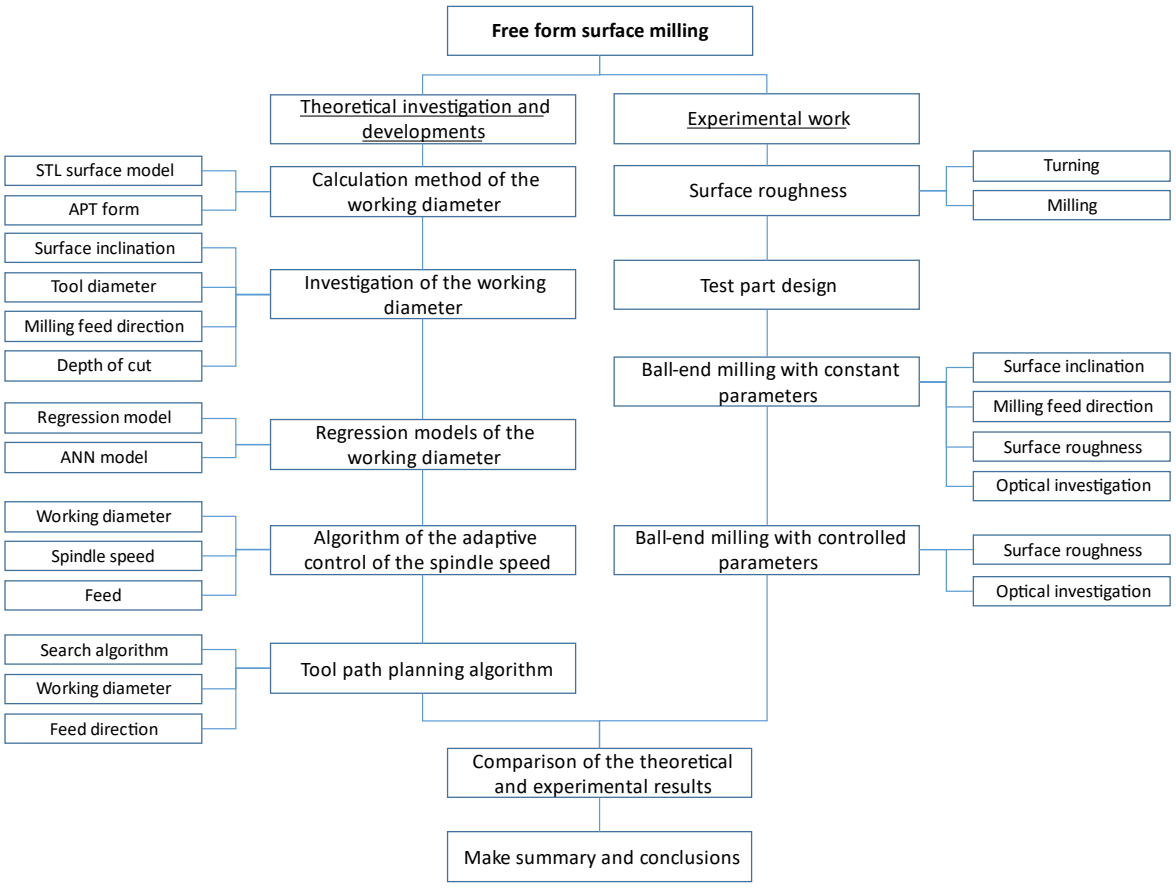


*Figure 1-3: Graphical overview of PhD research progress.*

# 2 State of the art

Free-form surfaces, unlike typical surfaces, lack translational symmetry or axes of rotation and are extensively used in industries such as automotive, aerospace, consumer products, and die/mould manufacturing [39][40]. These surfaces can be produced through forming methods, cutting methods, and additive manufacturing [41]. In mass production, forming methods often require moulds and dies, which are primarily manufactured using cutting methods like milling or electric discharge machining (EDM). Milling methods are also employed in machining EDM electrodes [42] [43]

Despite advancements in science and technology, milling free-form surfaces remains challenging due to the continuous change in contact between the cutting tool and the workpiece, leading to fluctuations in the tool's working diameter and cutting speed, which in turn affect surface quality [42], [43].

The primary tool for machining freeform surfaces, especially for finishing and pre-finishing, is the ball-end cutter. This tool is favored for its extended product life, high-precision machining, low manufacturing cost, axial feeding capability, and unique cutting-edge shapes (Helix-type, S-type, etc.) [44], [45], [46], [47].

However, when using a 3-axis milling machine, distinctions arise between the nominal and working (or effective) diameter of the ball-end cutter. This discrepancy is influenced by various parameters, including cutting parameters, workpiece inclination, and cutting strategy. Consequently, determining the working diameter that aligns with the process parameters is crucial for achieving the desired product quality.

## 2.1 Influence of cutting parameters:

The productivity of the milling process for freeform surfaces is determined by various machining conditions, such as the cutting tool properties, cutting parameters, and the applied tool path strategy. These parameters significantly affect both the micro- and macro-accuracy of the machined surface. To enhance machining performance and reduce production costs, several optimization methods can be employed.

Radhwan et al. [48] investigated the impact of various cutting parameters, such as cutting speed, feed rate, and depth of cut, on surface roughness. Their results indicate that both cutting speed and feed rate significantly influence surface roughness. Similarly, De Souza et al. [49] explored the influence of working diameter on cutting force, chip removal, and surface roughness, highlighting a decrease in surface roughness with higher cutting speeds. Mikó and Beňo [50] examined the impact of the inconstant effective diameter on surface roughness, reinforcing the importance of optimizing cutting parameters. Seikh et al. [51] examined the synergistic effects of cutting parameters on surface roughness in ball-end milling of oxygen-free high conductivity (OFHC) copper, identifying axial and radial depth of cut as the most influential parameters, followed by feed rate. Zhang et al. [52] delved into examining the impact of ball-end tool speed on the milling process, elucidating the relationship between cutting speed, feed direction, and inclination angle during free-form surface milling. Their findings underscored the pivotal role of cutting speed in influencing cutting force and chip formation. Varvruska et al. [53] proposed a method to regulate both cutting speed and feed rate, ensuring a consistent cutting speed. This approach contributed to enhancing the milling process efficiency by reducing machining time. Moreover, Käsemodel et al. [54] successfully reduced surface roughness and machining time by controlling spindle speed. In their methodology, spindle speed adjustment was facilitated by an algorithm dependent on the Grasshopper application within Rhino3D software, which obtained the normal vector of the

surface. Moreover, Mali et al. [55] delved into investigating the impact of cutting parameters and tool-path strategies on tool wear, cutting forces, and surface quality during the milling of curved surfaces.

Additionally, the orientation and inclination of the tool play critical roles in machining outcomes. Wojciechowski et al. [56] analyzed forces and process efficiency during the machining of hardened 55NiCrMoV6 steel using ball-end milling, finding that surface inclination notably affects cutting forces. Yao et al. [57] studied the influence of tool orientation on the surface of the TC17 titanium alloy, emphasizing the importance of tool orientation on surface roughness during ball-end milling. Gao et al. [58] investigated the effect of the tool inclination angle on surface roughness when machining the titanium alloy Ti-6Al-4V using a ball-end mill. They noted that tilting the tool significantly affects groove quality and employing an appropriate inclination angle can reduce surface roughness and improve form. Daymi et al. [59] emphasized the importance of inclination angle in ball-end milling when machining the titanium alloy Ti-6Al-4V. Additionally, Habibi et al. [60] and Burek et al. [61] emphasized tool orientation and directional changes to improve machining accuracy. Wojciechowski et al. [24] examined the effect of tool inclination on working diameter during ball-end milling, revealing that larger working diameters result in minor surface roughness, which decreases with increased cutting. Belguith et al. [62] explored the effect of tool bending on cutting force magnitude in ball-end milling, observing a decrease in uncut thickness with increasing tool bending due to equivalent radius diminution. Sadílek et al. [63] compared the quality of the surface roughness in the case of 3-axis and 5-axis milling machines, noting smaller deviations in accuracy with 5-axis milling. However, this deviation is higher in the case of 3-axis machines.

Building upon these insights into cutting parameters, the optimization of milling parameters has become a key focus in recent studies. Mersni et al. [64] used the Taguchi method to optimize the milling parameters to obtain a better surface finish using ball-end milling of a titanium alloy Ti-6Al-4V. They pointed out that the radial depth of cut ($a_p$) is the most important factor followed by the cutting speed ($v_c$) and then the feed per tooth ($f_z$). Matras and Zębala [65] optimized the cutting data and tool path pattern for machining the freeform surface of hardened steel using a ball-end mill, demonstrating that surface roughness and cutting-force components can be controlled by adjusting the feed rate based on the locally machined cross-sectional area. Fan [66] investigated the variation in cutting speed during the machining of sculptured surfaces using 3-axis ball-end milling, noting its significant impact on surface quality and tool longevity. Krajnik and Kopač [67] proposed a method to calculate the working diameter when using a ball-end milling cutter, emphasizing feed rate optimization to minimize tool load, with modifications made directly to the G-code.

## 2.2 Modeling and analysis:

In the realm of the manufacturing process, engineers grapple with two primary practical challenges. The initial challenge involves determining the values of process parameters that guarantee the desired product quality, aligning with technical specifications. The second challenge revolves around the optimization of manufacturing system performance, ensuring efficient resource utilization. In this context, researchers typically strive to create a model for the machining process, a mathematical equation illustrating the relationship between process parameters (decision variables) and machining performance (responses). Essentially, models fall into three categories: geometric models, analytical models, and Artificial Intelligent (AI) based models.

In the context of manufacturing industry, geometric models can be developed by emphasizing one or more aspects of machining theory, such as cutting tool properties, process

kinematics, and chip formation. Computer-aided design (CAD) methods are used to build the model that simulates the machined surface profile formation. Vyboishchik [68] presented a geometric model of the surface topology in the case of flat, concave (CV) and convex (CX) surfaces, highlighting the significant impact of surface inclination. Lotfi et al. [69] utilized this approach to compute cutting forces by determining the precise engagement region and instantaneous undeformed chip thickness. Similarly, Forootan et al. [70] introduced a model to calculate the cutter-workpiece engagement area and cutting forces for a ball-end tool. Feng and Su [71] proposed a model for calculating instantaneous cutting forces, incorporating static cutting system deflection feedback in 3D ball-end milling. Ko and Cho [72] utilized instantaneous cutting force parameters to develop a model for forces in ball end cutter applications. Ghorbani and Movahhedy [73] presented a model for calculating cutter-workpiece engagement boundaries in ball-end milling. In their study, Wei et al. [74] introduced a cutting force prediction approach for 3-axis ball end milling of sculptured surfaces with Z-level contouring tool paths. Addressing challenges in sculptured surface machining, Wei et al. [75] presented a unique method for predicting cutting forces in three-axis ball-end milling. Nishida et al. [76] introduced a distinctive approach to calculating uncut chip thickness, utilizing a voxel model to describe both the workpiece and cutting edge. In the realm of predicting working diameter, Miko and Zentay [77] presented a geometric model, later simulated using Matlab by Mgherony and Miko [78].

Analytical models, utilizing conventional approaches like the regression technique, have been applied innovatively in various studies. Cheng et al. [79] employed this approach to develop a new model predicting surface residual stress. In a similar vein, Lu et al. [80] utilized a Gaussian process regression model for accurate prediction of Ra surface roughness in compacted graphite cast iron. Addressing the intricacies of three and five-axis ball-end milling, Xu et al. [81] introduced a model to develop surface topography. This innovative model incorporates a discrete sweeping surface of the cutting edge, integrating time-varying feed speed profiles, thereby overcoming limitations in existing models. Denkena et al. [82] applied this method in their study, introducing a simulation approach that combines material removal simulation (MRS) and an empirical model to predict post-milling surface topography. Furthermore, Wojciechowski [83] contributed to this field by presenting a refined cutting force model specifically tailored for finishing ball end milling. This model factors in various elements such as cutting conditions, surface inclination angle, and cutter runout. Additionally, Baburaj [84] developed a predictive model for estimating cutting forces during the machining of free-form surfaces using a three-axis ball-end milling machine. Their model demonstrated effectiveness, with predicted cutting forces falling within an acceptable range of error.

While AI-based models, incorporating non-conventional techniques like Artificial Neural Network (ANN), have been instrumental in various studies. Santhakumar and Iqbal [85] employed a neural network to develop a model, focusing on predicting surface roughness, specific cutting energy, and temperature during end milling operations with the trochoid toolpath strategy for AISI D3 steel. Concurrently, Lin et al. [86] introduced a model for surface roughness in end milling, considering cutting parameters and machining vibration. Xie et al. [87] presented an ANN-based model for spindle speed power. Proposing an intelligent prediction model, Kannadasan et al. [88] utilized the ANFIS model to predict performance indexes like average surface roughness and geometric tolerances in milled products. Additionally, Shankar et al. [89] employed artificial intelligence to forecast the wear of the cutting tool during milling processes.

## 2.3 Tool path strategies

The term “tool path” denotes the specific trajectory along which a machine’s cutting tool moves to shape the desired surfaces [90]. Typically, Computer-Aided Manufacturing (CAM) systems are employed to generate this tool path for guiding CNC machines. This process gains even greater significance in the context of machining free-form surfaces, which have become increasingly prevalent across various industries like die and mold manufacturing, aerospace, and automotive production. Consequently, the automated generation of tool paths has assumed paramount importance since surface quality and machining efficiency hinge on the chosen tool path [91]. Various tool path planning strategies exist, including the iso-parametric line method, iso-scallop method, and iso-metric section plane method, among others [92]. However, these methods often lack clear guidance for selecting the optimal strategy. Thus, users are compelled to rely on a trial-and-error approach, which not only consumes time but is also suboptimal and prone to errors [93].

Hence, the paramount importance lies in devising an efficient and adaptable intelligent method for the individualized generation of tool paths customized to each specific surface. Nevertheless, the development of such a system presents a formidable challenge owing to the multifaceted variables influencing the machining of free-form surfaces, encompassing factors such as surface inclination, cutting speed, and various cutting parameters. This underscores the imperative for an advanced tool path planning approach capable of effectively addressing these intricate parameters to enhance surface quality and machining efficiency.

Many studies in this field primarily focus on optimizing cutting conditions through suitable milling strategies. While these approaches work well for machining numerous parts, they face challenges in achieving satisfactory surface quality on complex surfaces. For instance, Magalhães and Ferreira [91] investigated different tool path strategies for machining complex geometries from hardened H13 steel, finding that tool path significantly affects surface roughness of complex surfaces. Ižol et al. [94] emphasized the importance of milling strategies, suggesting that applied strategies exert a greater influence on surface roughness than the width of cut. Buj-Corral et al. [21] investigated surfaces at various slopes, recommending conventional milling for high-depth cuts and speeds, and ascendancy for reducing surface roughness, while preferring climb milling for descendent trajectories. J. Varga et al. [95] conducted a comparative study on four milling strategies using a ball-end tool and found that the constant Z strategy minimized shape deviations, resulting in an unoriented surface. D.-D. Vu et al. [96] optimized tool paths for sculpted surfaces during three-axis end milling, reducing tool path length by 20% compared to conventional methods. G. Huo et al. [97] introduced an innovative approach for generating tool paths for free-form surfaces using a three-axis machine, ensuring alignment with desired feed directions across the entire surface.

In a different approach, A. Kukreja and S. S. Pande [98] developed a machine learning system that selects the best toolpath planning strategy for CNC machining complex surfaces using performance parameters and a Convolutional Neural Network (CNN), achieving 96.8% accuracy. Simultaneously, U. Župerl et al. [99] presented a cloud-based system for real-time tool condition monitoring during end milling, employing IoT, an optical system, and AI to detect cutting chip size and analyze cutting force trends, achieving 85.3% accuracy in identifying tool breakage. Furthermore, J. Zhang et al. [100] developed an optimization model to plan tool paths, aiming to minimize path length while considering tolerance and complete milling constraints. In the study by Kukreja and S. Pande, [101], an optimized tool path was introduced utilizing the iso-scallop approach. Furthermore, the algorithm in the research offers two distinct strategies: iso-scallop and hybrid iso-scallop. This methodology involves the stitching and refinement of overlapping toolpaths. Meanwhile, in the study by Liu et al. [102],

a highly efficient method for generating iso-scallop tool paths was presented. This method directly computes scallop points and cutter location (CL) points for iso-scallop paths from scattered data points using iterative algorithms, eliminating the need for point offsetting surface fitting. Remarkably, this new approach has highlighted superior efficiency when compared to their previous method [103]. These distinct research endeavors collectively contribute to advancing tool path optimization and machining efficiency.

## 2.4 Classifying milling studies in light of the use of design of experiments

The design of experiments (DOE) is a powerful statistical methodology used to plan, conduct, analyze, and interpret controlled tests to evaluate the factors that may influence a particular outcome or set of outcomes. In the context of milling studies, DOE helps in systematically investigating the effects of multiple variables and their interactions on the milling process. This section classifies milling studies based on their use of DOE, highlighting the various approaches and their contributions to optimizing milling processes [104].

Selecting the right design of experiments helps achieve the goal of gaining the most information from these experiments. In manufacturing, it is not always possible to study all parameters and their effects on the output due to constraints such as time and cost. This necessity makes the use of Design of Experiments essential in investigating output parameters and obtaining the required manufacturing information through a minimal yet appropriate number of experiments [105].

In Figure 2-1, you can observe the various factors and the corresponding output response of the process. Each factor is associated with multiple levels. The number of levels may vary based on the specific experimental objectives, typically ranging from 2 to 5. Conversely, the number of factors and their respective levels play a crucial role in determining the appropriate approach for conducting Design of Experiments [105]. In the next chapters, four approaches of Design of Experiments will be discussed.

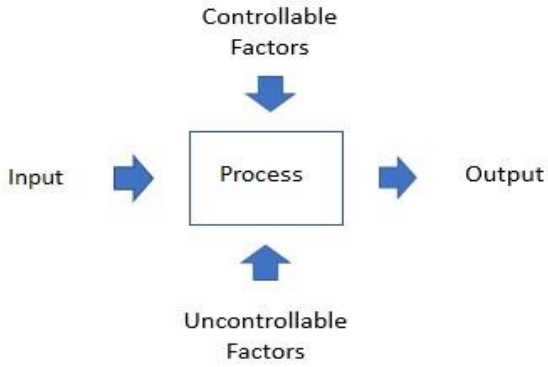


*Figure 2-1: Factors and output of a process.*

### 2.4.1 Full factorial design

In the case of full factorial design method, all the factors and their interactions are investigated. The number of levels is usually 2 and rarely 3. If the number of levels equals 2, the linear effect of the factors should be investigated. In case of 3 or more, not only the linear effects but also the quadratic effects of each factor should be studied.

The number of required experiments is calculated as $n^k$, where (k) represents the number of factors, and (n) signifies the number of levels for each factor. For instance, if we have three factors, each with two levels, the total number of experiments amounts to 8. In this scenario,

all potential combinations of factors at all levels are thoroughly examined. A full factorial design is well-suited when the number of factors is four or less. [106].

Many researchers rely on this method to identify the most influential factors that have a significant impact on the output. For example, in a study conducted by Noorani, Farooque and Ioi [107], the effect of four factors, namely spindle speed, depth of cut, feed rate, and tool size, on the surface roughness of aluminum alloy 6061 was investigated. Their findings revealed that feed rate and tool size have a substantial influence on surface roughness. The least surface roughness occurs when spindle speed and depth of cut are set to their highest levels, and the feed rate is kept low.

In a separate study focusing on tool life using the same workpiece material, M. Kasim et al. [108] identified cutting speed as the most critical factor affecting tool life. They observed that increasing cutting speed leads to a decrease in tool life. An optimum tool life of 97 minutes was achieved with a cutting speed of 115 m/min, a feed rate of 0.15 mm/tooth, and a depth of cut of 0.5 mm.

Furthermore, Kiran and Kumar [109] conducted a multi-objective optimization study. They found that the lowest total cost and the maximum tool life of 170.19 minutes could be achieved by setting the feed rate to 0.3 mm/rev, cutting speed to 50 m/min, and depth of cut to 0.3 mm.

In another investigation, Lakshmi and Subbaiah [110] explored the impact of cutting speed, feed rate, and depth of cut on surface roughness. Their results indicated that feed rate had the primary effect on surface roughness, followed by cutting speed. Additionally, they performed a multi-objective optimization with the aim of maximizing metal removal rate (MRR) and minimizing surface roughness ($R_a$). The optimal conditions were found to be a feed rate of 800 mm/min, a cutting speed of 160 m/min, and a depth of cut of 0.5 mm.

Shahrajabian and Farahnakian [111] explored the influence of several factors on surface roughness and machining forces in CFRPs, maintaining the same factors but replacing cutting speed with spindle speed. Their findings were as follows: as the feed rate increased, surface roughness also increased, whereas it decreased with spindle speed. Likewise, when the feed rate increased, machining forces rose, but they decreased with spindle speed.

In a similar vein, Abbas et al. [112] investigated the impact of these same factors on the surface roughness of high-strength steel and conducted a multi-objective optimization aimed at maximizing metal removal rate while minimizing surface roughness (Ra). They determined the optimal parameters to be a depth of cut of 1.0 mm, spindle speed of 1250 rpm, and feed rate of 67 mm/min, resulting in a composite desirability of 0.83, which yielded Ra = 0.15 μm and MRR = 233.3 $mm^3$/min.

On the other hand, Vipindas et al. [113] obtained different results based on tool diameter. When using a 0.5 mm tool diameter, they found that the most significant factor affecting surface roughness was the depth of cut, followed by spindle speed and feed rate. The interaction between feed rate and spindle speed had a notable impact. However, when using a 1 mm tool diameter, their results aligned with those of other studies. In both cases, the interaction between feed rate and spindle speed significantly affected surface roughness.

Deshmukh et al. [114] delved into material removal rate and found the following outcomes: surface roughness is predominantly influenced by feed rate, while material removal rate is most affected by the depth of cut. They observed a proportional relationship between material removal rate and surface roughness. Notably, the minimum surface roughness (Ra = 1.2 μm) was achieved with a feed rate of 250 m/min, a depth of cut of 0.2 mm, and a spindle speed of 600 rpm. Conversely, maximum material removal (29.214 $mm^3$/s) occurred at a feed rate of

300 m/min, a depth of cut of 0.6 mm, and a spindle speed of 800 rpm. They also determined the minimum time required for maximum material removal rate to be 13.03 seconds.

Bolar, Das and Joshi [115] explored the impact of tool diameter, feed rate, and axial and radial depth of cut on surface roughness, revealing several findings:

1. The best surface finish was achieved with lower values of feed rate, axial depth of cut, and radial depth of cut when using an 8 mm tool diameter.
2. Tool diameter had a significant effect on both surface roughness and cutting force.
3. Tool breakage was observed when using a 4 mm diameter tool with high depth of cut and feed rate.

Mikó and Nagy [116] focused on the effect of tool corner radius, feed rate, and depth of cut on surface roughness, and summarized their results as follows:

1. The impact of depth of cut and feed rate was similar.
2. A higher feed rate had a minor effect on surface roughness but slightly improved surface accuracy.
3. Increasing the depth of cut negatively affected both investigated parameters.
4. A larger tool corner radius reduced surface roughness but increased surface error.

Table 2-1 provides a summary of studies utilizing full factorial design. It is evident that the number of input factors is three in eight studies, with only two studies incorporating four input factors. However, the number of levels varies across the research; some studies have 2 levels, others 3 levels, and one study employs 4 levels. Notably, the highest number of required experiments across these studies is $3^4$ (81).

In the context of milling machines, feed rate, depth of cut, spindle speed, and cutting speed emerge as the most crucial factors. Furthermore, surface roughness (Ra) is the predominant output variable in the majority of these investigations. Using full factorial design helps studying all the possibilities of the levels of the factors. It gives enough information about the output response of the process. However, a limitation of this method is that the number of experiments required increases with the number of factors and their levels. This can make applying the method impractical in some cases due to constraints on time and cost. In such cases, another method could be chosen like fractional factorial design which will be discussed in the next chapter.

*Table 2-1: Full factorial design in milling machine experiments*

| Author/ year | Work piece Material | Input Factors | No. levels | No. Experiments | Response Variables |
|---|---|---|---|---|---|
| Noorani Farooque Ioi 2009 [107]. | AL 6061 | Spindle Speed<br>Depth of Cut<br>Feed Rate<br>Tool Size | 2 | 24<br>3 replications | Surface roughness $R_a$ |
| Lakshmi Subbaiah 2012 [110] | EN24 alloy steel | Cutting speed<br>Feed rate<br>Depth of cut | 3 | 33<br>no replication | Surface roughness $R_a$<br>Material removal rate |
| Kiran Kumar 2013 [109] | AISI 304 Stainless Steel | Cutting speed<br>Feed rate<br>Depth of cut | 3 | 33 | Tool life<br>Total cost |
| Kasim et al. 2015 [108] | AL 6061-T6 | Cutting speed<br>Feed rate<br>Depth of cut | 2 | 23<br>no replication | Tool life |
| Shahrajabian Farahnakian | CRFP | Spindle speed<br>Feed rate | 3 | 33<br>no replication | Surface roughness $R_a$ |

| | | | | | |
|---|---|---|---|---|---|
| 2015 [111] | | Depth of cut | | | Machining force |
| Vipindas<br>Kuriachen<br>Mathew<br>2016 [113] | Titanium alloy Ti-6Al-4V | Spindle speed<br>Feed rate<br>Depth of cut<br>Tool type | 3<br><br><br>2 | $3^3*2$<br>no replication | Surface roughness $R_a$<br>Top burr formation |
| Abbas et al.<br>2016 [112] | High strength steel | Spindle speed<br>Depth of cut<br>Feed rate | 4 | 33<br>no replicate | surface roughness $R_a$ and $Rt$<br>Material removal rate |
| Deshmukh et al.<br>2017 [114] | AISI 1020 Mild Steel | Cutting speed<br><br>Depth of cut<br>Feed rate | 4<br><br>3 | $3^2*4$<br>no replication | Surface roughness $R_a$<br>Material removal rate |
| Bolar<br>Das<br>Joshi<br>2018 [115] | AL 2024-T35 | Tool diameter<br>Feed rate<br>Axial depth of cut<br>Radial depth of cut | 3 | 34<br>no replication | Surface roughness $R_a$<br>Cutting force |
| Mikó<br>Nagy<br>2019 [116] | C45 steel | Tool's corner radius<br><br>Feed rate<br>Depth of cut | 3<br><br>2 | $2^2*3$<br>no replication | Surface roughness $R_a$ |

### 2.4.2 Fractional factorial

In the industry, the constraints of time, resources, and budget are of paramount importance. This practical consideration often renders full factorial experiments unfeasible, especially when dealing with a large number of factors. As an alternative, fractional factorial design is implemented, allowing researchers to conduct a reduced number of experiments to obtain crucial information about main effects and desired interaction effects. This approach involves omitting the investigation of certain interactions that are considered less significant[106].

The number of experiments in a fractional factorial design can be calculated using the formula $n^{k-p}$, where 'n' is the number of levels, 'k' is the number of factors, and 'p' is the exponent indicating the fraction of the full factorial design being used. For two-level factors, the formula simplifies to $2^{k-p}$. Here, $½^p$ denotes the fraction of the full factorial design being conducted. For example, when 'p' equals 1, it results in a half-fractional factorial design. Thus, with 3 factors at 2 levels, only four experiments are needed, which is half the number required for a full factorial design.[117].

Below, we review some studies that have employed fractional factorial design in the context of milling machinery:

Saini and Pradhan [118] applied this method to investigate the impact of four machining parameters (speed, feed, depth of cut, and coolant) on high carbon alloy steel. Their findings revealed that the depth of cut had the most significant effect on material removal rate, followed by feed, the interaction effect of depth of cut and feed, and, lastly, the impact of coolant. The optimal result for material removal rate was achieved at 52.1512 gm/min, with a depth of cut of 3.0 mm, a feed rate of 0.15 mm/tooth, and the use of coolant.

Conversely, Catherine, Ma'arof and Suresh [119] considered five factors (depth of cut, feed rate, step-over, spindle speed, and plunge rate) in their study on surface roughness. They found that step-over had the most significant influence on surface roughness.

Tseng et al. [120] employed a half fractional design to explore the impact of five factors (cutting speed, feed rate, depth of cut, nose radius, and cutting fluid) on surface roughness. Their research highlighted that the most critical factors were feed rate, cutting speed, and depth of cut.

El-Taybany et al. [121] conducted a study involving two levels for six factors, focusing on the cutting forces and moment as the experiment outputs. Their findings can be summarized as follows:

- The application of cutting fluid had a significant impact on cutting forces. It was observed that when cutting fluid was used, the moment decreased while cutting forces increased. A similar effect was noted when ultrasonic vibration was applied, resulting in a reduction in moment and an increase in cutting forces.
- Feed rate, spindle speed, and depth of cut were identified as key factors affecting cutting forces. Increasing the depth of cut and feed rate led to higher cutting forces, while decreasing the spindle speed had a similar effect.

Table 2-2 presents five studies that employed fractional factorial design. It is apparent that the number of factors considered in these studies exceeds the number of factors in Table 1. Three of these studies utilized half fractional factorial designs, with two of them having 5 factors and one with 6 factors.

Fractional factorial design proves to be an invaluable tool for investigating the most influential factors with primary effects on the output. When time and cost constraints are present, this approach becomes necessary, as it provides a wealth of information with fewer experiments compared to a full factorial design. However, it is worth noting that this method may yield insufficient information processes, and a prior understanding of the main factors to be studied is essential.

*Table 2-2: Fractional factorial design in milling machine experiments*

| **Author/ year** | **Work piece material** | **No. Factors** | **Input Factors** | **No. levels** | **Fractional Design** | **Response Variables** |
|---|---|---|---|---|---|---|
| Saini Pradhan 2014 [118] | EN-31 | 4 | Speed<br>Feed<br>Depth of cut<br>Coolant | 2 | $2^{4-1}$<br>no replication | Material removal rate |
| Catherine et al 2015 [119] | PE board | 5 | Depth of cut<br>Feed rate<br>Step-over<br>Spindle speed<br>Plunge rate | 2 | $2^{5-1}$<br>no replication | Surface roughness $R_a$ |
| Tseng Konada Kwon 2015 [120] | AL 6061 T6 | 5 | Cutting Speed<br>Feed rate<br>Depth of cut Nose radius<br>Cutting fluid | 2 | $2^{5-1}$<br>3 replications | Surface roughness $R_a$ |
| El-Taybany Hossam El-Hofy 2017 [121] | Soda glass | 6 | Spindle speed<br>Feed rate<br>Depth of cut<br>Ultrasonic vibration | 2 | $2^{6-1}$<br>2 replications | Cutting forces and the moment |

| | | | | | | |
|---|---|---|---|---|---|---|
| | | | Grain structure<br>Cutting Fluid | | | |

### 2.4.3 Taguchi method

This method, developed by Dr. Taguchi, a renowned Japanese engineer, has gained widespread popularity for its revolutionary approach to enhancing product quality in the industry. Central to Taguchi's methodology is the concept of the "loss of society," emphasizing that both society and individual firms suffer when well-made products do not perform as effectively as they could [117].

According to Taguchi's perspective, the journey to improving product quality commences with bringing the population distribution closer to the target value. Subsequently, the focus shifts to minimizing variation around this target [122].

Dr. Taguchi's approach incorporates a set of standard orthogonal arrays, which serve to determine the number of experiments to be conducted. The choice of the most suitable array depends on the number of factors and their respective levels [117]. By using these arrays, it becomes possible to examine the linear effects of the factors and relevant interactions among them.

Taguchi's method also accounts for noise or uncontrollable factors, often disregarded due to economic constraints and their perceived minimal impact on process responses. However, by including these factors, Taguchi developed a robust design [19]. In this robust design, an outer array represents the noise variables, integrated with an inner array that represents the main factors [117].

Now, let's delve into some research examples where this approach was employed in investigations within the field of milling machines.

Singh and Mall [123] conducted a study to optimize the surface roughness of aluminum by investigating the effects of cutting speed, feed rate, and depth of cut. Their findings indicated that the most crucial factor for surface roughness was the feed rate, followed by cutting speed and depth of cut.

In a separate study, Ramesh [124] focused on minimizing cycle time during the machining of stainless steel AISI 304 by examining the spindle speed, feed rate, and depth of cut. The results of this research revealed that, for cycle time, the spindle speed emerged as the most significant factor, followed by feed rate and depth of cut, while in terms of surface roughness; the feed rate was identified as the primary influencing factor.

Malay et al. [125] explored the same factors to optimize the milling process for machining Al 6351. Their results diverged from previous findings as they highlighted that spindle speed was the most critical factor in modeling surface roughness. However, Ghalme, Mankar, and Bhalerao [126] emphasized that achieving the optimal surface roughness was contingent on specific values: spindle speed = 200 rpm, depth of cut = 1.2 mm, and feed = 40 mm/min.

In a study by Ratnam et al. [127] the effects of process factors on surface roughness, surface hardness, and tool vibrations were investigated. Their findings can be summarized in the following three points:

1. The most influential factors for surface roughness were the feed rate and tool speed.
2. For surface hardness, tool speed and depth of cut played the most significant roles.

3. In the context of orthogonal turn-milling, depth of cut had a vital impact on surface hardness and tool vibrations, while in tangential turn-milling, tool speed emerged as the most crucial factor.

In their research, Gupta, Krishna and Suresh [128] concentrated on the flatness of the workpiece. Their study revealed that increasing spindle speed and feed rate led to a reduction in flatness, while an increase in depth of cut resulted in higher flatness values. In their study Kumar et al [129] found that, the most important factor is spindle speed, then depth of cut and feed.

Conversely, Sosa, Makwana and Acharya [130] not only considered surface roughness but also examined material removal rate. They found that feed rate had the most significant effect on material removal rate, while cutting speed primarily influenced surface roughness.

In another investigation conducted by Kim and Lee [131], cutting force and tool wear were studied alongside surface roughness. The key findings are as follows:

1. Spindle speed played a major role in tool wear.
2. Depth of cut had the most significant impact on cutting force.
3. Feed rate was the primary influencing factor for surface roughness.

In an attempt to minimize energy consumption while maintaining surface roughness, Ahmed and Arora [132] concluded that spindle speed was the most important factor for surface roughness, while feed rate had the most significant effect on energy consumption.

Table 2-3 shows that the L9 orthogonal array is the most commonly used, especially when dealing with three levels and either four or three factors. This choice aligns well with investigating surface roughness, given that the most critical factors for surface roughness are spindle speed, depth of cut, and feed rate, as indicated in Table 2. For a higher number of factor levels, orthogonal arrays such as L16 and L25 are more suitable.

The Taguchi method emphasizes achieving a target value rather than merely conforming to specified limits, which has significantly improved product quality. It enables the analysis of multiple factors with a minimal number of experiments and allows for a focus on key factors while ignoring less important ones.

*Table 2-3: Taguchi design in milling machine experiments*

| Author/ year | Work piece material | No. factors | Input factors | No. levels | Ortho-gonal matrix | Response variables |
|---|---|---|---|---|---|---|
| Singh Mall 2015 [123] | AL | 3 | Cutting speed<br>Feed rate<br>Depth of cut | 3 | $L_9$ | Surface roughness |
| Ramesh 2015 [124] | AISI 304 Stainless steel | 3 | Spindle speed<br>Feed rate<br>Depth of Cut | 3 | $L_9$ | Surface roughness<br>Cycle time |
| Malay et al. 2016 [125] | AL 6351 | 3 | Spindle speed<br>Feed rate<br>Depth of cut | 3 | $L_9$ | Surface roughness |
| Ghalme1 Mankar Bhalerao 2016 [126] | GFRP | 3 | Spindle speed<br>Feed rate<br>Depth of cut | 3 | $L_9$ | Surface roughness |
| Ratnam et al. 2016 [127] | Extruded brass (leaded) | 3 | Tool speed<br>Feed rate<br>Depth of cut | 4 | $L_{16}$ | Surface roughness<br>Surface hardness<br>Tool vibrations |

| | | | | | | |
|---|---|---|---|---|---|---|
| Gupta Krishna Suresh 2017 [128] | AL/Si alloy | 4 | Spindle speed Feed Rate Depth of Cut Step over ratio | 3 | $L_9$ | Flatness |
| Kumar et al. 2017 [129] | Al2024-SiC | 4 | Spindle speed Feed Rate Depth of Cut Number of Flutes | 3 | $L_{27}$ | Surface roughness |
| Sosa Makwana Acharya 2108 [130] | Medium carbon steel | 3 | Spindle speed Feed Rate Depth of Cut | 5 | $L_{25}$ | Surface roughness Material removal rate |
| Kim Lee 2019 [131] | Inconel 718 | 3 | Spindle speed Feed rate Depth of cut | 3 | $L_9$ | Tool wear Cutting force Surface roughness |
| Ahmed Arora 2019 [132] | Low carbon steel A36 K02600 | 4 | Spindle speed Feed rate Depth of cut Cutting speed | 3 | $L_9$ | Surface roughness Energy consumption |

### 2.4.4 Response surface methodology

Response Surface Methodology (RSM) is an integrated approach that combines mathematical and statistical techniques to enhance, develop, and optimize processes. It also plays a crucial role in formulating and designing new products [133]. In most RSM problems, both first and second-order models are utilized. Linear terms are associated with the first-order model, while the second-order model incorporates quadratic terms.

This method has been employed in numerous research studies to optimize cutting parameters in machining operations. Subramanian et al. [134] developed a second-order quadratic model to predict vibration amplitude. Their research revealed that increasing the feed rate led to an increase in vibration amplitude, while decreasing the cutting speed also resulted in higher vibration amplitudes. These increases in vibration amplitudes were observed at low nose radii and low radial rake angles, whereas decreases in vibration amplitudes occurred at high nose radii and high radial rake angles.

In another study, Jeyakumar et al. [135] investigated the influence of machining parameters on cutting force, tool wear, and surface roughness. Their findings were as follows:

1. The z-component of the cutting force exhibited a significantly higher magnitude compared to the other components in the x-direction.
2. Tool wear rates were higher at low cutting speeds.
3. Lower feed rates were associated with higher surface roughness, while higher speeds led to reduced surface roughness.
4. Machining with a high depth of cut resulted in increased tool wear, cutting force, and surface roughness.

Patel et al. [136], explored the effect of cutting parameters on workpiece temperature. They discovered that increasing the depth of cut, feed rate, and speed also increased the workpiece temperature. However, the depth of cut was identified as the most critical parameter. To minimize temperature, a lower depth of cut was found to be desirable.

Kumar and Rajamohan [137] studied the effects of spindle speed, feed rate, axial depth of cut, and radial depth on surface roughness and flatness. Their research highlighted the

significance of the feed rate in surface roughness. Increasing the feed rate or axial depth of cut resulted in higher surface roughness, while increasing cutting speed or spindle speed led to reduced surface roughness. In terms of flatness, axial and radial depth of cut significantly influenced the outcome.

In their study, Rao and Murthy [138] used a multi-response optimization technique to minimize surface roughness and workpiece vibration velocity by optimizing cutting parameters. The optimal parameters identified were a cutting speed of 210 m/min, a nose radius of 0.6828 mm, and a feed rate of 0.10 mm/min.

Khairusshima et al. [139] developed a statistical model to investigate the impact of cutting parameters on tool wear. They found that the most critical factor influencing tool wear was the feed rate. The optimal parameters for minimizing tool wear were identified as a feed rate of 200 mm/min, a cutting speed of 3510 rpm, and a depth of cut of 0.5 mm, resulting in a tool wear of 0.0267 mm.

On the other hand, Başar, Kahraman and Önder [140] delved into the impact of cutting parameters on surface roughness and developed a model for estimating surface roughness. They determined that spindle speed and feed rate had the most significant effects on surface roughness. In their model, the minimum surface roughness was achieved at spindle speed of 5981 rpm, feed rate of 3008 mm/min, and a depth of cut of 0.54 mm.

Singh, Samad and Saraf [141] the effects of machining parameters on surface roughness during turning of AL6061 were analyzed. Their model closely matched experimental values with a 95 percent confidence level. The minimum surface roughness parameters—Ra= 0.6943 μm, Rq = 1.0314 μm, and Rz = 4.1229 μm— were achieved with a feed rate of 73.37 mm/min, cutting speed of 187.84 m/min, and a depth of cut of 0.48 mm.

Based on the data presented in Table 2-4, several key points emerge:

1. Surface roughness has been a common response variable in numerous research studies, with efforts aimed at reducing roughness using various machining parameters.
2. In addition to conventional factors like cutting speed, feed rate, and depth of cut, researchers have also explored the influence of nose radius.
3. Various response variables beyond surface roughness have been investigated, including tool wear, vibration, and cutting force.

*Table 2-4: Response surface methodology in milling machine experiments*

| Author/ year | Work piece material | No. factors | Input factors | No. levels | Type | Response Variables |
|---|---|---|---|---|---|---|
| Subramanian et al. 2013 [134] | Al 7075-T6 | 5 | Radial rake angle<br>Nose radius<br>Cutting speed<br>Cutting feed<br>Axial depth of cut | 5 | CCD | vibration amplitude |
| Jeyakumar Marimuthu Ramachandran 2013 [135] | Al6061/SiC | 4 | Spindle speed<br>Feed rate<br>Depth of cut<br>Nose radius | 3 | CCD | Cutting force<br>Tool wear<br>Surface roughness $R_a$ |
| Patel et al. 2014 [136] | Mild steel | 3 | Speed<br>Feed rate<br>Depth of cut | 3 | CCD | Temperature of work piece |
| Kumar Rajamohan 2015 [137] | AL 6063-T6 | 4 | Spindle speed<br>Feed rate<br>Axial depth of cut<br>Radial depth | 5 | CCD | Surface roughness $R_a$<br>Fatness |

| | | | | | | |
|---|---|---|---|---|---|---|
| Rao; Murthy 2016 [138] | AISI 316 | 3 | Nose radius<br><br>Cutting speed<br>Feed rate | 2<br><br>3 | CCD | Tool wear<br>Vibration of work piece |
| Khairusshima et al. 2018 [139] | CFRP | 3 | Cutting speed<br>Feed rate<br>Depth of cut | 5 | CCD | Tool wear |
| Başar Kahraman Önder 2019 [140] | AL 5083 | 3 | Feed rate Spindle speed<br>depth of cut | 3 | FCD | Surface roughness $R_a$ |
| Singh; Samad Sara; 2019 [141] | AL 6061 | 4 | Feed<br>Depth of cut<br>Spindle speed<br>Nose radius | 2 | CCD | Surface roughness $R_a$, $R_z$ and $R_q$ |

Following the state-of-the-art review and the introduction of design of experiment techniques in the milling process, with an emphasis on key input and output factors, the subsequent two chapters will delve into surface roughness analysis. Initially, a comparison will be made between longitudinal turning and constant Z-level milling technologies, focusing on the Ra/Rz ratio. In the following chapter, the impact of surface inclination on roughness will be explored, assessing concave and convex workpieces machined under identical cutting parameters.

# 3 Comparison of surface roughness when turning and milling

## 3.1 Objective

This chapter presents a geometric model of surface roughness in both turning and contour milling processes, addressing these two cutting procedures based on a common theoretical foundation. Through the meticulous measurement of workpiece surface roughness, this chapter provides an insightful examination, comparing results between turning and milling operations.

The aim of this chapter is to highlight the importance of the Ra (arithmetic average roughness) and Rz (average maximum height of the profile) parameters in accurately describing surface roughness. These parameters are crucial for evaluating and ensuring the quality of machined surfaces. By understanding their significance, we can better assess the performance and effectiveness of different machining processes. This chapter will delve into the definitions and applications of Ra and Rz, demonstrating how they provide a comprehensive understanding of surface roughness.

In the case of turning, two turning tools with different corner radius were used. The effect of the feed and depth of cut were studied. The same in milling, two different cutters with different corner radius were used. The depth of cut is investigated on two levels.

Figure 3-1 shows the geometric model of the cusp height (CH), which is the base of the estimation process of surface roughness.

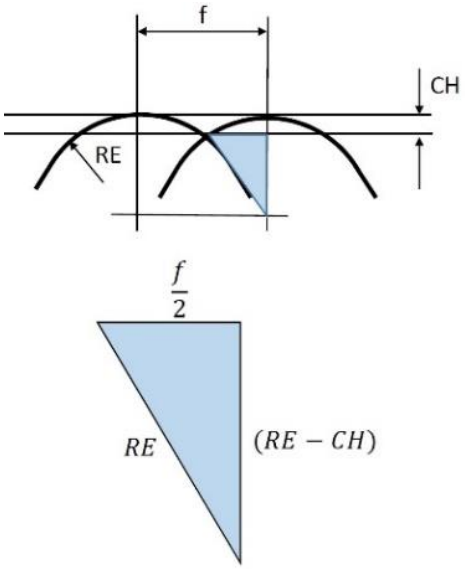


*Figure 3-1: Cusp height in case of a longitudinal turning.*

Based on Figure 3-1 the cusp height in turning can be calculated from equation:

$$RE^2 = (\frac{f}{2})^2 + RE \quad (3\text{-}1)$$

Because of the small value of CH, the square of it is small too, so it is negligible. The cusp height is:

$$CH = \frac{f^2}{8 \cdot RE} \quad (3\text{-}2)$$

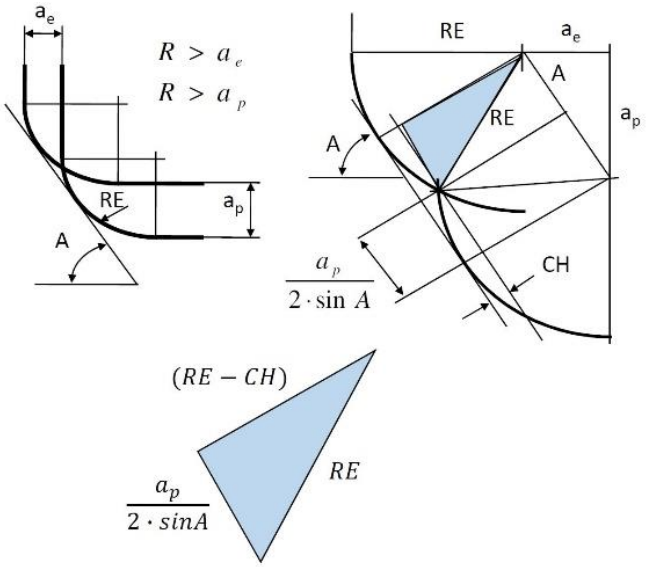


*Figure 3-2: Cusp height in case of the Z-level milling.*

Because of the similarity of the geometric model Figure 3-2, in case of Z-level milling the cusp height can be calculated in the same way:

$$RE^2 = \left(\frac{a_p}{2 \cdot sinA}\right)^2 + (RE - CH)^2 \quad (3\text{-}3)$$

$$CH = \frac{{a_p}^2}{8 \cdot RE \cdot sin^2 A} \quad (3\text{-}4)$$

## 3.2 Materials and methods

The workpiece material used for the present study was C45 (1.0503) medium-carbon unalloyed steel. C45 steel is utilized in the manufacturing of parts with high strength requirements, such as gears, shafts, piston pins, etc., as well as parts subjected to lower stress levels, such as machined parts, forgings, stampings, bolts, nuts, and pipe joints. The tensile strength of C45 steel ranges from Rm=650 to 800 MPa. The chemical composition of C45 is provided in Table 3-1.

*Table 3-1: Chemical composition of C45 steel (analysis in %)*

| C | Si | Mn | P | S | Cr | Mo | Ni |
|---|---|---|---|---|---|---|---|
| 0.42-0.5 | <0.4 | 0.5-0.8 | <0.045 | <0.045 | <0.4 | <0.1 | <0.4 |

During the experiments turning and milling technologies were compared. The turning test parts were machined by the type E400 conventional lathe engine (tuning machine). Two different turning tools were used with varying corner radii (RE): CNMG 120404-PM and CNMG 120408-PM inserts. The same cutting speed was maintained, and three different feed rates were applied (Table 3-2).

Surface roughness was measured using the Mitutoyo SJ-301 instrument. The Ra and Rz parameters were measured in 8 positions around the test part, and the presented values were calculated as their averages.

*Table 3-2: Cutting parameters in case of turning.*

| | T1 | T2 | T3 | T4 | T5 | T6 |
|---|---|---|---|---|---|---|
| Cutting speed $v_c$ (m/min) | 100 | 100 | 100 | 100 | 100 | 100 |
| Depth of cut $a_p$ (mm) | 1.0 | 1.0 | 1.0 | 1.5 | 1.5 | 1.5 |
| Feed rate f (mm/rev) | 0.1 | 0.15 | 0.2 | 0.1 | 0.15 | 0.2 |
| Corner radius RE (mm) | 0.4 | 0.4 | 0.4 | 0.8 | 0.8 | 0.8 |

In the case of milling, the test parts were machined using a Mazak 410-AII CNC machining center. The surface inclination was 80°. Two different milling cutters were employed with the same cutting speed ($v_c$ = 160 m/min), but two values of the depth of cut were utilized (Table 3-3). The diameter of solid carbide milling cutters was 8 mm, with a 4-tooth configuration (type: Fraisa U45319.388 and U45319.391). The Z-level milling strategy was implemented, wherein the milling cutter moves solely in the x-y plane, machining the surface slice-by-slice.

Surface roughness was assessed using the Mitutoyo SJ-301 instrument. The Ra and Rz parameters were measured at 3 positions, and the presented values were calculated as the averages of these measurements.

*Table 3-3: Cutting parameters in case of milling.*

| | M1 | M2 | M3 | M4 |
|---|---|---|---|---|
| Cutting speed vc (m/min) | 160 | 160 | 160 | 160 |
| Depth of cut ap (mm) | 0.15 | 0.25 | 0.15 | 0.25 |
| Feed per tooth fz (mm/rev) | 0.05 | 0.05 | 0.05 | 0.05 |
| Corner radius RE (mm) | 0.5 | 0.5 | 1 | 1 |

## 3.3 The results

Table 3-4 contains the values of the calculated cusp height and the measured surface roughness. The measured data was analyzed by three aspects: (1) visual inspection of the surface profile, (2) the ratio of Rz/Ra and (3) the relationship between the cusp height and the surface roughness.

*Table 3-4: Values of cusp height and the measured surface roughness.*

| Part ID | CH [µm] | Ra [µm] | Rz [µm] |
|---|---|---|---|
| T1 | 3.13 | 1.36 | 7.69 |
| T2 | 7.03 | 2.00 | 10.17 |
| T3 | 12.50 | 3.06 | 15.10 |
| T4 | 1.56 | 1.09 | 7.06 |
| T5 | 3.52 | 1.46 | 8.50 |
| T6 | 6.25 | 1.99 | 10.31 |
| M1 | 5.80 | 2.40 | 9.66 |
| M2 | 16.11 | 4.84 | 19.25 |
| M3 | 2.90 | 1.38 | 6.15 |
| M4 | 8.06 | 2.50 | 10.63 |

### 3.3.1 Characterization of surface roughness

Representative surface profiles obtained from turning and milling operations are presented in Figure 3-3 and Figure 3-4 respectively.

From a practical standpoint, the comparison of maximum surface height (Rz) and arithmetic mean height (Ra) is of fundamental importance, commonly used by technologists and constructors.

Based on Figure 3-3, it can be observed that the surface appears smoother at smaller feed rates, with roughness increasing as feed rate increases. This trend holds true for both values of the depth of cut, with the optimal scenario occurring at the smallest feed rate ($f_z$ = 0.1 mm). At smaller feed rates, the profile appears irregular and becomes progressively more regular with increasing feed rate. However, with larger corner radii (RE), the profile remains irregular. This irregularity can be attributed to factors beyond geometric parameters, including machining environment conditions such as vibration and chip removal processes.

In the case of milling (Figure 3-4) the smoothest surface can be achieved with larger depth of cut ($a_p$ = 0.25 mm) and larger corner radius (RE = 1.0 mm). The profiles exhibit regularity, with identifiable cusps.

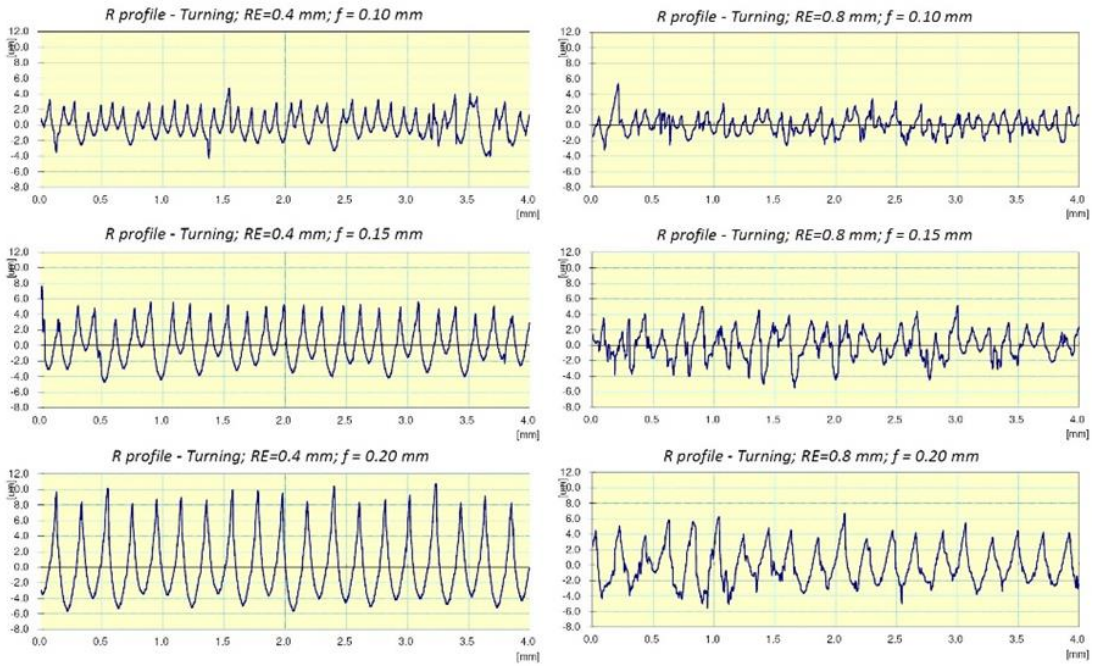


*Figure 3-3: Surface profiles at turning operation.*

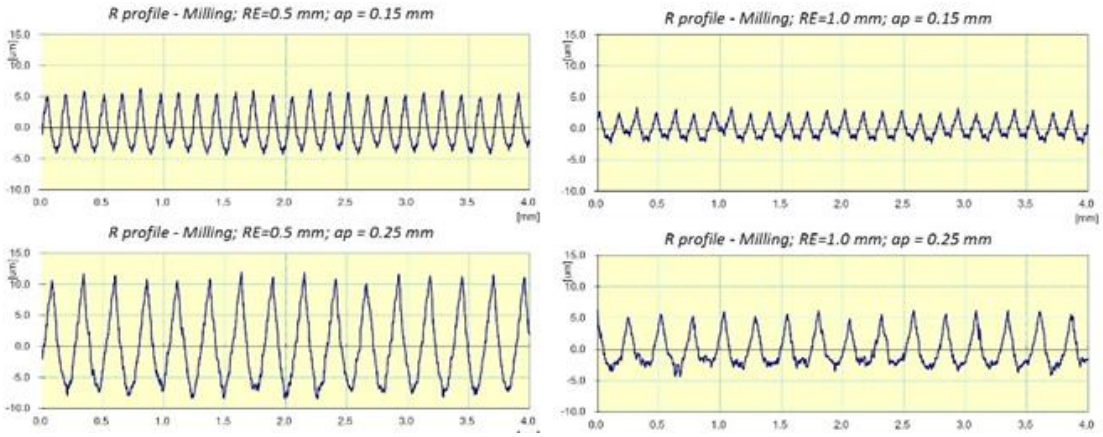


*Figure 3-4: Surface profiles at milling operation.*

### 3.3.2 The ratio of Rz/Ra

In the machine design, both Ra and Rz parameters are utilized, with certain design steps, such as fitting and lubrication, placing more emphasis on either Ra or the Rz. Although the conversion between Ra and Rz is important, the ratio of Rz/Ra is not a constant value, it depends on the production technology.

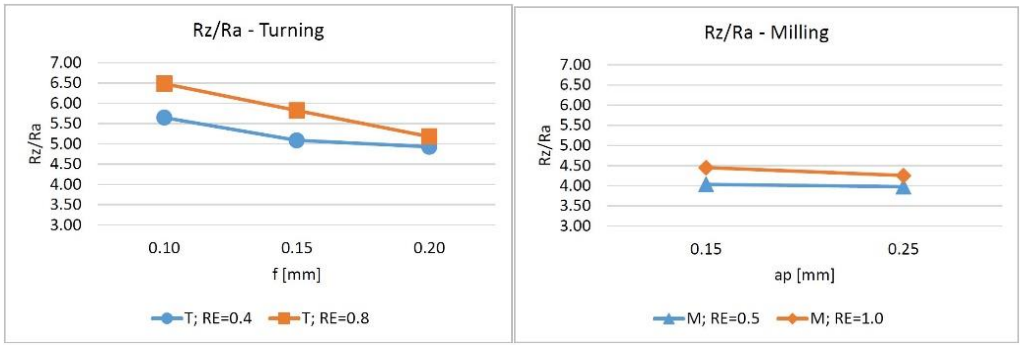


*a)* *b)*

*Figure 3-5: The ration Rz/Ra*

During turning, both the workpiece material and cutting conditions exert significant influence on surface roughness. The average ratio of Rz/Ra is 5.52, with an increase in corner radius (RE) leading to a higher ratio, while an increase in feed rate results in a decrease in this ratio (Figure 3-5 a). Notably, the feed rate has a greater impact on the ratio.

In milling operations, the average ratio is 4.18, with the ratio of Rz/Ra decreasing as the depth of cut increases (Figure 3-5 b). However, the difference between smaller and larger corner radii (RE) is less pronounced compared to turning. Specifically, with a smaller corner radius (RE = 0.5 mm), the change is minimal.

### 3.3.3 Comparison of cusp height and surface roughness

Based on the machining theory-based approach, there is relationship between the cusp height and the surface roughness. Figure 3-6 shows the measured surface roughness that is machined with different cutting conditions and the calculated cusp height at turning. In the case of Ra and Rz the linear regression works with good R2 factors (R2Ra=99.62%; R2Rz=98.33%). The relationship can be described with a linear regression:

$$Ra = 0.1794 \cdot CH + 0.8108 \qquad (3\text{-}5)$$

$$Rz = 0.7341 \cdot CH + 5.6444 \quad (3\text{-}6)$$

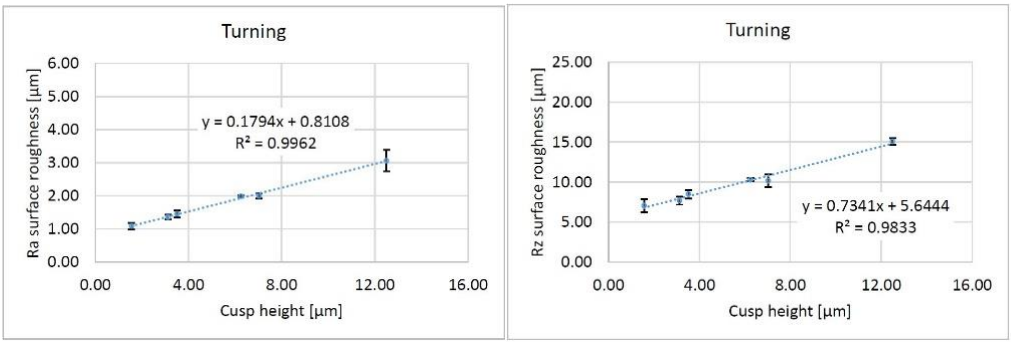


*a)* *b)*

*Figure 3-6: Measured Ra and Rz in function of cusp height in case of the longitudinal turning.*

If surface roughness is analyzed in the case of milling, the relationship between cusp height and surface roughness can be described by linear regression (Figure 3-7). The R2 coefficients are highly satisfactory ($R2R_a$=98.21%; $R2R_z$=99.15), indicating a strong correlation and precise estimation.

$$Ra = 0.2557 \cdot CH + 0.6793 \quad (3\text{-}7)$$

$$Rz = 0.9762 \cdot CH + 3.4013 \quad (3\text{-}8)$$

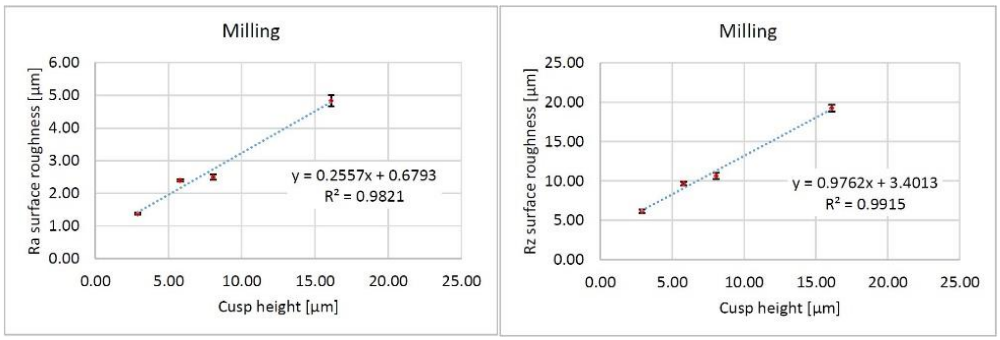


*a)* *b)*

*Figure 3-7: Measured Ra and Rz in function of cusp height in case of the Z-level milling.*

Let's combine the measured data from both the turning and milling experiments to investigate the general application of the cusp height parameter. Figure 3-8 shows the regression of the united database. In case of Ra surface roughness, the regression is satisfactory ($R2R_a$=93.66%), while the Rz parameter can be estimated with even greater accuracy using the cusp height. The R2Rz value is 96.61%, and the corresponding calculated equation is:

$$Rz = 0.8495 \cdot CH + 4.7714 \quad (3\text{-}9)$$

The surface roughness can be estimated based on cusp height, taking into account the tool and cutting parameters. In the investigated case, the following form was utilized:

$$Rx = C(RE, p) \cdot CH \quad (3\text{-}10)$$

where:

- *RE* represents the corner radius of the tool, and

- $p$ denotes the feed in the case of turning and the depth of cut in the case of contour milling.

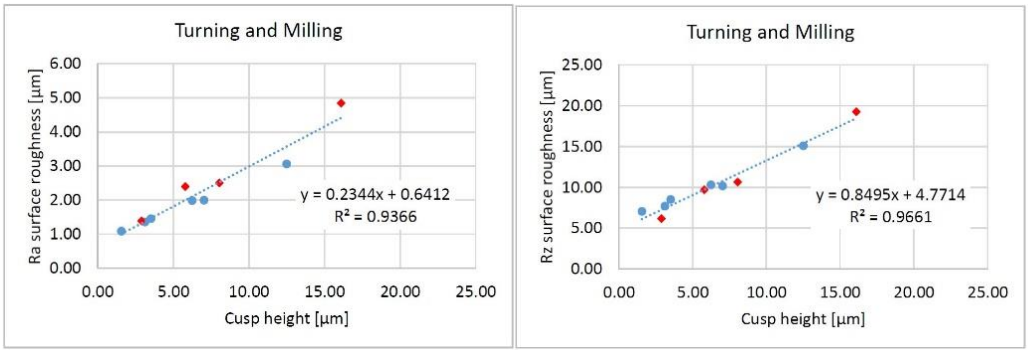


*a)* *b)*

*Figure 3-8: Ra and Rz surface roughness in function of cusp height in case of turning an z-level milling.*

Based on the measured data, the results of the hybrid estimation approach are:

$$Ra = (1.94 - 1.68 \cdot RE + 11.6 \cdot p) \cdot CH \quad (3\text{-}11)$$

$$Rz = (0.24 - 0.37 \cdot RE + 3.45 \cdot p) \cdot CH \quad (3\text{-}12)$$

The coefficient of determination for C(RE, p) is R2C_Ra=70.0% in case of Ra parameter and R2C_Rz=88.8% in case of Rz parameter.

Based on all measured data and statistical analyses, it appears that the Rz parameter is more suitable for the estimation method based on cusp height.

## 3.4 Conclusion

This chapter provides a comprehensive review of the significance of surface roughness and the various approaches utilized for predicting it. In recent years, there has been a growing interest in predicting surface roughness to develop more precise models, despite the multitude of uncontrollable factors that influence the machined surface. Notably, cutting conditions and cutting tool parameters wield a significant impact on surface roughness.

In this chapter, a comparison between longitudinal turning and Z-level milling technologies is conducted. For turning, the effect of corner radius and feed is investigated, while for milling, the impact of corner radius and depth of cut is studied. The presented geometric model of cusp height highlights the logical equivalency between the feed in turning and the depth of cut in milling. The research aims to demonstrate the application of cusp height as a geometric parameter in estimating surface roughness, taking into account both geometric and technological parameters.

Analysis of the measured data reveals that increasing feed in turning or increasing depth of cut in milling results in higher surface roughness, whereas increasing corner radius of the tool leads to a decrease in surface roughness. Furthermore, the calculated cusp height exhibits the same trend as the measured surface roughness parameters. Although both Rz and Ra parameters show a strong correlation with cusp height, the hybrid model indicates that the Rz parameter is more suitable for estimating surface quality based on cusp height. These findings underscore the importance of optimizing cutting parameters to achieve the desired surface roughness.

# 4 The effect of the surface inclination and the cutting speed on the surface roughness when ball-end milling

## 4.1 Objective

This chapter examines how changing the surface inclination affects cutting speed and explores the consequences of varying cutting speed on surface roughness. It also provides insights into the importance of feed rate and width of cut in the machining process when using a 3D ball-end mill.

## 4.2 Materials and methods

The machining experiments were conducted on both concave (CV) and convex (CX) surfaces made of the same material, namely low-alloy steel 42CrMo4. 42CrMo4 is commonly employed in the manufacturing of parts requiring high tensile strengths, such as compressors, turbines, and working elements of heavy equipment used both aboveground and underground, as well as components of agricultural machinery. The chemical composition of 42CrMo4 is provided in Table 4-1.

*Table 4-1: Chemical composition of the low-alloy steel 42CrMo4: (analysis in %)*

| C | Si | Mn | P | S | Cr | Mo | Cu |
|---|---|---|---|---|---|---|---|
| 0.38-0.45 | 0.10-0.40 | 0.60-0.90 | ≤ 0:025 | ≤ 0:035 | 0:9 - 1:2 | 0:15−0:3 | ≤ 0:4 |

The CV and CX parts consist of a cylindrical surface with a 45 mm radius connected to a horizontal plane with a 10 mm radius. Figure 4-1 shows both workpieces and Table 4-2 shows the angles of the normal vector of the surface.

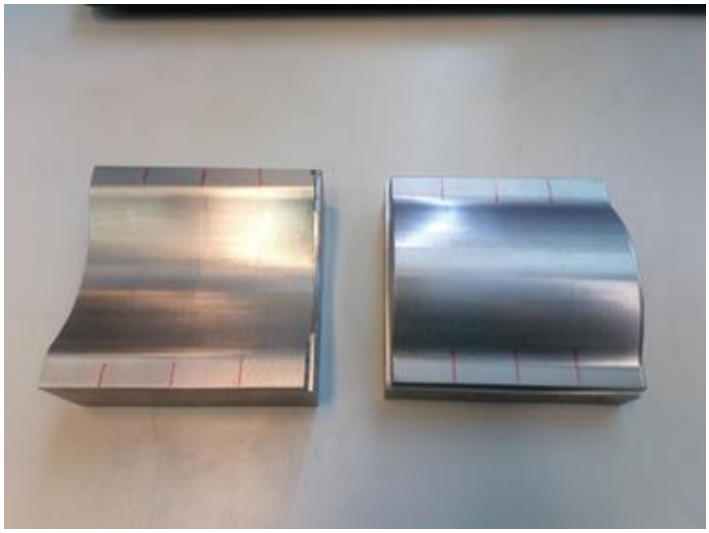

*Figure 4-1: The CV and CX workpieces.*

*Table 4-2: Angles of the normal vector of the surface*

| Measuring position (y) | 25 | 20 | 15 | 10 | 5 | 0 | 5 | 10 | 15 | 20 | 25 |
|---|---|---|---|---|---|---|---|---|---|---|---|
| CX angles (°) | 30 | 23.6 | 17.5 | 11.5 | 5.7 | 0 | −5.7 | −11.5 | −17.5 | −23.6 | −30° |
| CV angles (°) | −38.7 | −30 | −22 | −14.5 | −7.2 | 0 | 7.2 | 14.5 | 22 | 30 | 38.7 |

The machining was performed by a Mazak Vertical Center Nexus 410A-II CNC vertical machining center. The surface roughness was measured by a Mahr's MarSurf GD120 instrument. The Ra and Rz parameters were measured in the x-direction perpendicular to the milling direction at 11 different positions. The milling was done using a Fraisa X7450.450 ball-end milling cutter with a diameter of 10 mm (Dc = 10 mm) and 4 teeth (z = 4).

Five test surfaces were created by ball-end milling with different feed rates and widths of cut.

Table 4-3 shows the applied cutting parameters in machining these surfaces.

*Table 4-3: Cutting parameters used in the test.*

| Test id. | CV-01 | CV-02 | CV-05 | CV-03 | CV-04 |
|---|---|---|---|---|---|
| | CX-01 | CX-02 | CX-05 | CX-03 | CX-04 |
| Cutting speed $v_c$ [m/min] | 1600 | | | | |
| Spindle speed n [rpm] | 5100 | | | | |
| Feed per tooth $f_z$ [mm] | 0.08 | 0.08 | 0.08 | 0.12 | 0.16 |
| Feed speed $v_f$ [mm/min] | 1630 | 1630 | 1630 | 2450 | 3260 |
| Depth of cut $a_p$ [mm] | 0.3 | | | | |
| Width of cut $a_e$ [mm] | 0.35 | 0.25 | 0.15 | 0.15 | 0.15 |

Since the surface inclination changes, the effective diameter also changes. A geometrical model is presented by Mikó and Zentay [77] to calculate the effective diameter was implemented. Figure 4-2 shows the calculated effective diameter at each measured point in the case of the CV and CX workpieces.

The actual cutting speed can be calculated depending on the effective diameter at each measured point using the following formula:

$$v_c = \frac{D_{eff} * n * \pi}{1000} \quad (4\text{-}1)$$

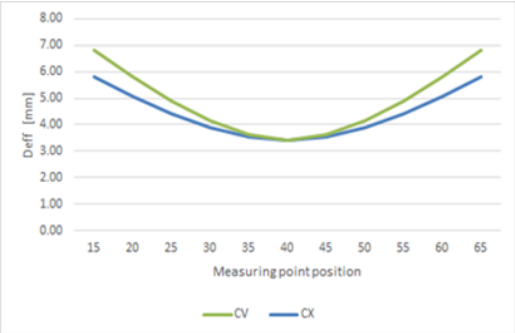


*Figure 4-2: The Effective diameters at each measured point*

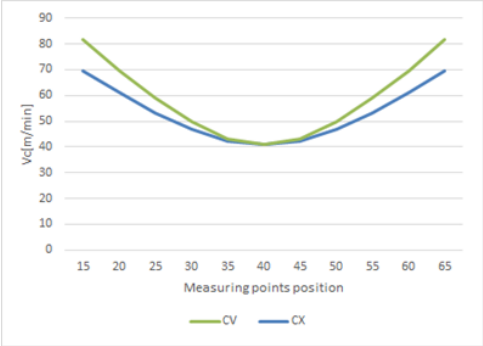


*Figure 4-3: shows the actual cutting speed for CV and CX surfaces.*

Figure 4-2 and Figure 4-3 show the effective diameter and actual cutting speed. Even though the diameter of the tool is 10 mm, the actual cutting diameter is smaller. In the case of the CV surfaces, it changes between (3.4 and 6.8 mm), while in the case of the CX surfaces, it changes between (3.4 and 5.8 mm). On the other hand, the effective diameter and, as a result, the cutting speed are the smallest in the middle of the workpieces, where the value of the normal vector is 0° and. In addition, although it can be seen from Figure 4-3 that the value of the cutting speed is higher in the case of the CV surfaces compared to the CX equivalents. However, the cutting speed curve is similar for both CV and CX test pieces.

## 4.3 Results and discussion

Figure 4-4 illustrates the average surface roughness of the test specimens. The graph indicates that the surface quality of the CV test specimens surpasses that of the CX counterparts under identical cutting parameters, owing to the higher actual cutting speed achieved in the case of CV surfaces compared to CX equivalents.

Conversely, when the feed rate is set at 0.08 mm and the width of cut is 0.35 mm, the surface roughness is observed to be poorest for both CV and CX surfaces.

The surface roughness of the workpieces was measured at several points revealing a notable influence of surface inclination on surface quality, as evident in Figures (Figure 4-5, Figure 4-6, Figure 4-7, Figure 4-8, Figure 4-9), This effect is particularly pronounced at the center of the test pieces, where the cutting speed is at its minimum, resulting in lower surface quality.

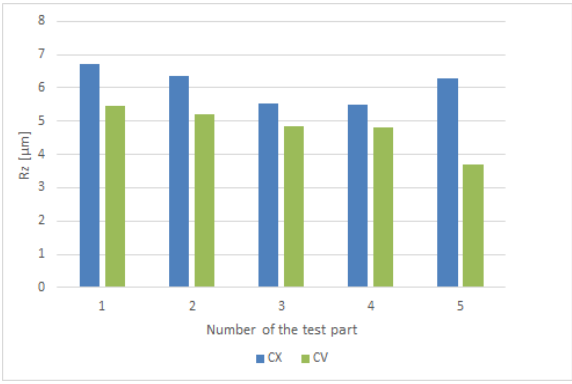


*Figure 4-4: Average Rz of each test piece.*

In the case of CX-01 and CX-02, the surface roughness is inferior, compared to the other three pieces. On these two pieces, Rz measures approximately 16 µm at the middle, whereas it is around 10 µm at the middle of the other pieces. In contrast, among the CV pieces, CV-05

demonstrates the best surface roughness, with Rz measuring less than 8 µm at the middle. In comparison, it is approximately 12 µm on the other pieces.

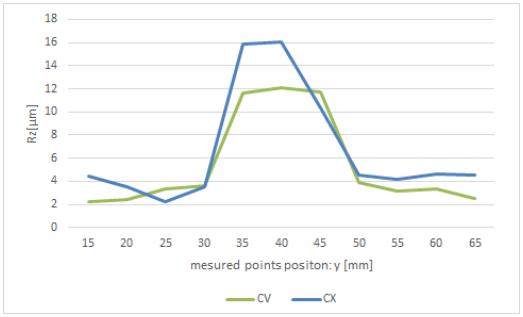


*Figure 4-5: Rz surface roughness in the case of CX-01 and CV-01*

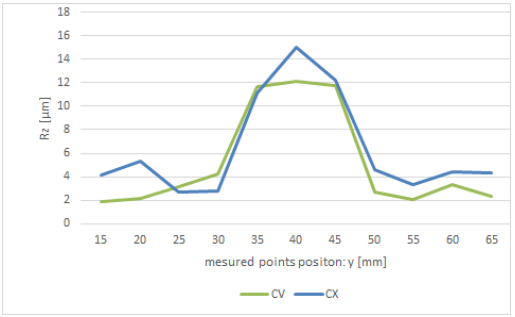


*Figure 4-6: Rz surface roughness in the case of CX-02 and CV-02*

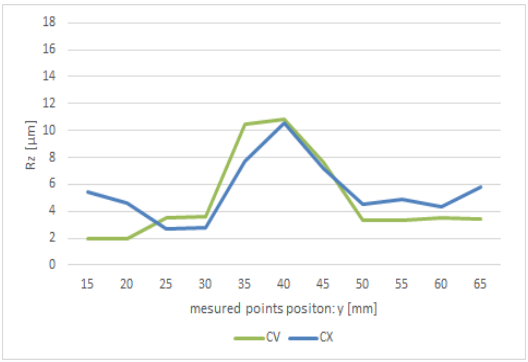


*Figure 4-7: Rz surface roughness in the case of CX-03 and CV-03*

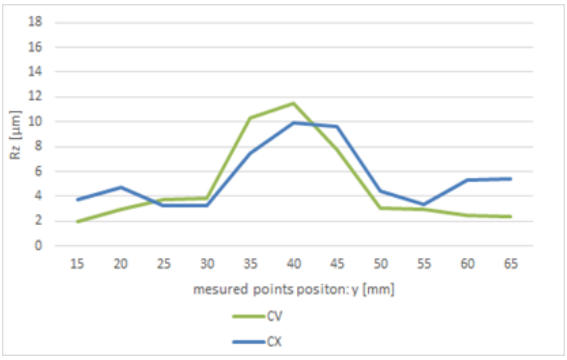


*Figure 4-8: Rz surface roughness in the case of CX-04 and CV-04*

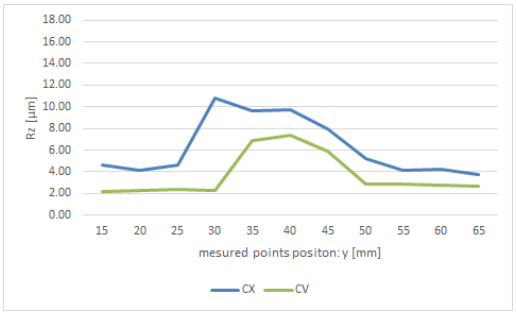


*Figure 4-9: Rz surface roughness in the case of CX-05 and CV-05*

The variation in surface roughness from piece to piece can be attributed to changes in the feed rate and width of cut. The feed rate is at its minimum during the machining of CX-01 and CV-01 but increases to its maximum during machining of CX-04 and CV-04. Conversely, the width of cut gradually decreases to its minimum during machining of CX-04 and CV-04.

Figure 4-10 and Figure 4-11 depict the main effect of changing the width of cut and feed rate on surface roughness for CV and CX surfaces. It is evident that the width of cut significantly affects surface roughness, with an increase in width of cut leading to higher Rz values of surface roughness. However, the feed rate has a minor effect on surface roughness, particularly for CV surfaces.

The actual cutting speed and the effective diameter exhibit the same effect on the surface roughness, as illustrated in Figure 4-12 and Figure 4-13. The Rz value of surface roughness

decreases with increasing the effective diameter and the cutting speed. However, in the case of CX surfaces, surface roughness increases by approximately 1 µm at a cutting speed of 70 m/min.

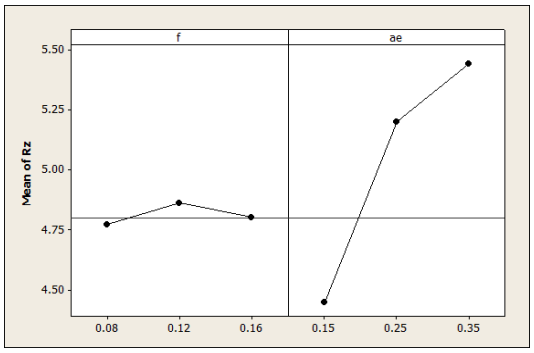


*Figure 4-10: The effect of the width of cut and feed rate in the case of CV surfaces.*

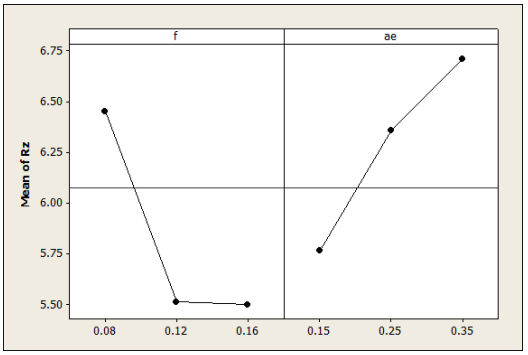


*Figure 4-11: The effect of the width of cut and feed rate in the case of CX surfaces.*

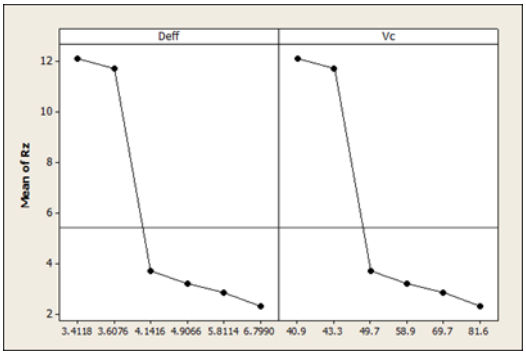


*Figure 4-12: The effect of the effective diameter and actual cutting speed in the case of CV surfaces*

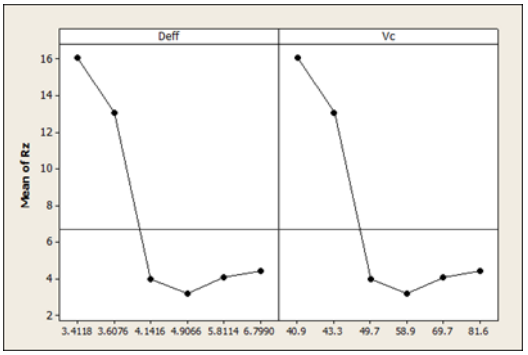


*Figure 4-13: The effect of the effective diameter and actual cutting speed in the case of CX surfaces*

## 4.4 Conclusion

Throughout this chapter, the impact of cutting speed on surface roughness has been thoroughly examined. The data obtained indicate that, under identical cutting parameters, the surface roughness of CV test pieces outperforms that of the CX counterparts. However, variations in surface inclination led to fluctuations in the actual cutting speed, thereby influencing surface quality. Notably, the cutting speed diminishes significantly when the ball-end mill's normal axis is applied to the workpiece surface. Given that fluctuations in cutting speed pose a significant challenge in 3-axis milling machines, adjusting the cutting speed during the milling process can mitigate this issue and ensure higher surface quality.

Furthermore, surface roughness is also influenced by other cutting parameters, such as feed rate and width of cut. It has been observed that increasing the width of cut results in higher surface roughness, whereas changes in the feed rate have only a minor effect.

Upon examining surface roughness, the subsequent chapter centers its discussion on the effective diameter. This chapter introduces a geometric model alongside a MATLAB simulation.

# 5 Simulation of the working diameter in 3-axis ball-end milling of free-form surface

## 5.1 Objective

The previous chapters emphasize the predominant focus of optimization procedures in ball-end milling on factors such as surface quality and tool path planning. However, they also highlight the need to emphasize the significance of cutting depth and surface geometry, given their direct impact on the working diameter, which subsequently influences cutting speed and surface quality.

In this chapter, a geometric approach is proposed to calculate the effective diameter during the finishing of free surfaces using a ball-end tool. The objective is to determine the working diameter across the surface and investigate the influence of surface inclination angles, axial and radial depth of cut, and feed direction on the working diameter. To achieve this, a Matlab simulation was used to illustrate the variation in working diameter with respect to the aforementioned factors.

## 5.2 Effective diameter

The nominal and effective diameters differ in ball-end milling operations. For a horizontal surface, the effective diameter, as illustrated in Figure 5-1, can be calculated by Eq 5-1

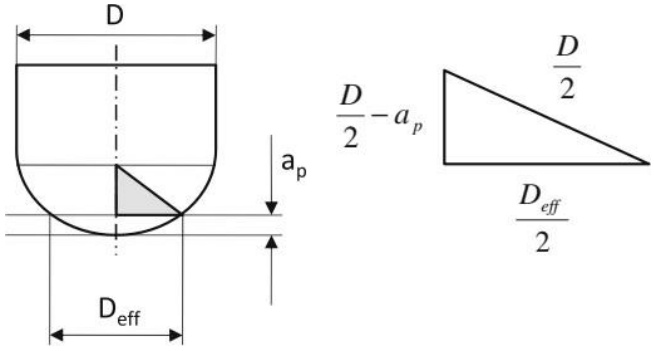


*Figure 5-1: Definition of the effective diameter in the case of a horizontal surface.*

$$D_{eff} = 2 * \sqrt{\left(\frac{D}{2}\right)^2 + \left(\frac{D}{2} - a_p\right)^2} \quad (5\text{-}1)$$

Whereas $a_p$ is the depth of cut, and D is the cutter's nominal diameter.

As previously discussed, the diameter of the cutting tool varies due to changes in surface inclination, resulting in different sections of the tool's edge being engaged. Figure 5-2 depicts an inclined surface alongside a ball-end milling cutter.

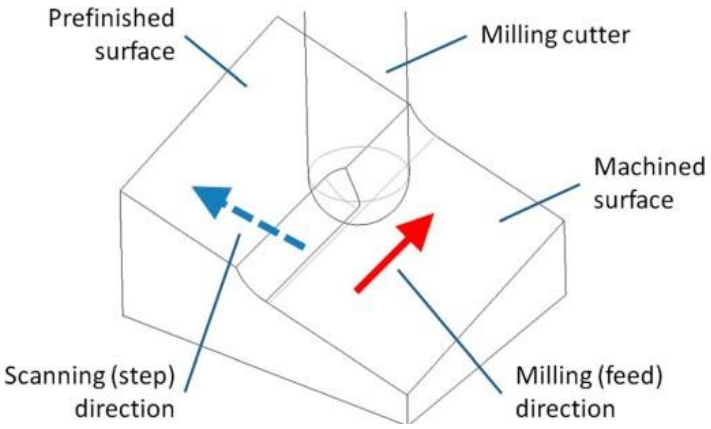


*Figure 5-2: Ball-end milling of an inclined plane surface.*

The working (effective) diameter can be defined as the distance between the intersection circle and the tool axis. This intersection circle is generated by parallel surface to the machined surface, with the distance between surfaces representing the depth of cut ($a_p$). According to the geometric model proposed by Mikó and Zentay [77], the intersection circle can be described. However, relocating the coordinate system's origin to the center of the ball simplifies further transformations. The equation of the intersection circle, in case of horizontal surface, can be described by Eq (5-2).

$$\underline{Cr}_{eff} = \begin{bmatrix} R_{eff} \cdot cos(2\pi t) \\ R_{eff} \cdot sin(2\pi t) \\ -R + a_p \\ 1 \end{bmatrix}, t \in [0,1] \qquad (5\text{-}2)$$

Surface inclination can be characterized by the angular position of the normal vector. $A_{N1}$ denotes the angular position relative to the x-axis, while $A_{N2}$ refers to the z-axis. With this information, two rotation operators are sufficient to compute the current equation of the intersection circle.

Utilizing the intersection plane instead of the offset surface facilitates calculations but may lead to slight differences in results.

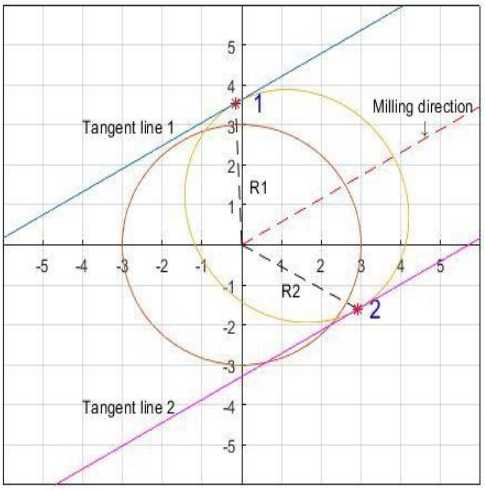


*Figure 5-3: Tangent points on the transformed circle.*

The current working diameter can be determined by considering the feed direction. To find the needed point to measure the working diameter, the tangent plane perpendicular to the xy plane must align parallel with the feed direction, as depicted in Figure 5-3. The central circle represents the original section curve, while the other one illustrates the view of the transformed circle. Mathematically, the description of the transformed curve can be generated using two rotation matrices (Eq 3-4, 3-5). On the transformed circle, two points can be defined by the tangent line aligned with the feed direction of the milling ($A_f$) (Eq 3-6).

$$\overline{\overline{Tr}} = \begin{bmatrix} cos(A_{N1}) \cdot cos(A_{N2}) & -sin(A_{N1}) & -cos(A_{N1}) \cdot sin(A_{N2}) & 0 \\ sin(A_{N1}) \cdot cos(A_{N2}) & cos(A_{N1}) & -sin(A_{N1}) \cdot sin(A_{N2}) & 0 \\ sin(A_{N2}) & 0 & cos(A_{N2}) & 0 \\ 0 & 0 & 0 & 1 \end{bmatrix} \quad (5\text{-}3)$$

$$\overline{C_{eff}^{T}} = \overline{\overline{Tr}} \cdot \overline{Cr_{eff}} = \begin{bmatrix} cos(A_{N1}) \cdot cos(A_{N2}) & -sin(A_{N1}) & -cos(A_{N1}) \cdot sin(A_{N2}) & 0 \\ sin(A_{N1}) \cdot cos(A_{N2}) & cos(A_{N1}) & -sin(A_{N1}) \cdot sin(A_{N2}) & 0 \\ sin(A_{N2}) & 0 & cos(A_{N2}) & 0 \\ 0 & 0 & 0 & 1 \end{bmatrix} \cdot \begin{bmatrix} R_{eff} \cdot cos(2\pi t) \\ R_{eff} \cdot sin(2\pi t) \\ (-R + a_p) \\ 1 \end{bmatrix} \quad (5\text{-}4)$$

The location of the tangent point can be calculated by first differential of the curve:

$$\frac{d\,\overline{\overline{C_{eff}^{T}}}}{dt} = tg\,A \quad (5\text{-}5)$$

Considering the width of cut, additional 4 points can be identified, indicating the starting or ending point of the cutting (Figure 5-5).

The step-over parameter ($a_e$) defines two additional points per side, depending on the milling process, whether it is down-milling or up-milling. By drawing a parallel line to the tangent line at a distance equal to the width of cut, two points can be identified on the transformed circle (Figure 5-4).

Depending on the direction of the width of cut, the milling cutter can operate on side 1 or side 2. In the case of up-milling, the cutting cycle begins at point 1 and ends at point 1' (Figure 5-5 a), while in the case of down-milling, the cutting process starts at point 1'' and ends at point 1 (Figure 5-5 b). If the tool operates on side 2, in the case of down-milling, chip removal begins at point 2' and ends at point 2 (Figure 5-5 c), while in the case of up-milling, chip removal occurs between points 2 and 2" (Figure 5-5 d)

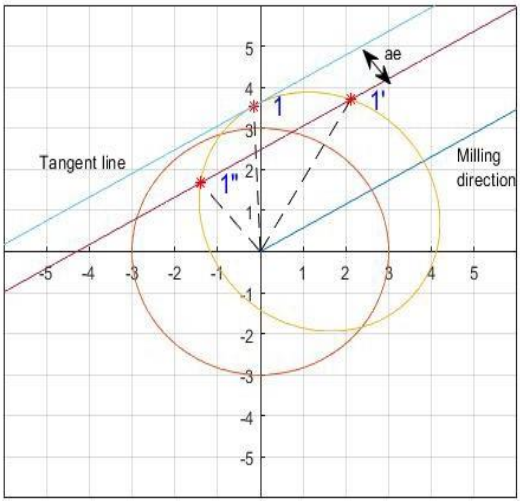


*Figure 5-4: The extreme points defined by the width of cut.*

With a larger width of cut ($a_e$), the variation in the effective diameter will be more pronounced. This implies that the cutting speed fluctuates throughout a single chip removal process, leading to inconsistencies in cutting speed and potentially resulting in inadequate surface roughness.

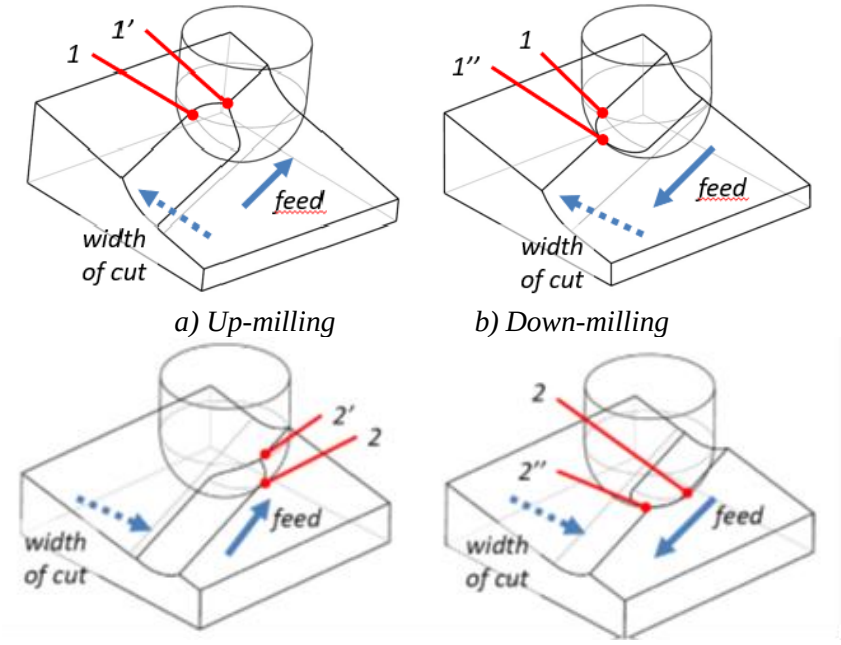


*a) Up-milling* *b) Down-milling*

*a) Up-milling* *b) Down-milling*

*Figure 5-5: Extreme points.*

The simulation was implemented in Matlab. The pseudo-code of the Matlab program is the next:

1. Set the tool parameter: $D_c$.
2. Set the input cutting parameters $A_f$, $a_e$, $a_p$, n.
3. Set the surface inclination: $A_{N1}$, $A_{N2}$.
4. Calculate the effective diameter in horizontal plane.
5. Create the transformed circle considering the inclination of the surface.
6. Find the two tangent points (1, 2) when the slope of the tangent line is equal to the feed direction ($A_f$).

7. Find the parallel line to the tangent line with a distance equal to the width of cut.
8. Find the intersect between the transformed circle and the parallel line (1', 1", 2', 2")
9. Calculate the distance between the tangent points and the tool center.
10. Calculate the distance between the tool center and the intersecting points.
11. Output Working diameters: $D_{eff}$ and current $v_c$

## 5.3 The effect of the depth of cut and the width of cut.

The cutting diameter is contingent upon the tool diameter, surface inclination, and depth of cut ($a_p$). Their impact was explored through simulations. Initially, the influence of the tool diameter, depth of cut, and width of cut was demonstrated for a specific surface position and feed direction. The values of these cutting and tool parameters were selected according to industrial norms to illustrate the individual effect of each parameter.

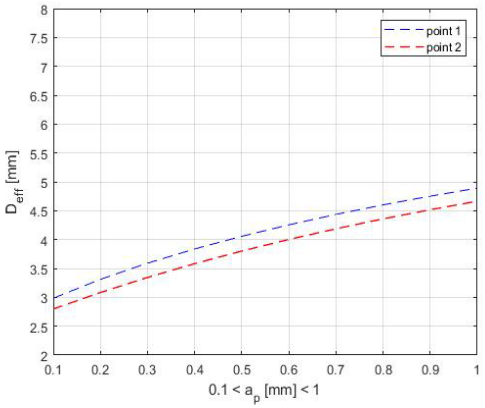


*a) Tool diameter $D_c$ = 6mm*

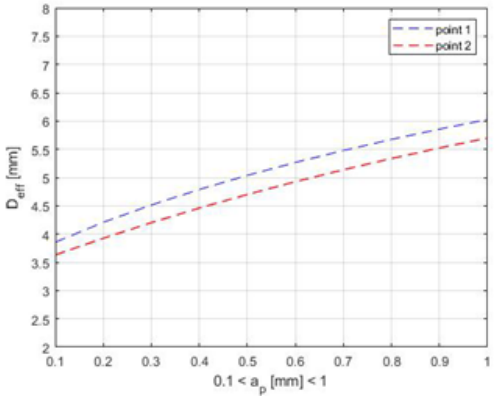


*b) Tool diameter $D_c$ = 8mm*

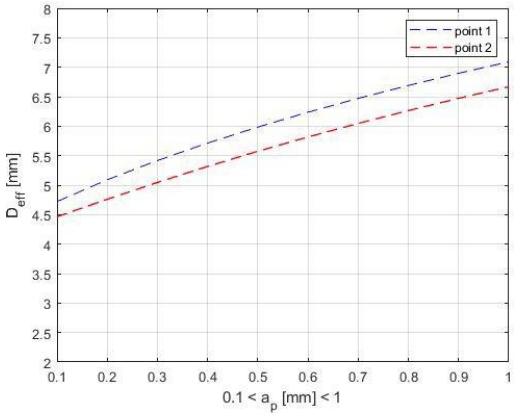


*c) Tool diameter $D_c$ = 10 mm*

*Figure 5-6: The effective diameter in the function of depth of cut.*

The depth of cut, or axial depth of cut ($a_p$), signifies the extent to which the tool penetrates the workpiece along the z-axis. Consequently, defining a greater depth of cut enhances the material removal performed by the tool. This is evident in Figure 5-6, where $A_{N1}$=35°, $A_{N2}$=25° and $A_f$=30°. As the depth of cut increases, so does the working diameter. When milling is conducted from bottom to top, the working diameter is larger, the disparity depending on the surface inclination. The figure illustrates the impact of depth of cut on the working diameter, using various tool diameters (6, 8, and 10 mm). At $a_p$ = 0.1 mm, the tool operates with half its diameter.

Figure 5-7 demonstrates how changes in the width of cut ($a_e$) affect the working diameter in the context of up milling and down milling, employing different tool diameters (6, 8, and 10 mm) when $a_p$ = 1 mm at cutting point.

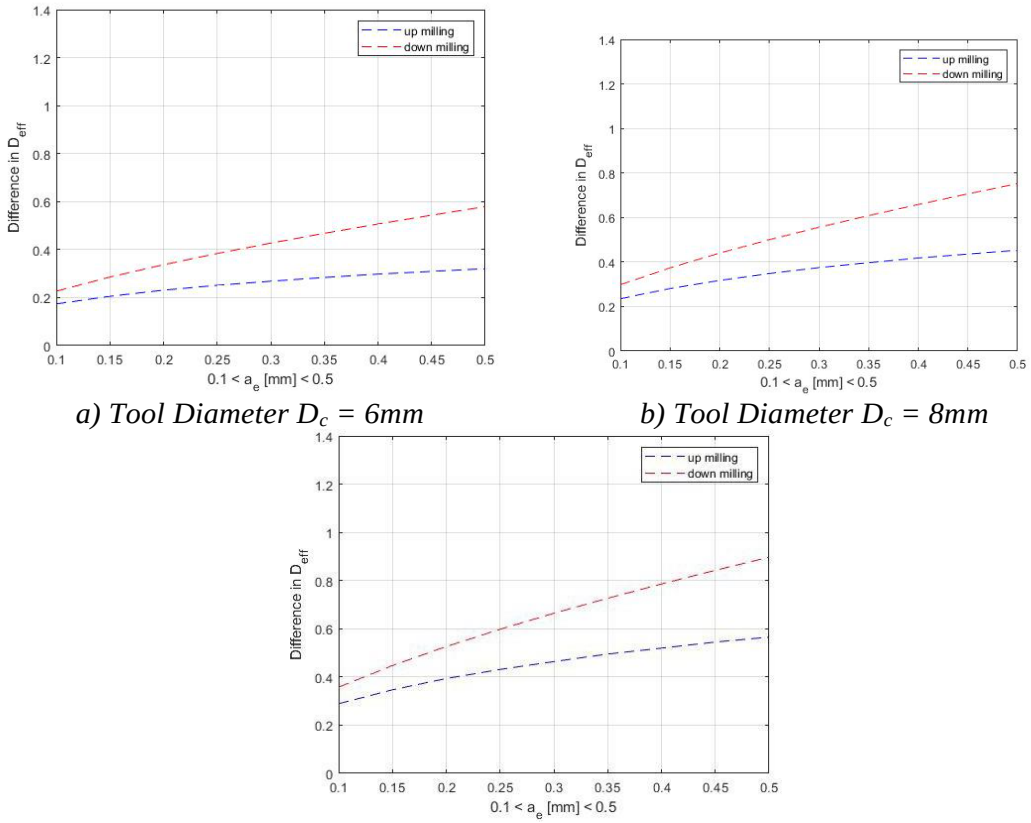


*a) Tool Diameter $D_c$ = 6mm*

*b) Tool Diameter $D_c$ = 8mm*

*c) Tool Diameter $D_c$ = 10mm*

*Figure 5-7: The change of the working diameter during chip removal.*

As depicted in Figure 5-7, the variations in working diameter exhibit similar ranges despite employing different tool diameters. This outcome is anticipated since increasing the nominal diameter of the tool augments the working diameter but does not influence the magnitude of change in the working diameter for the same tool. This change is linked to the cutting parameters such as depth and width of cut, as discussed earlier, as well as the surface inclination, which will be elaborated upon in the subsequent section.

## 5.4 The effect of the feed direction

The working diameter is also impacted by the feed direction. Therefore, in addition to considering the tool diameter, depth of cut, width of cut, and surface inclination, the feed direction must also be taken into account. Figure 5-8 illustrates the alteration in the working diameter resulting from variations in the feed direction, with the following parameters: $D_c$ = 10 mm; $A_{N1}$ = 35°; $A_{N2}$ = 25°; $a_p$ = 1 mm; $a_e$ = 1 mm.

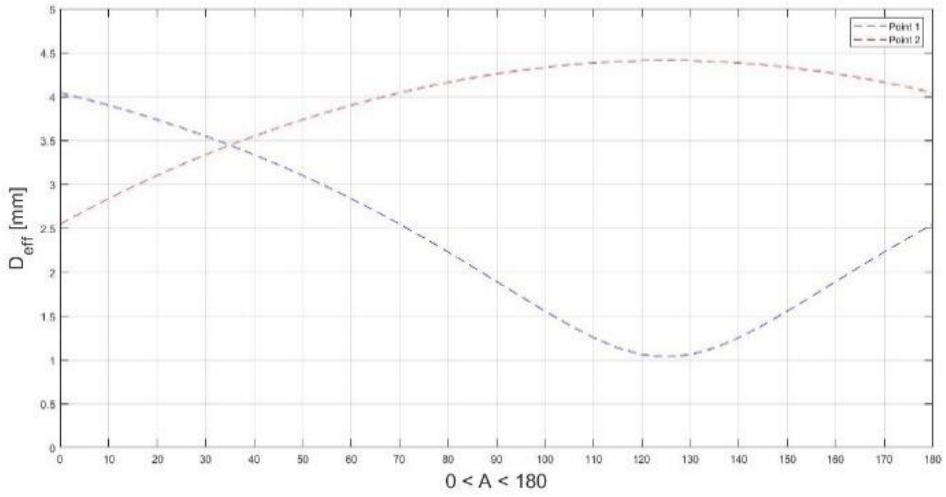


*Figure 5-8: The effective diameter as a function of the feed direction ($a_p$=1 mm).*

The working diameter undergoes significant variations with changes in milling direction. At point 2, this change falls within the range of 2.5 to 4.5 mm, while at point 1, it fluctuates between 1 to 4 mm. Interestingly, the working diameter at point 1 with $A_f$ = 180° matches the working diameter at point 2 with $A_f$ = 0°. When the feed direction angle exceeds 180°, points 1 and 2 are switched. In this simulation, the width of cut does not play a role.

With a depth of cut of 0.3 mm, which is a realistic value for machining, the overall character of the curves remains consistent, albeit with lower values. The effective diameter ranges from 0.5 to 3.5 mm in this scenario.

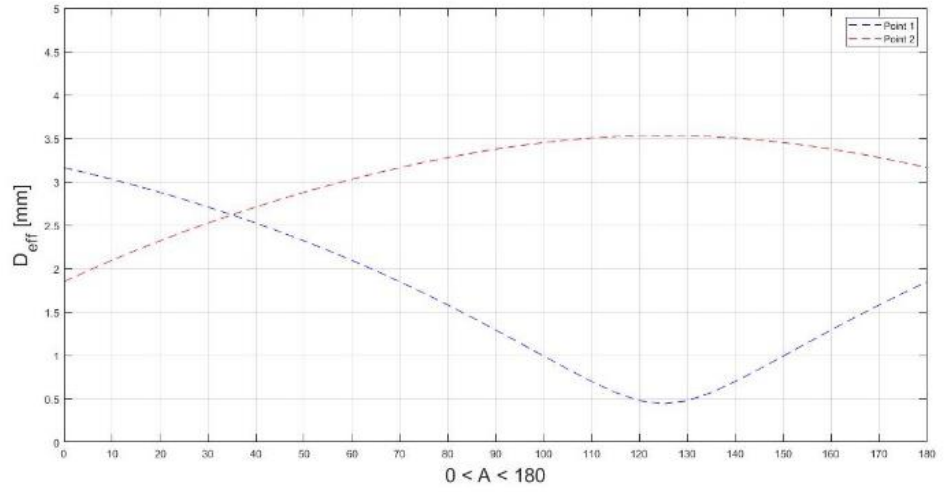


*Figure 5-9: The effective diameter as a function of the feed direction ($a_p$=0.3 mm).*

Figure 5-8 and Figure 5-9 highlight the critical role of selecting the appropriate feed direction to minimize fluctuations in the working diameter. This visualization can be generated for any point on a surface, allowing for the selection of the optimal feed direction based on the working diameter criterion.

## 5.5 The effect of the surface inclination

As mentioned earlier, the working diameter undergoes variations during the milling process due to changes in the surface inclination ($A_{N1}$, $A_{N2}$). In this case study, we examine the effect of surface inclination and its impact on the cutting speed. Throughout the simulation, the tool diameter remained constant at 10 mm, with a nominal cutting speed of $v_c$ = 120 m/min and a spindle speed of n = 3820 1/min.

In Figure 5-10, the fluctuation of the working diameter of the ball-end mill is depicted when the depth of cut is set to 1 mm, and the feed direction is $A_f$ = 30°. It's evident that the surface inclination exerts a significant influence on the working diameter, resulting in substantial changes from one point to another. The changing of the surface normal vector ($A_{N1}$, $A_{N2}$) means changing the character of the surface. In Figure 5-10 a), the working diameter is calculated between the center of the tool and point 1 on the transformed circle, whereas, in Figure 5-10 b), it is calculated between the center of the tool and point 2 on the transformed circle. The lowest value is 0.055 mm at $A_{N1}$ = 120°, $A_{N2}$ = -37.5° in the case of points 1, and $A_{N1}$ = 120°, $A_{N2}$ = 37.5° in the case of point 2. The highest diameter is 4.950 mm at $A_{N1}$ = 120°, $A_{N2}$ = 45° in the case of point 1, and $A_{N1}$ = 120°, $A_{N2}$ = - 45° in the case of point 2. The minimum and maximum values of the $D_{eff\_1}$ and $D_{eff\_2}$ are the same, the role of point 1 and 2 changes by the changing of $A_{N1}$ and $A_{N2}$, and the two diagrams are symmetrical.

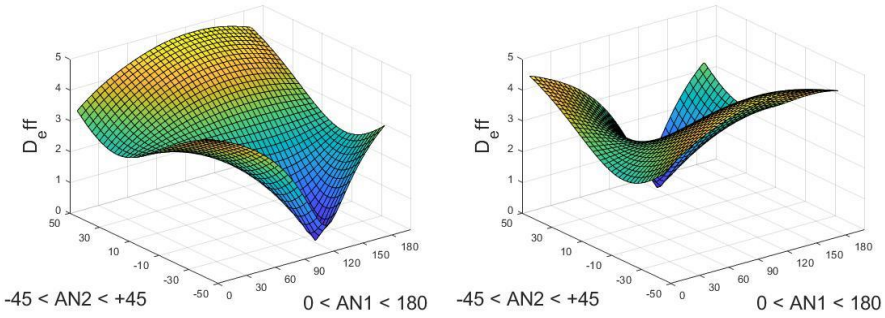


*a) At cutting point 1* *b) At cutting point 2*

*Figure 5-10: The change of the effective diameter as a function of the surface inclination ($A_f$ = 30°)*

Figure 5-11 demonstrates the variations in cutting speed resulting from changes in surface inclination. The actual cutting speed at each point is determined by the effective diameter, calculated using the formula:

$$v_c = \frac{D_{eff} * n * \pi}{1000} \qquad (5\text{-}6)$$

Certainly, the positions with the highest and lowest cutting speeds align with those of the minimum and maximum values of the working diameter, resembling the trends observed in the $D_{eff}$ diagrams. For instance, at point 1, the highest speed of 59.4 mm/min occurs at $A_{N1}$ = 120◦, $A_{N2}$ = 45° and the lowest speed of 0.66 mm/min is recorded at $A_{N1}$ = 120°, $A_{N2}$ = -37.5°, Similarly, for point 2, the highest and lowest speeds are attained at $A_{N1}$ = 120°, $A_{N2}$ = -45° and at $A_{N1}$ = 120°, $A_{N2}$ = 37.5°, respectively.

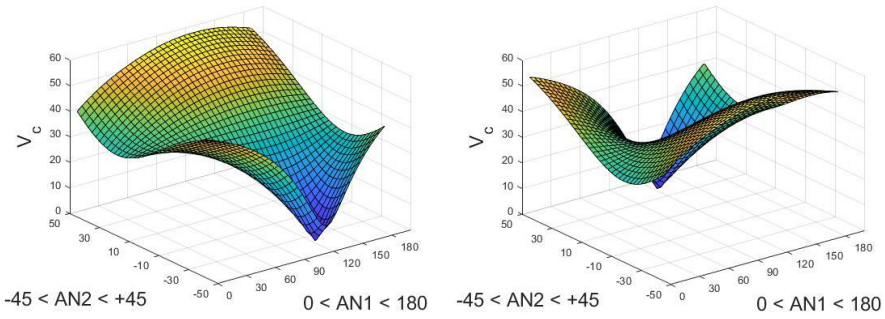


*a) At cutting point 1* *b) At cutting point 2*

*Figure 5-11: The change of the cutting speed as a function of the surface inclination ($A_f$ = 30°)*

When the depth of cut is reduced to 0.3 mm, resulting in a smaller working diameter, the surface's characteristics remain similar to those observed previously, and both the point 1 and point 2 surfaces exhibit symmetry. Table 5-1 presents the data obtained from these simulations.

*Table 5-1: The data of the simulation.*

| **$A_f$ [°]** | **30** | | **60** | |
|---|---|---|---|---|
| **Cutting point** | **1** | **2** | **1** | **2** |
| $D_{eff}$ min [mm] | 0.005 | 0.005 | 0.005 | 0.005 |
| $v_c$ min [m/min] | 0.06 | 0.06 | 0.06 | 0.06 |
| $A_{N1}$ [°] | 120 | 120 | 150 | 150 |
| $A_{N2}$ [°] | -20 | 20 | -20 | 20 |
| $D_{eff}$ max [mm] | 4.530 | 4.530 | 4.530 | 4.530 |
| $v_c$ max [m/min] | 54.36 | 54.36 | 54.36 | 54.36 |
| $A_{N1}$ [°] | 120 | 120 | 150 | 150 |
| $A_{N2}$ [°] | 45 | -45 | 45 | -45 |

In this simulation, two different feed directions were employed: $A_f$ = 30° and $A_f$ = 60°. Figure 5-12 illustrates the change in working diameter. The minimum working diameter is recorded at 0.005 mm, and the maximum at 4.530 mm, both smaller than those observed with $a_p$ = 1 mm. While the minimum and maximum values remain consistent across both investigated cases, their respective locations differ. The surface of the diagram is shifted along $A_{N1}$ by 30°. Additionally, the cutting speed changes proportionally with the working diameter, ranging from 0.05 to 54.5 m/min.

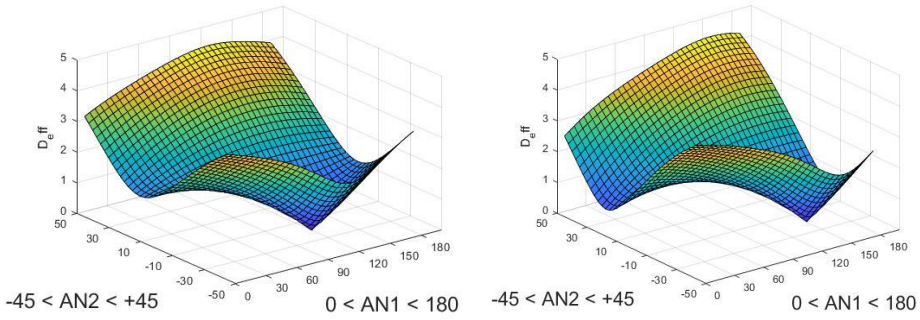


*a) $A_f$ = 30°* *b) $A_f$ = 60°*

*Figure 5-12: Working diameter at point 1, $a_p$=0.3 mm.*

When comparing the actual cutting speed to the nominal cutting speed, the impact of surface inclination becomes evident. The highest actual cutting speed reaches half of the nominal cutting speed, while at certain points, the speed decreases significantly, nearing zero. This variation in cutting speed directly influences the surface roughness and quality, highlighting the importance of considering surface inclination in machining processes.

The Figure 5-13 shows additional examples for the changing of the working diameter of the ball end milling cutter and the cutting speed in case of different surface inclination and feed direction. As shown, the feed direction shifts the data, the result surface is the same, but the position is different.

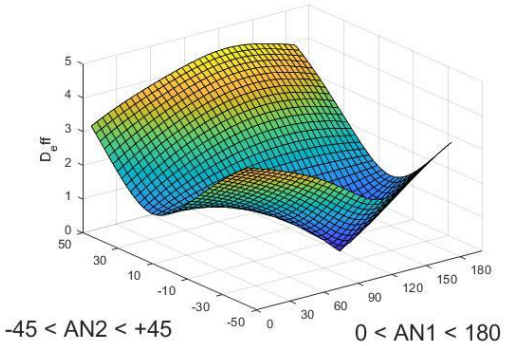


*a) Working diameter at cutting point 1*
$a_p = 0.3$ mm $A_f = 30°$

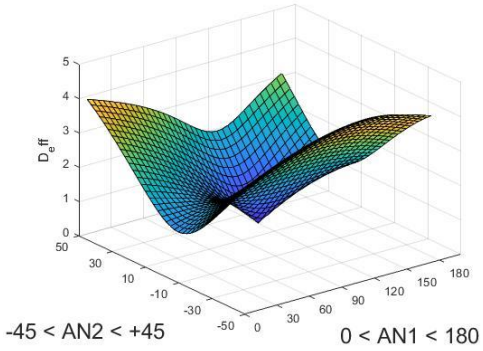


*b) Working diameter at cutting point 2*
$a_p = 0.3$ mm $A_f = 30°$

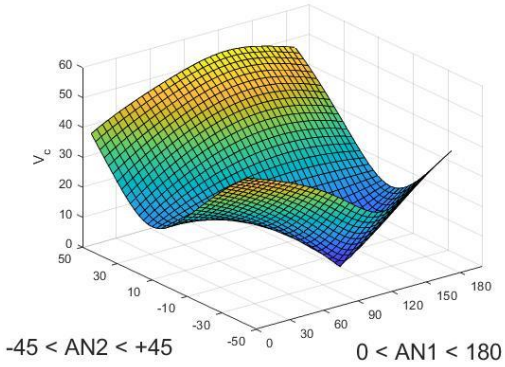


*c) Cutting speed at cutting point 1*
$a_p = 0.3$ mm $A_f = 30°$

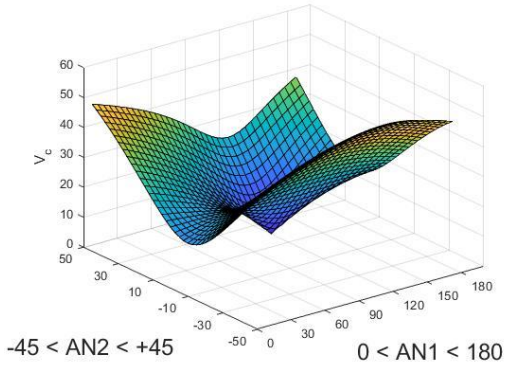


*d) Cutting speed at cutting point 2*
$a_p = 0.3$ mm $A_f = 30°$

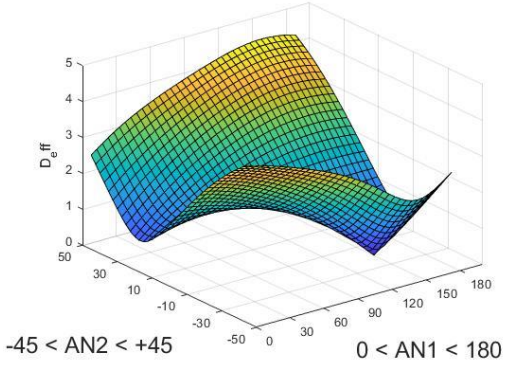


*e) Working diameter at cutting point 1*
$a_p = 0.3$ mm $A_f = 60°$

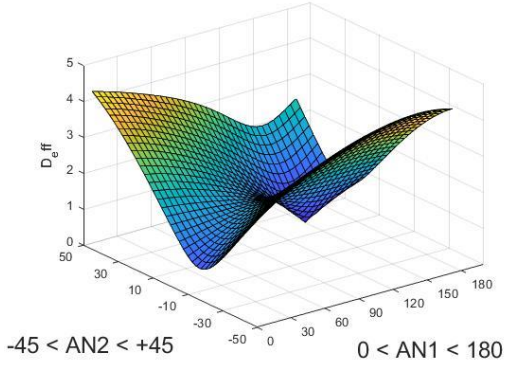


*f) Working diameter at cutting point 2*
$a_p = 0.3$ mm $A_f = 60°$

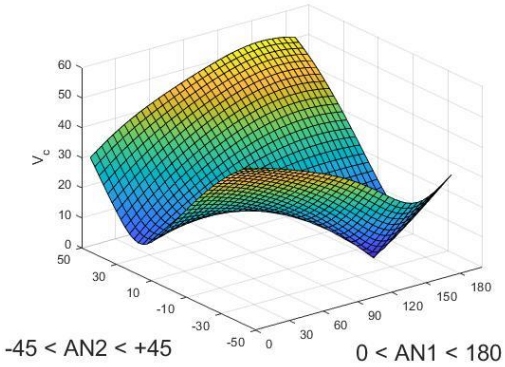


*g) Cutting speed at cutting point 1*
*$a_p$ = 0.3 mm $A_f$ = 60°*

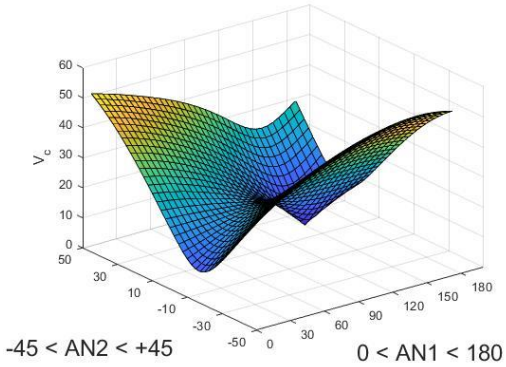


*h) Cutting speed at cutting point 2*
*$a_p$ = 0.3 mm $A_f$ = 60°*

*Figure 5-13: Cutting speed and working diameter at different cases.*

## 5.6 Conclusion

This chapter delves into the dynamic changes of the working diameter of a ball-end milling cutter, examining how alterations in surface inclination and feed direction influence the uniformity of the machined surface. Additionally, it explores the influence of depth and width of cut on the working diameter with the goal of devising an optimization algorithm to enhance surface quality for milled free-form surfaces by controlling the working diameter of the milling cutter.

A simulation model was constructed to compute the working diameter in a general setting. The results of this simulation, conducted using Matlab, were presented. By leveraging the geometric method proposed by Mikó and Zentay [77] adjustments were made to facilitate easier implementation within the Matlab environment. This simulation application allowed for a more comprehensive investigation of each parameter. The steps undertaken in implementing the simulation model are outlined as follows:

The intersection circle formed by the milling cutter and the surface is initially defined in the horizontal plane to establish the theoretical effective diameter.

- Considering the surface inclination at the contact point, the intersection circle can be transformed accordingly.
- The effective diameter at each point is represented by the distance between the center of the milling cutter and a point on the transformed circle.
- Two points on the transformed circle, corresponding to the cutting points, are determined by parallel tangent lines aligned with the feed direction.
- Additionally, the width of cut designates two points on the transformed circle, signifying the start or end of the chip removal process.

The findings shed light on how cutting parameters affect the effective diameter and offer a clear understanding of how feed direction and surface inclination influence both the effective diameter and cutting speed. Employing a relatively high depth of cut enhances the effective diameter, promoting greater tool engagement with the workpiece, albeit at the expense of increased cutting tool load. Conversely, widening the cut augments the variation in effective diameter across the chip removal section, underscoring the importance of considering this parameter to mitigate fluctuations in working diameter.

The impact of the feed direction and surface inclination is demonstrated. However, while nothing can be done related to the surface inclination, the feed direction is the parameter that

can be chosen carefully to achieve a constant working diameter. The change in the working diameter leads to a change in the real cutting speed, which will affect the changing of the surface roughness of the milled surface. Therefore, as a solution, the milling speed should be controlled and adjusted at each point to keep the cutting speed at the same value. During the optimization algorithm of the ball-end milling process, the working diameter must be calculated point-by-point. The geometric information and the technological data are determined by the connection of the CAD model of the surface and the NC program.

Building upon of what has been presented in this chapter, the next chapter will emphasize the importance of the working diameter by employing both a regression model and an Artificial Neural Network (ANN) to predict it during milling operations with a ball-end cutter. This approach will take into account several influencing factors, including the tool diameter, depth of cut, feed direction, and surface inclination, thus offering a more dynamic and accurate estimation method.

# 6 Regression analysis and neural network model of working diameter of ball-end mill

## 6.1 Objective

This chapter aims to underscore the importance of the working diameter by employing both a regression model and an Artificial Neural Network (ANN) to predict it during milling operations with a ball-end cutter. The effective (working) diameter is contingent upon several factors including the tool diameter (D), depth of cut ($a_p$), feed direction ($A_f$), and surface inclination, described by the angular position of the surface normal vector ($A_{N1}$, $A_{N2}$). Notably, $A_{N1}$ can be eliminated if the feed direction is treated as a relative parameter, indicating the feed direction to the $A_{N1}$ angle. In the analysis, this relative feed direction is applied.

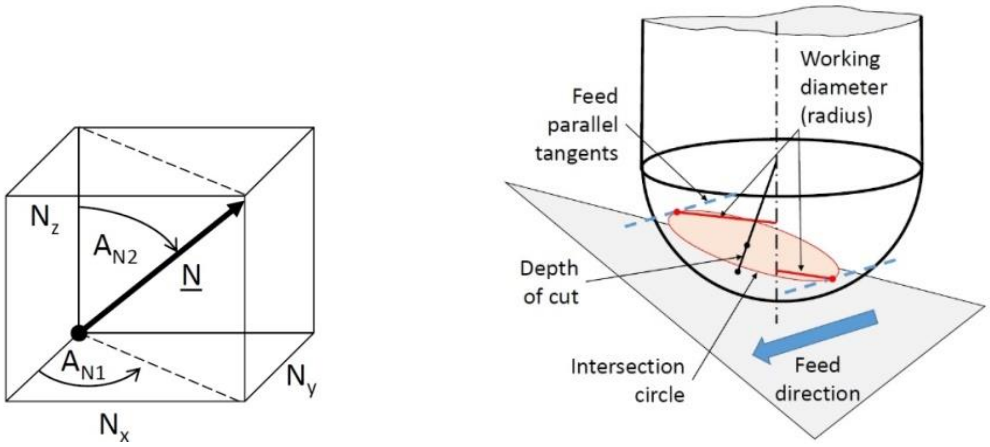


*Figure 6-1: Orientation of the surface normal vector and the interpretation of the tool working diameter.*

## 6.2 Method

For deeper analyses of effective diameter, it is essential to establish a mathematical model that describes effective diameter concerning cutting parameters. Two different methods were compared, regression modeling and the artificial neural network.

The base of the analysis is the set of data, which was generated by the geometry-based algorithm.

The tool diameter and the depth of cut were varied in 4 levels, the surface inclination, and the relative feed direction in 13 levels, as the Table 6-1 shows. The full factorial plan was used, because of the fast and easy calculation of the working diameter, so 2704 data were generated (4 x 4 x 13 x 13 = 2704).

*Table 6-1 Input parameters*

| **Parameter** | **Values** | | | |
|---|---|---|---|---|
| D | 6 | 8 | 10 | 12 |
| $a_p$ | 0.15 | 0.25 | 0.35 | 0.45 |

| | | | | | | | | | | | | | |
|---|---|---|---|---|---|---|---|---|---|---|---|---|---|
| $A_{N2}$ | 40 | 30 | 20 | 15 | 10 | 5 | 1 | -5 | -10 | -15 | -20 | -30 | -40 |
| $A_f$ | 89 | 74 | 61 | 44 | 31 | 14 | 1 | -14 | -31 | -44 | -61 | -74 | -89 |

The statistical analysis of the data and the regression analysis were performed by MiniTab v14 and Excel. The neural network model was created by Matlab.

The regression model and the ANN model were compared based on statistical parameters. The coefficient of determination (R2) is the percentage of variation in the response that the model explains. The R2 is between 0 and 1, the higher R2 value indicates the better model.

$$R^2 = 1 - \left(\frac{\sum_{i=1}^{n}(x_i - \hat{x_i})^2}{\sum_{i=1}^{n}(x_i - \bar{x})^2}\right) \quad (6\text{-}1)$$

Where:

$x_i$: original (measured) value
$\hat{x_i}$: estimated value
$\bar{x}$: mean value of $x_i$
$n$: number of data

Root means square error (RMSE) measures the accuracy of the regression model also. The RMSE is the root square of the average value of the square of the difference of the original and estimated values.

$$RMSE = \sqrt{\frac{1}{n} \cdot \sum_{i=1}^{n}(x_i - \hat{x_i})^2} \quad (6\text{-}2)$$

Mean absolute percentage error (MAPE) means the average of the absolute value of the relative difference of the original and estimated values.

$$MAPE = \frac{1}{n} \cdot \sum_{i=1}^{n}\left|\frac{x_i - \hat{x_i}}{x_i}\right| \quad (6\text{-}3)$$

## 6.3 Results

### 6.3.1 The regression model:

The main effects plot shows the importance of each input parameter on the output parameter. The graphs show the mean values for each factor level connected by line. The surface inclination ($A_{N2}$) has the largest effect on the working diameter as the Figure 6-2 shows. In the case of the shallow section, this effect is smaller, but at the steep region, the working diameter is larger, and the relationship is not linear. The diameter of the tool and the depth of cut have increasing and linear effect on the working diameter. The smallest effect can be seen in the case of the feed direction.

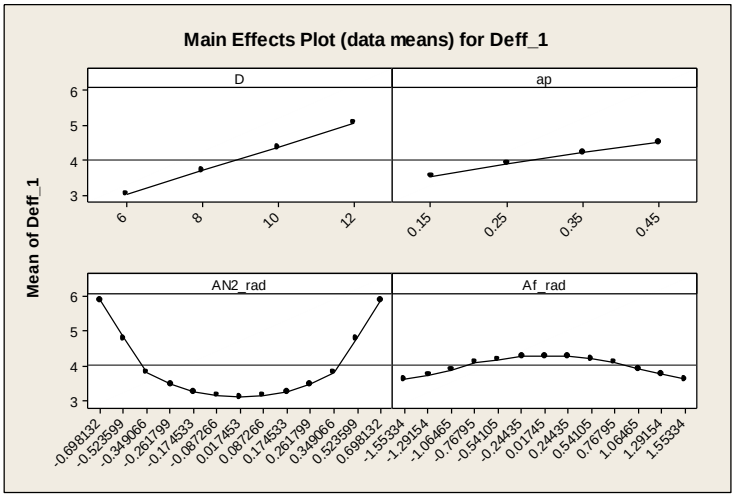


*Figure 6-2: The main effects plot.*

The Figure 6-3 shows how the relationship between one factor and the continuous response depends on the value of the second factor. This plot displays the average of one factor level on the x-axis, and a separate row for each level of another factor. If the lines of the diagram are parallel, there is no interaction between the factors, if the lines are not parallel, an interaction occurs and then in this case, the multiplication of the factors must also be included in the model.

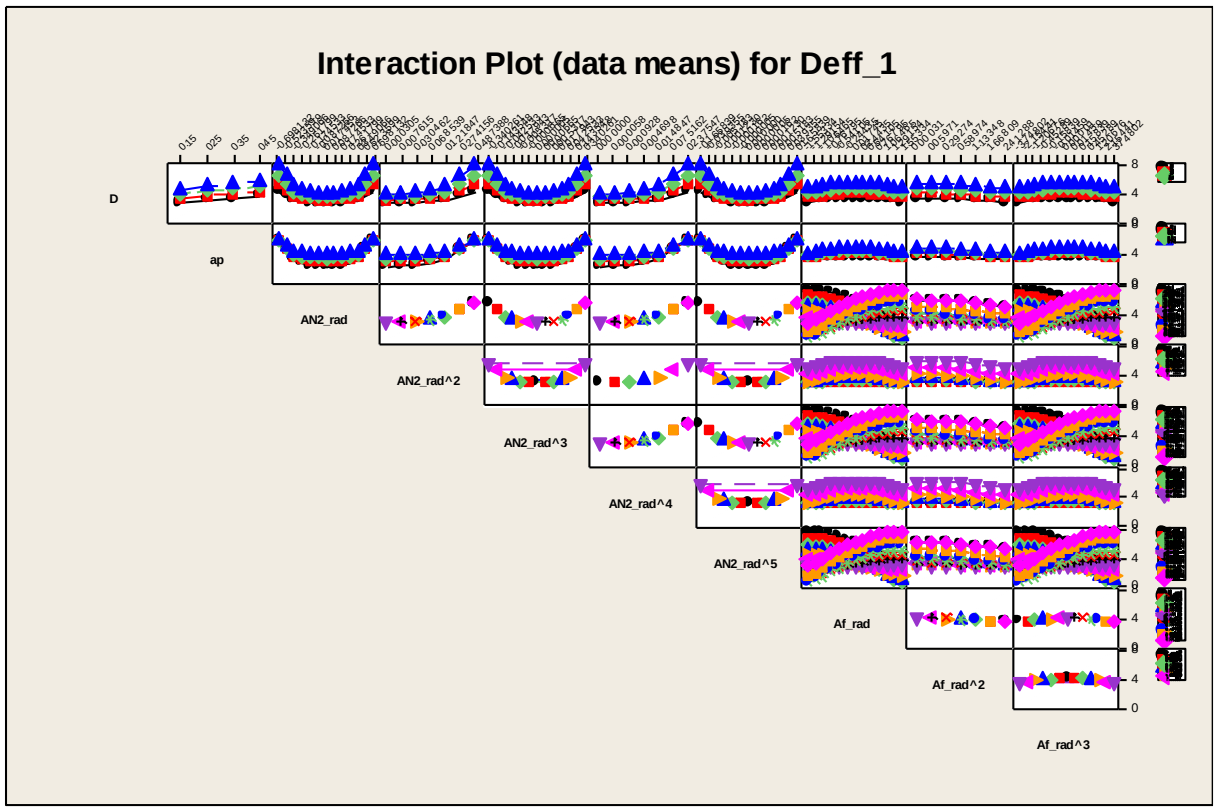


*Figure 6-3: The interaction plot*

Based on the Main effects plot, the Interaction plot and iterations, the following equation was defined (marked as r1 model):

$$D_{eff} = C + c_1 \cdot D + c_2 \cdot a_p + c_3 \cdot {AN_2}^2 + c_4 \cdot {AN_2}^4 + c_5 \cdot {A_f}^2 + c_6 \cdot AN_2 \cdot A_f + c_7 \cdot AN_2 \cdot {A_f}^3 + c_8 \cdot {AN_2}^3 \cdot A_f + c_9 \cdot {AN_2}^3 \cdot {A_f}^3 + c_{10} \cdot {AN_2}^5 \cdot A_f + c_{11} \cdot {AN_2}^5 \cdot {A_f}^5 \quad (6\text{-}4)$$

The value of the coefficients of the r1 model are the next:

```
Deff_1 = - 0.696 + 0.342 D + 3.29 ap + 6.55 AN2^2 - 1.61 AN2^4
         - 0.282 Af^2 + 7.78 (AN2xAf) - 0.741 (AN2xAf^3)
         - 19.9 (AN2^3xAf) + 3.46 (AN2^3xAf^3)
         + 18.5 (AN2_rad^5xAf_rad) - 4.36 (AN2_rad^5xAf_rad^3)
```

| Predictor | Coef | SE Coef | T | P |
|---|---|---|---|---|
| Constant | -0.69634 | 0.05688 | -12.24 | 0.000 |
| D | 0.341616 | 0.004844 | 70.52 | 0.000 |
| ap | 3.28969 | 0.09688 | 33.96 | 0.000 |
| AN2^2 | 6.5483 | 0.2513 | 26.05 | 0.000 |
| AN2^4 | -1.6055 | 0.5047 | -3.18 | 0.001 |
| Af^2 | -0.28226 | 0.01303 | -21.67 | 0.000 |
| (AN2 x Af) | 7.7777 | 0.2868 | 27.12 | 0.000 |

```
(AN2 x Af^3)          -0.7411    0.1577      -4.70  0.000
(AN2^3xAf)           -19.900     2.335       -8.52  0.000
(AN2^3xAf^3)           3.456     1.283        2.69  0.007
(AN2^5xAf)            18.542     3.852        4.81  0.000
(AN2^5xAf^3)          -4.363     2.117       -2.06  0.039
S = 0.563235   R-Sq = 91.9%   R-Sq(adj) = 91.8%
```

In the case of the two values of the working diameter the regression model is the same, only the values of the coefficients are different.

In order to improve the accuracy of the regression model, four separated equations were created for the different tool diameter (marked as r2 model). The structure of the regression equation was the same. Table 6-2 shows the values of the coefficients.

The accuracy of the regression is improved, the values of the R2adj parameter are up to 95% in every case. However, the result is better, but instead of one equation four equation should be used, and the tool diameter is not taken into account. The suggested solution is to use a linear function of the tool diameter instead of constant coefficients. As the Table 6-2 presents, the coefficients show linear regression in function of the tool diameter (D) with good accuracy, so the separated equations could be unified in the next form:

$$D_{eff} = \sum f_i(D) \cdot C_i \tag{6-5}$$

*Table 6-2: The coefficients in r2 regression model for $D_{eff\_1}$*

| $C_i$ | D=6 | D=8 | D=10 | D=12 | $f_i(D)$ | R-Sq(adj) |
|---|---|---|---|---|---|---|
| C | 1.88518 | 2.23381 | 2.54862 | 2.84520 | 0.1597D+0.9405 | 99.87 |
| $a_p$ | 2.89268 | 3.20990 | 3.44240 | 3.61380 | 0.1198D+2.2116 | 98.17 |
| $A_{N2}^2$ | 2.63420 | 4.98210 | 7.76160 | 10.81520 | 1.3661D-5.7468 | 99.66 |
| $A_{N2}^4$ | 0.61640 | -0.46070 | -2.20430 | -4.37350 | -0.8357D+5.9155 | 97.89 |
| $A_f^2$ | -0.21801 | -0.26535 | -0.30474 | -0.34095 | -0.0204D-0.0986 | 99.62 |
| $A_{N2}$ x $A_f$ | 5.25760 | 6.98720 | 8.64290 | 10.22300 | 0.8276D+0.3293 | 99.96 |
| $A_{N2}$ x $A_f^3$ | -0.65230 | -0.71700 | -0.77200 | -0.82310 | -0.0284D-0.4858 | 99.70 |
| $A_{N2}^3$ x $A_f$ | -12.00600 | -17.17600 | -22.48100 | -27.93600 | -2.6548D+3.9930 | 99.99 |
| $A_{N2}^3$ x $A_f^3$ | 3.66500 | 3.62800 | 3.36800 | 3.16300 | -0.0883D+4.2507 | 93.46 |
| $A_{N2}^5$ x $A_f$ | 10.40900 | 15.60000 | 21.10500 | 27.05200 | 2.7717D-6.4038 | 99.91 |
| $A_{N2}^5$ x $A_f^3$ | -4.83400 | -4.73600 | -4.17300 | -3.70900 | 0.1969D-6.1351 | 94.01 |
| R-Sq(adj) | 95.7 | 96.3 | 96.8 | 97.1 | | |

### 6.3.2 The artificial neural network (ANN) model

Another way of mathematical modeling is the use of Artificial Neural Networks (ANN). The ANN is a multi-layered structure comprising one or more hidden layers positioned between the input and output layers. Each of these layers consists of numerous processing units called neurons, which are interconnected with adjustable weights. Within the network, every neuron receives input from all the neurons in the previous layer [142], and this is calculated as follows:

$$net_j = \sum_{j=0}^{N} w_{ij} * x_i \tag{6-6}$$

Whereas:

- netj represents the total or net input, N is the number of inputs to the $j^{th}$ neuron in the hidden layer.
- $w_{ij}$ is the weight of the connection from the $i^{th}$ neuron in the forward layer to the $j^{th}$ neuron in the hidden layer
- $x_i$ is the input from the $i^{th}$ neuron in the preceding layer.

Each neuron in the network generates its output ($out_j$) by processing the net input through an activation (transfer) function. In this study, the logistic sigmoid transfer function (also known as the sigmoid or logistic function) was used for hidden layers and a linear transfer function for the output layer in a regression task [143].

The logistic sigmoid transfer function, often used in artificial neural networks, is defined by the following formula:

$$f(x) = \frac{1}{1+e^{-x}} \tag{6-7}$$

- x represents the input to the function.
- e is the base of the natural logarithm (Euler's number), approximately equal to 2.71828.

The logistic sigmoid function maps any real-valued number x to an output in the range (0, 1), making it suitable for problems that require modeling probabilities or introducing non-linearity in the neural network.

The sigmoid function's characteristic S-shaped curve is typically used in the hidden layers of feedforward neural networks for tasks like classification. It helps transform the weighted sum of inputs into a range where the network can learn complex relationships between features.

For this study, we have designed an optimal neural network architecture using the Matlab Neural Network Toolbox. In the first case (marked as a1 model) the network architecture comprises one input layer, one hidden layer, and one output layer. 10 neurons in the hidden layer, while the input layer has four neurons, and the output layer contains two neurons during both the training and testing phases. The input layer neurons correspond to the tool diameter (D), the depth of cut ($a_p$), the surface inclination ($A_{N2}$) and the relative feed direction ($A_f$), while the output layer represents effective diameter ($D_{eff}\_1$ and $D_{eff}\_2$). While in the second case (marked as a2 model) the network has two hidden layers, 10 neurons in the first hidden layer, and 5 in the second.

In Figure 6-4 and Figure 6-5, it is evident that more than 1000 samples, in addition to approximately 400 validation and test samples, exhibit an error of 0.01034 in the context of a neural network configuration with a single hidden layer.

In contrast, when employing a model with two hidden layers, approximately 1200 samples and 400 validation and test samples display a notably reduced error of 0.001365. This implies that by increasing the complexity of the model, achieved by adding more neurons and hidden layers, the model's performance has been enhanced.

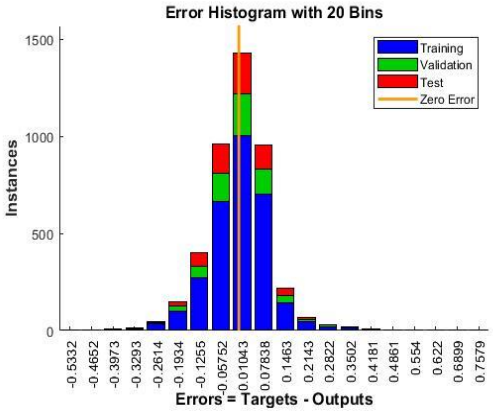


*Figure 6-4: Histogram error in the case of 1 hidden layer.*

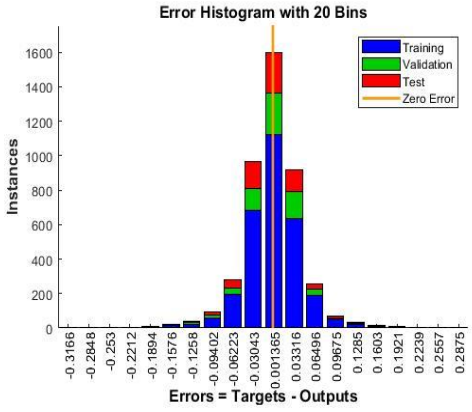


*Figure 6-5: Histogram error in the case of 2 hidden layers.*

The discernible distinctions in accuracy are apparent in Figure 6-6 and Figure 6-7 presented below, where the performance of the two-layer configuration surpasses that of the single-layer arrangement. In the first case, the accuracy for training data stands at 0.99512. In contrast, the second case exhibits superior accuracy with a value of 0.99892. This pattern is similarly reflected in the validation data, where the initial scenario registers an accuracy of 0.99408, while the second case excels with a higher accuracy score of 0.99886. The trend continues in the testing data, with the first case recording an accuracy of 0.9949, while the second case excels further with an accuracy of 0.9989.

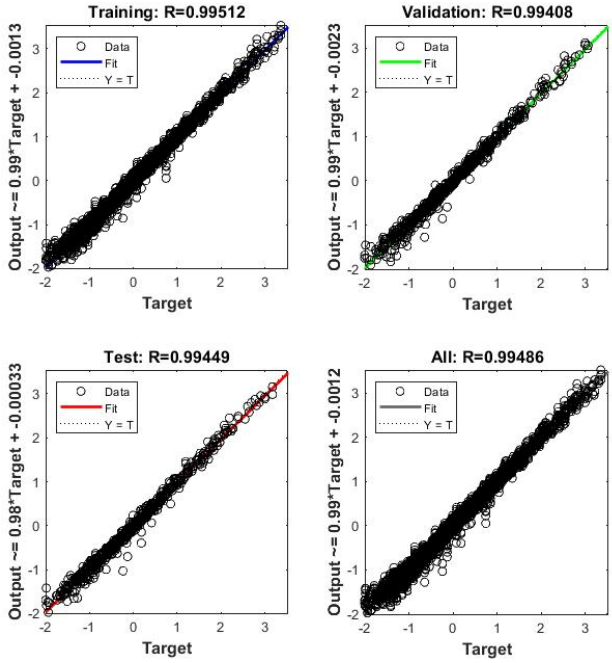


*Figure 6-6: Training, testing and validation data in the case of 1 hidden layer.*

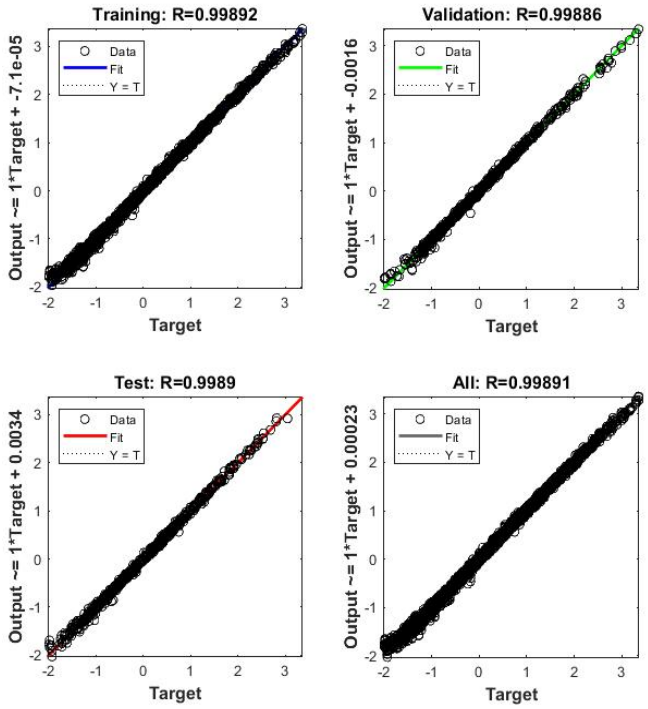


*Figure 6-7: Training, testing and validation data in the case of 2 hidden layers.*

Consequently, when utilizing a neural network architecture featuring two hidden layers, we observe enhanced performance in comparison to the one-layer counterpart. This improvement is particularly evident in the validation results, achieved within a reduced number of training epochs. In case of two hidden layers, the learning process was faster (Figure 6-8 and Figure 6-9).

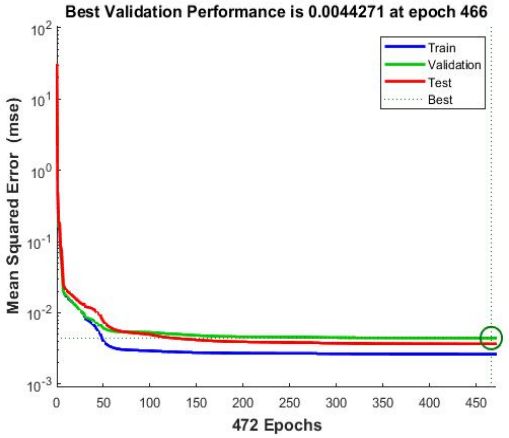


*Figure 6-8:Validation performance in the case of 1 hidden layer (a1).*

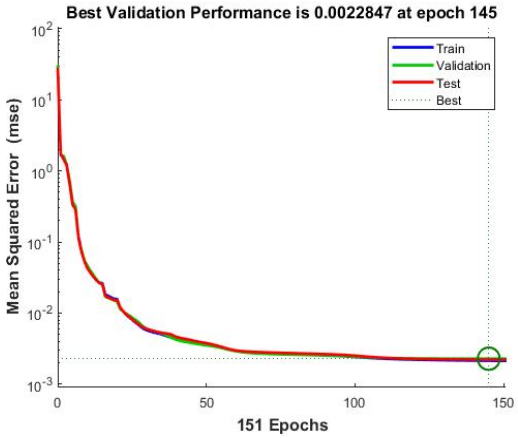


*Figure 6-9:Validation performance in the case of 2 hidden layers (a2).*

### 6.3.3 Comparison of the models

The base of the comparison is the analysis of the error. Figure 6-10 and Figure 6-11 present the calculated and the estimated values of the effective diameter and the distribution of the differences. The data of $D_{eff1}$ is presented only, the results of $D_{eff2}$ shows similar tendencies.

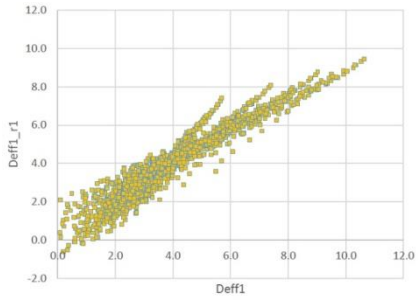


*a) r1*

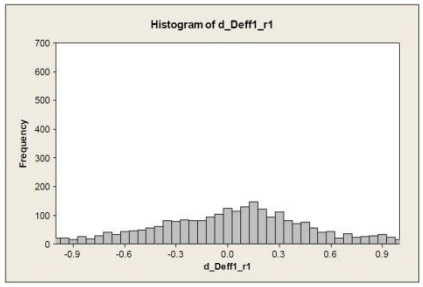


*b) r1*

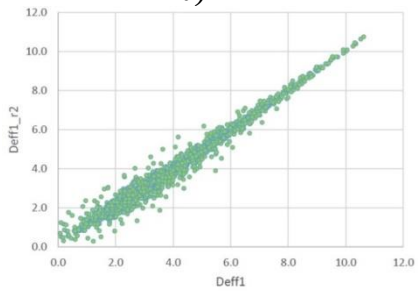


*c) r2*

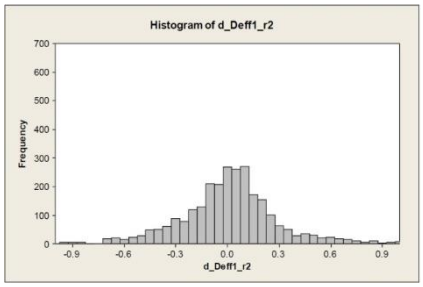


*d) r2*

*Figure 6-10: The calculated and the estimated values of the effective diameter and the distribution of the error of regression models*

In case of r1 model, as shown in Figure 6-10 a) and b), the estimated values have remarkable error. The point clouds follow the ideal line, but the area is too wide. Moreover, some negative values are also included. The inaccuracy of the regression can be seen in the histogram of the differences. The range of the differences is 3.899 mm, and the histogram is flat, the standard deviation is 0.562 mm. Four peaks can be seen at the top region, which correspond to the four different tool diameters.

The r2 regression model shows better accuracy (Figure 6-10 c) and d)). The point cloud is narrower, and the histogram has a higher peak. The range is little bit smaller (3.118 mm), and the standard deviation is 0.329 mm. The larger deviation can be observed under 6 mm.

The artificial neural network models show better performances. The a1 model (Figure 6-11 a) and b)) has narrow point cloud, but some outlier data can be observed. In the case of small working diameter, the error is larger; a small curve can be seen in the diagram. The histogram of the error shows normal distribution, the range is 2.601 mm, and the standard deviation is 0.194 mm.

The a2 neural model shows the best accuracy. The point cloud in Figure 6-11 c) is very thin, but under 1 mm a similar pattern can be observed in case of a1 model. The histogram is narrow and tall, the range is 1.113 mm, and the standard deviation is 0.080 mm only. The a2 ANN model results in the smallest error in all cases.

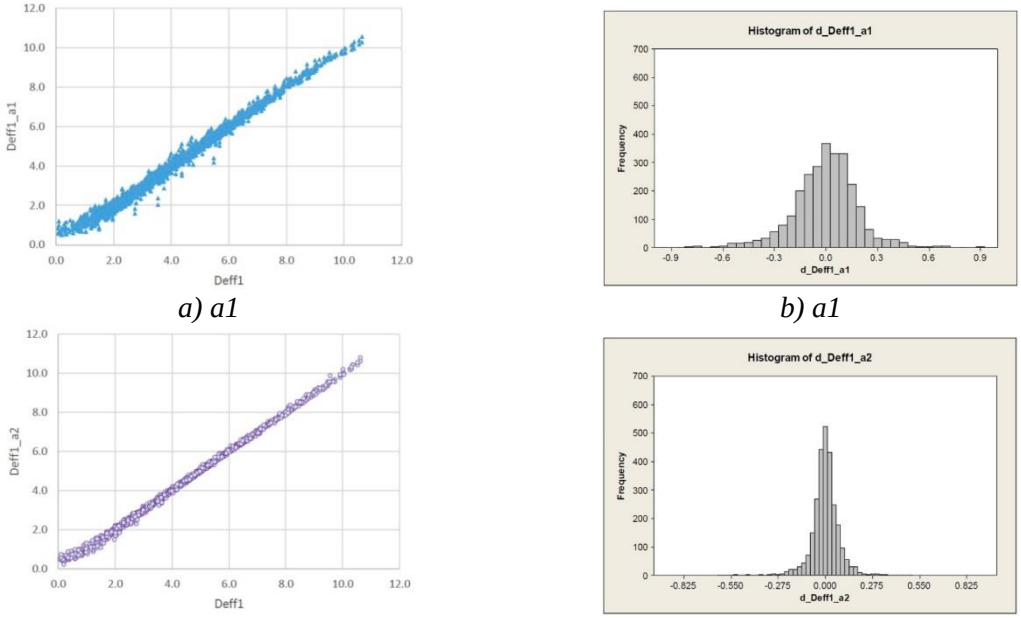


*a) a1* *b) a1*

*c) a2* *d) a2*

*Figure 6-11: The calculated and the estimated values of the effective diameter and the distribution of the error of ANN models.*

The improving accuracy of the different methods is shown in the previously presented diagrams, but the statistic parameters can describe it more precisely (Table 6-3 and Figure 6-12). The range of the error values indicates the inaccuracy of the methods, but it means just a rough characterization. The standard deviation can describe the nature of the histogram, the distribution of the values of the error. In the case of the presented models, the range and the standard deviation had smaller and smaller values.

The coefficient of determination ($R^2$) is 91.9% in the case of the r1 model, which is a good regression generally, but as the previous analysis shown, the error can be large in some cases. In the case of artificial neural network model, the $R^2$ values are 99.0% and 99.8%, which means a very good regression for both cases.

The standard deviation, the relative mean square error (RMSE) and the mean absolute percentage error (MAPE) changed in parallel (Figure 6-12). The relative values of the standard deviation, the RMSE and the MAPE changed in similar way. In the case of the r2, the values are 58% - 58% - 59%; in the case of the a1: 35% - 37% - 42% and in case of the a2: 14% - 14% and 19% comparing to the r1 model. Although these parameters measure the different aspects of the deviation, their values changed in parallel.

*Table 6-3: The values of the statistical parameters of the differences*

| Model | r1 | r2 | a1 | a2 |
|---|---|---|---|---|
| Range | 3.899 | 3.118 | 2.601 | 1.113 |
| St.Dev | 0.562 | 0.329 | 0.194 | 0.080 |
| $R^2$ | 0.919 | 0.972 | 0.990 | 0.998 |
| RMSE | 0.562 | 0.329 | 0.194 | 0.080 |
| MAPE | 0.194 | 0.114 | 0.082 | 0.038 |

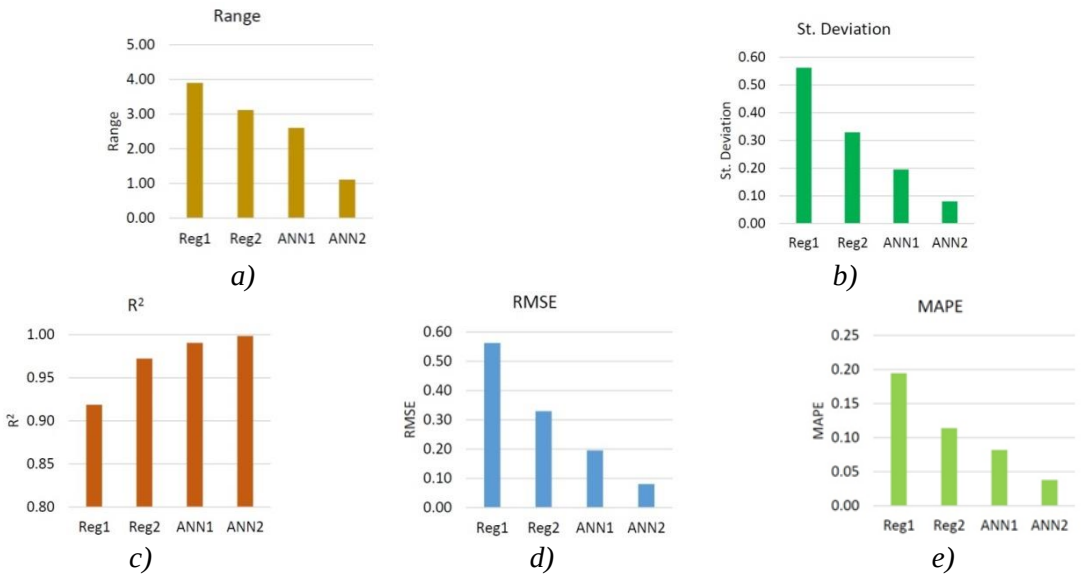


*Figure 6-12: The range, the standard deviation, the $R^2$, the RMSE and the MAPE values of the differences.*

## 6.4 Conclusions

In the case of ball-end milling of free-form surfaces, the working diameter changes parallel with the surface inclination. The working diameter depends on the tool diameter, the depth of cut, the surface inclination and the feed direction. In this chapter two types of regression models and two artificial neural network models were compared based on the statistical parameters of the error values. The base of the investigation was a set of data, which contains 2704 variations of input parameters. The performance of the models was compared by the range of the error, the standard deviation, the coefficient of determination (R2), the relative mean square error (RMSE) and the mean absolute percentage error (MAPE).

The results can be summarized as follow:

- Introducing the relative feed direction allows us to reduce the number of input parameters due to the periodic nature of the geometric model. Using the relative feed direction in the regression equation for the working diameter has proven beneficial. To create an effective regression model, we need to multiply the first, third, and fifth powers of the surface inclination and the relative feed direction.
- A separate regression model based on the tool diameter improves accuracy, as the coefficients can be calculated according to the tool diameter. This method helps create a unified regression model, making the modeling process simpler and consistent for different tool diameters.
- Integrating Artificial Neural Networks (ANNs) into prediction models aims to use their learning abilities to create accurate and reliable models for predicting the working diameter in ball-end milling. This approach ensures precision and dependability in real-world milling by using relevant cutting parameters. The ANN-based model performed the best, with the standard deviation, RMSE, and MAPE values all improving consistently.
- The working diameter of the ball-end milling cutter is crucial for the adaptive modification of cutting parameters to maintain a constant cutting speed and feed rate. During the tool path planning for finishing milling of a free-form surface, the current value of the working diameter can be utilized to minimize its variations. These

applications require a fast and accurate calculation method to effectively adjust the cutting parameters in real-time.

The exploration of working diameter concludes with this chapter. Subsequent chapters unveil suggested algorithms aimed at tackling the thesis problem. First, the next chapter delves into the algorithm for speed control, accompanied by a Matlab simulation. This is followed by an experimental study highlighting the enhancements in surface roughness attained through the implementation of this algorithm. Following that, an algorithm optimizing tool path planning, along with its simulation, is presented.

# 7 Controlling the spindle speed when milling free-form surfaces using ball-end cutter

## 7.1 Objective

The chapter introduces a post-processing algorithm designed to control spindle speed independently of CAD/CAM systems by modifying the NC code. It outlines the general concept, algorithm steps, and data sources. Geometric surface data can be extracted from an STL file, while tool path data can be retrieved from an APT format process file. These standard file formats ensure CAD/CAM system independence.

The chapter illustrates the algorithm's functionality through an example, demonstrating its effectiveness in modifying NC code to control spindle speed independently of the CAD/CAM system.

## 7.2 Spindle speed control concept

To calculate the spindle speed and ensure effective machining, the working diameter of the ball-end milling cutter needs to be determined point-by-point. This calculation relies on the geometric model applied [77], necessitating the description of the free-form surface, the cutting tool path, and cutting data.

To calculate the working diameter, both surface data and tool path data are essential. The STL file format is commonly used for describing free-form surfaces, while the APT language is utilized for describing tool paths. Briefly, the STL file format represents objects in CAD systems by defining the surface geometry using a mesh of triangles. On the other hand, the APT language provides a means to describe tool paths, including tool movements, feed rates, and spindle speeds.

By utilizing the STL file format for surface geometry and the APT language for tool path data, the algorithm can calculate the angle of surface inclination at each cutting point, facilitating the determination of the working diameter of the ball-end milling cutter. This comprehensive approach ensures accurate spindle speed control and effective machining, independent of the CAD/CAM system used.

### 7.2.1 STL file format

For describing the geometric data of a free-form surface, various file formats are available, ranging from native CAD system formats to neutral, standard formats. For the specific application discussed, where only the orientation of surface normal vectors at different positions is needed, different tessellation-based formats were examined.

CAD systems support numerous file formats, including STL, AMF, and OBJ. Each format contains data such as texture, color, and geometry about the object to be manufactured. However, the data encoded in these formats differs, with variations from file to file. For instance, while an STL file solely describes surface geometry without color or texture representation, AMF and OBJ can store information about texture and color [144], [145].

Furthermore, the difference between these formats extends beyond the type of information stored; it also pertains to how the surface is represented. For instance, STL employs planar triangles to describe the object, while AMF includes curved triangles alongside planar ones. OBJ offers even more advanced representation options, such as free-form surfaces and curves [144], [145].

Given that surface geometry is the primary concern in the application and considering the widespread use of the STL format, it has been chosen for this specific purpose. Its simplicity and focus on surface geometry make it suitable for the task at hand.

STL stands for *Standard Triangle Language / Standard Tessellation Language / Stereolithography*. This widely used file format is supported by many CAD systems [146]. It comprises a list of triangle facet data, with each facet containing facet normal and three vertices (see Figure 7-1). Both the facet normal and vertices are represented in the three-dimensional Cartesian coordinate system. Below is an example of an STL file. The file begins with a "*SOLID*" name, then a list of facets, and ends with an "*ENDSOLID*" followed by the name of the solid. The STL file includes only surface geometry data, while other information such as material, color, and texture are not stored in this file format.

```
solid
…
facet normal ni nj nk
    outer loop
        vertex v1x v1y v1z
        vertex v2x v2y v2z
        vertex v3x v3y v3z
    endloop
endfacet
…
endsolid
```

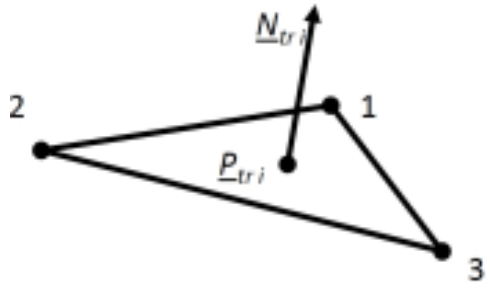


*Figure 7-1: Definition of a triangle in the STL language.*

### 7.2.2 APT file

To acquire information about the tool path, the CNC code of the milling process needs to be parsed. Presently, G-code serves as the most prevalent method for instructing numerical control machines. Although G-code programming is standardized, different control manufacturers use different variations or add their own code. Furthermore, obtaining the precise location of the cutter directly from the G-code proves challenging for the requirements of this application [147]. Hence, the APT language is preferred for retrieving the tool position during the milling process. The Automated Programming Tool (APT) is a high-level computer programming language developed by the Massachusetts Institute of Technology (MIT) in 1958 [148], [149]. It is primarily utilized for automating the generation of programs for NC machines.

In the APT, all tool movement parameters, including contact points, vectors, cutting information, and tool paths, are recorded comprehensively. By analyzing the data stored in the APT program, the corresponding NC code can be generated [150]. This approach facilitates precise extraction of tool path information, aiding in accurate calculation of the working diameter for the milling process. The APT language offers the capability to retrieve the position of the cutter at each point during the milling process. Below is an excerpt from an APT program:

```
$$-> MFGNO / MFG0002
PARTNO / MFG0002
$$-> FEATNO / 13
MACHIN / MILL, 1
$$-> CUTCOM_GEOMETRY_TYPE / OUTPUT_ON_CENTER
UNITS / MM
LOADTL / 37 $$-> D10 R5 FRISA
$$-> CUTTER / 10.000000
$$-> CSYS / 1.0000000000, 0.0000000000, 0.0000000000, -25.0000000000,  $
        0.0000000000, 1.0000000000, 0.0000000000, -25.0000000000,  $
        0.0000000000, 0.0000000000, 1.0000000000, 0.0000000000
SPINDL / RPM, 2000.000000,  CLW
RAPID
FROM / -20.100, 25.249, 30.000
$$-> SETSTART / -20.100, 25.249, 30.000
RAPID
GOTO / -20.100, 25.249, 9.994
FEDRAT / 500.000000,  MMPM
GOTO / -19.975, 25.249, 9.994
GOTO / -18.996, 25.249, 9.990
GOTO / -18.871, 25.249, 9.994
```

In this example, the APT program begins with metadata regarding the part, like the part name (MFG0002), the machine tool ID (MILL, 1), the unit of measure (MM), the tool properties (D10 R5) and the direction of the coordinate system. Comments are marked with $$. The subsequent section contains machining information, including commands like SPINDL for spindle speed control. RAPID denotes rapid motion, while FEDRAT initiates working motion. The GOTO command specifies the x, y, and z coordinates of the endpoint for linear motion. This explicit marking of tool positions in the APT program is advantageous, particularly for distinguishing between cutting motions and rapid motions. As the location of the cutter is crucial only during contact with the workpiece, the algorithm can effectively differentiate between cutting and rapid motions. Furthermore, additional process data such as cutting tool diameter, nominal cutting speed, feed speed, depth of cut, width of cut, and milling direction can be derived from the APT file or provided as user inputs. This comprehensive approach ensures accurate calculation and control of the machining process.

### 7.2.3 The algorithm description

To achieve the objective of this study, an algorithm has been developed to control and adjust the spindle speed point-by-point to maintain a constant cutting speed. Figure 7-2 illustrates the functioning of this algorithm in calculating the spindle speed required at each point of the surface.

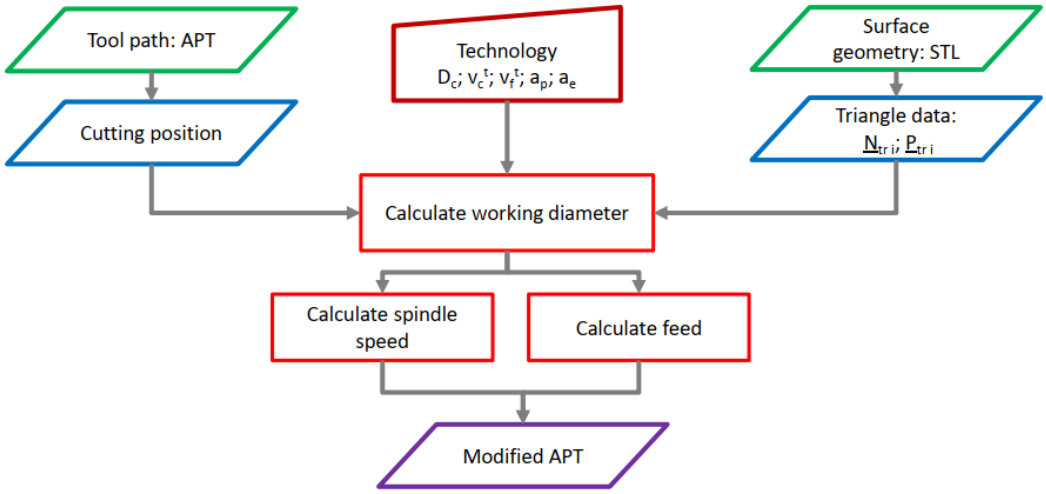


*Figure 7-2: Diagram illustrates the algorithm.*

The algorithm initiates by reading the STL file (Figure 7-3), which is generated by the CAD system to describe the workpiece surface. It parses the file and computes the incentre point for each triangle by averaging the coordinates of its three corners. Subsequently, the algorithm stores a list of incentre points (Ptr i) of the triangles along with their corresponding normal vectors (Ntr i). To enhance efficiency, triangles that do not belong to the machined surface are eliminated. This elimination process involves examining the normal vector of each triangle. If the normal vector is parallel to the coordinate axes, except for the Z+ direction, the triangle is disregarded.

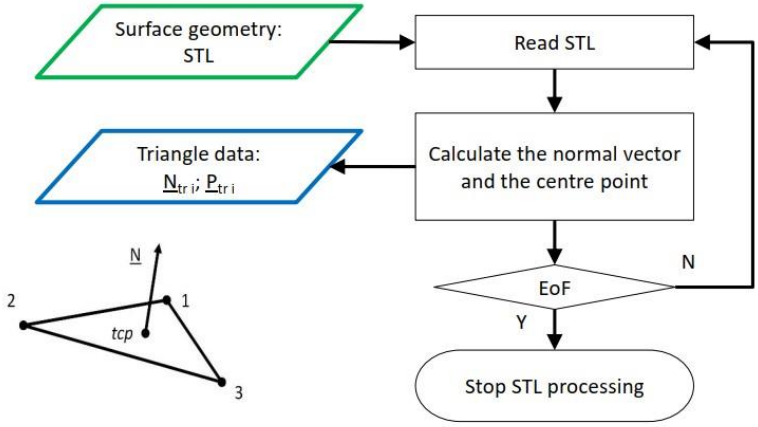


*Figure 7-3:Processing of the STL file.*

The algorithm proceeds by reading the APT file (Figure 7-4). This file includes coordinates of tool locations, although these points do not precisely represent the actual contact between the tool and the surface. Nonetheless, they serve as useful data for calculations. The disparity between the tool nose point and the actual tool/surface contact point is minimal, particularly for shallow surfaces. In the APT file, machining points are specified following the "FEDRAT" command, while "RAPID" designates points of rapid tool motion. By analyzing these keywords, the algorithm can differentiate between various tool locations and determine the appropriate spindle speed adjustments accordingly.

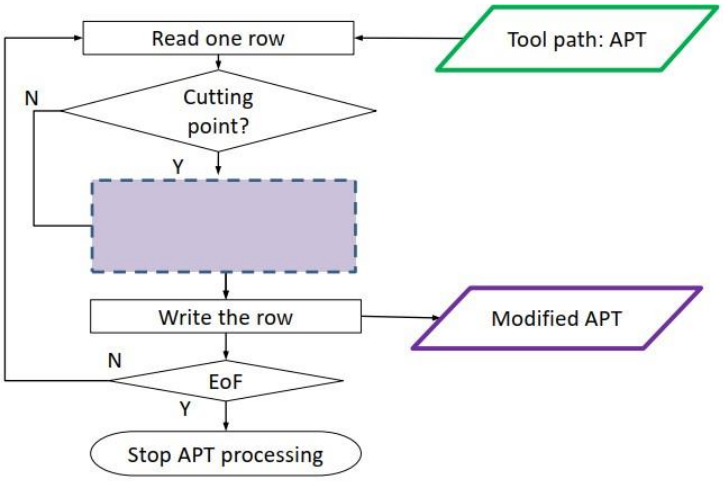


*Figure 7-4: Processing of the APT file.*

The subsequent step involves determining the normal vector at each tool position. This is achieved by connecting the tool position to the corresponding triangle. To accomplish this, the algorithm computes the distance between the tool location and all the incentre points, returning the incentre point with the shortest distance to the tool position. This indicates that the tool is within the triangle associated with that incentre point and shares the same normal vector as the triangle.

It's worth noting that depending on the resolution of the STL file, one triangle may be assigned to multiple tool positions. While this could introduce some error in the calculation of the working diameter, its impact is typically minimal and can be mitigated by increasing the resolution of the surface description.

By determining the normal vector of the surface at each tool position, the surface inclination angles $A_{N1}$ and $A_{N2}$ can be calculated as depicted in Figure 7-5.

$$A_{N1} = arctg(\frac{N_y}{N_x}) \quad (7\text{-}1)$$

$$A_{N2} = \arccos(N_z) \quad (7\text{-}2)$$

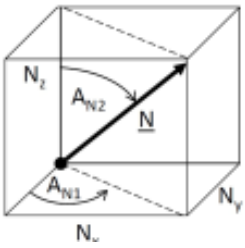


*Figure 7-5: Calculation of the inclination angles (AN1, AN2)*

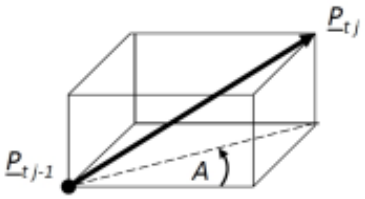


*Figure 7-6: Calculation of the feed direction (Af)*

If the cutter location is known, the feed direction can be calculated as well (Figure 7-6).

$$A = arctg(\frac{P_{y_j} - P_{y_{j-1}}}{P_{x_j} - P_{x_{j-1}}}) \quad (7\text{-}3)$$

The feed direction can be constant, like in the presented example. In this case, there is no need to calculate it point-by-point, it can be input data.

This data is necessary to calculate the working diameter at each tool position, which is an important step to calculate the required spindle speed Figure 7-7. To calculate the working diameter, a geometric model presented by Mikó and Zentay [77] was used. At technology parameters the *t* means the theoretical (nominal) values, and the *o* is the optimized.

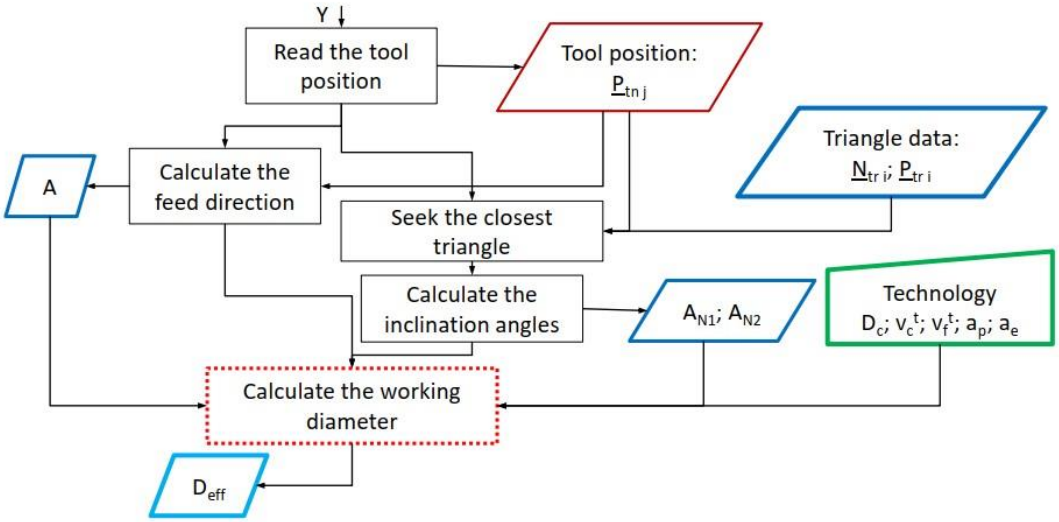


*Figure 7-7: The algorithm segment responsible for computing the working diameter.*

In this model, the working diameter is defined as the distance between the tool center line and an intersection circle. This intersection circle is generated by a plane with the same normal as the current surface point, and the distance is equal to the depth of cut. The transformation required to calculate the working diameter is determined by the inclination angles $A_{N1}$ and $A_{N2}$. The direction of the working diameter is defined by the feed direction.

In this approach, the geometry of the machined part of the free-form surface is locally approximated. This method aligns well with the use of the STL description of the surface geometry, which allows for efficient handling of complex surface geometries by approximating them with triangles.

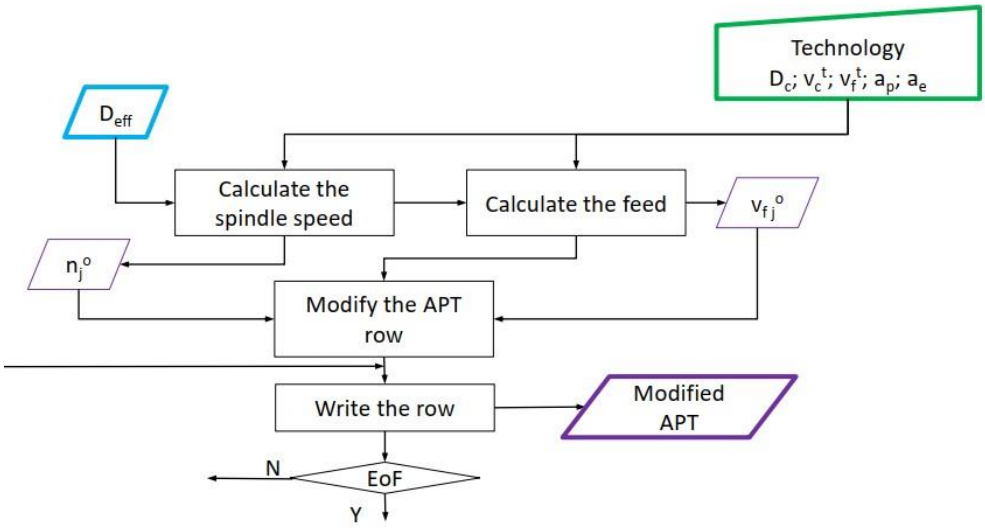


*Figure 7-8: Updating the APT file.*

In order to ensure the constant cutting speed, the spindle speed has to be calculated point-by-point. The required spindle speed at each point is calculated by the following formula:

$$n = \frac{1000 * v_c}{D_{eff} * \pi} [1/\text{min}] \quad (7\text{-}4)$$

For constant cutting condition, the feed rate must be modified parallel with the spindle speed:

$$v_f = f_z * z * n [\text{mm/min}] \quad (7\text{-}5)$$

## 7.3 The results and the simulation

A simulation was conducted to investigate the variation in cutting speed and the corresponding adjustments in spindle speed necessary to maintain a constant cutting speed, utilizing the presented algorithm. Table 7-1 outlines the cutting parameters, which were utilized in this simulation. Additionally, Figure 7-9 depicts a simulation of the down milling process within CAM software.

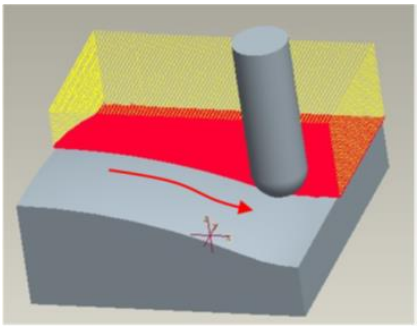

*Figure 7-9: Down milling process in CAM simulation.*

*Table 7-1: Cutting parameters.*

| | | |
|---|---|---|
| Cutting speed | vc [m/min] | 63 |
| Spindle speed | n [rpm] | 2000 |
| Feed per tooth | fz [mm] | 0.125 |
| Feed rate | vf [mm/min] | 500 |
| Feed direction | A [°] | 0 |
| Depth of cut | ap [mm] | 0.30 |
| Width of cut | ae [mm] | 0.25 |
| Tool diameter | D [mm] | 10.0 |
| Number of teeth | z [-] | 2 |

The STL file describes a workpiece with dimensions of 50x50 mm (Figure 7-10). Meanwhile, the APT file contains instructions for a down milling process. By parsing this file, the algorithm can determine the tool location, as illustrated in Figure 7-11.

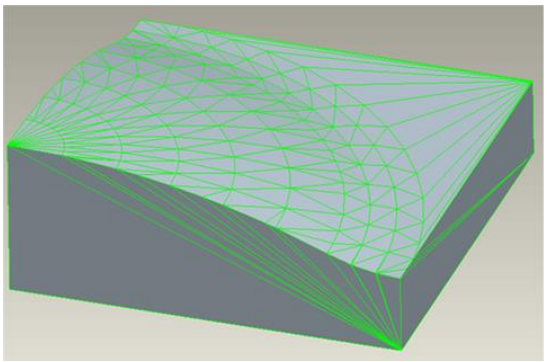

*Figure 7-10: The STL file, representing the workpiece.*

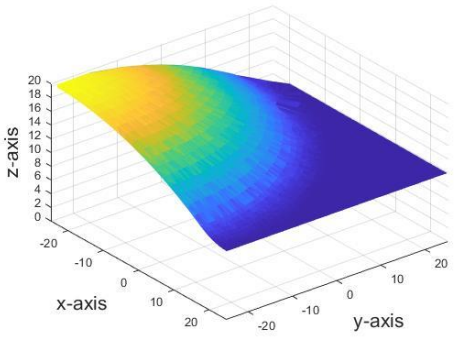


*Figure 7-11: The tool position determined by reading the APT file.*

However, it is important to note that the resolution of the STL file may be lower than the resolution of the tool path description. While this difference in resolution could introduce some errors, it is typically not significant for the spindle speed adjustment process.

Additionally, it is essential to recognize that the coordinates of the tool position differ from those of the surface points because the tool contact point is located at the nose point of the tool.

Therefore, the tool position may not perfectly align with the surface geometry, but this discrepancy is accounted for in the algorithm's calculations.

The working diameter and cutting speed were calculated in the case of feed direction A =0. Figure 7-12 and Figure 7-13 show the change in the working dimeter and cutting speed from point to point along the surface of the workpiece. Notably, these changes occur in parallel.

When the surface normal close to vertical direction (the surface is horizontal), the working diameter is small, resulting in a decrease in cutting speed. As depicted in Figure 7-12, the working diameter drops to the lowest value (about 1.5 mm) when the surface is horizontal, in this section of the workpiece, the axis of the tool is normal on the surface.

Conversely, in the middle section, the diameter of the work increases as the tool engages more deeply into the workpiece. Similarly, the actual cutting speed varies from point to point along the surface, mirroring the changes observed in the working diameter.

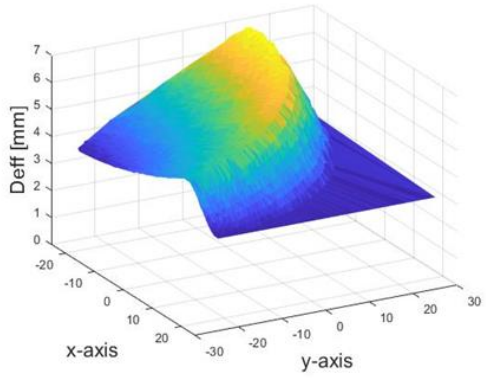


*Figure 7-12: The working diameter*

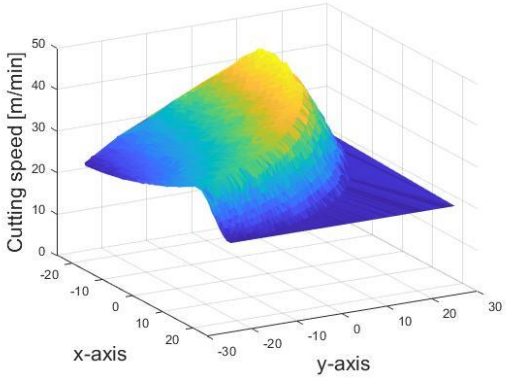


*Figure 7-13: The cutting speed*

Similarly, Figure 7-14 and Figure 7-15 show the working diameter and cutting speed as a function of the surface slope. When $A_{N1} = 0$ and $A_{N2} = 0$, the working diameter is of low value. As the surface slope increases, the working diameter also increases, indicating that more work is being done by the cutter. This relationship holds true for cutting speed as well higher surface slopes correspond to higher cutting speeds.

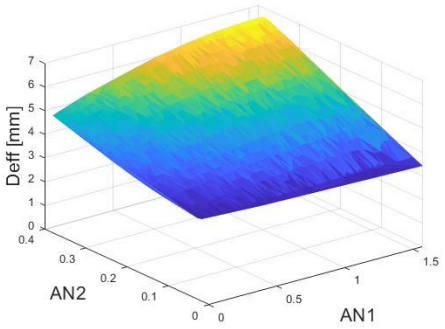


*Figure 7-14: Working diameter versus surface inclination.*

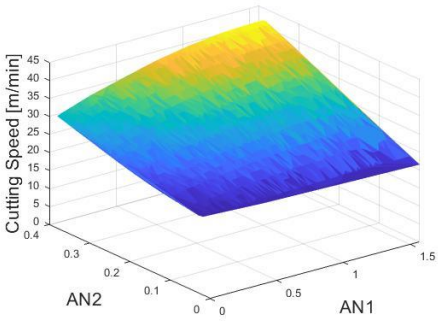


*Figure 7-15: Cutting speed versus surface inclination.*

Although despite the constancy of cutting parameters, including spindle speed, the actual cutting speed fluctuates from point to point during the milling process due to variations in the tool's working diameter, which in turn varies with different surface inclination angles.

Although the nominal cutting speed is set at 63 [m/min], the actual cutting speed varies significantly, ranging from a maximum of 42 [m/min] at certain points to a minimum of about 21 [m/min] at others. To maintain a constant cutting speed, adjustments to both spindle speed and feed rate are necessary. The presented algorithm offers a solution to this challenge by controlling both spindle speed and feed rate. Figure 7-16 and Figure 7-17 illustrate the modified spindle speed and feed rate at each point, ensuring a constant cutting speed of 63 [m/min].

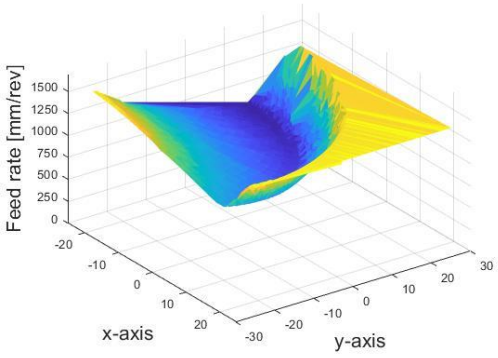


*Figure 7-16: Modified feed rate.*

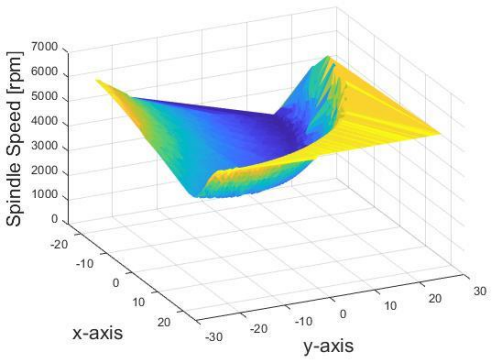


*Figure 7-17: Modified spindle speed.*

At certain points, an increase in spindle speed is necessary to compensate for the decrease in cutting speed resulting from a decrease in the working diameter. The spindle speed required at these points can reach up to 5877 [rpm]. Conversely, the lowest spindle speed required is 3002 [rpm]. Similarly, to maintain a constant cutting speed, the feed rate must also be adjusted. The increase in the required feed rate is directly proportional to the spindle speed. Therefore, both parameters exhibit similar characteristics, with the increase in feed rate reaching 1500 [mm/min], three times greater than the nominal feed rate. The feed rate ranges from 750 to 1469 mm/min.

With the presented algorithm, it becomes possible to fix the cutting speed to a specific value. Figure 7-18 illustrates the theoretical cutting speed as a function of surface slope, demonstrating a constant cutting speed of 63 [m/min] regardless of changes in surface angles. In simulation, a small difference in cutting speed may occur depending on the resolution of the calculation, which is influenced by the density of the tool path points and the STL surface model.

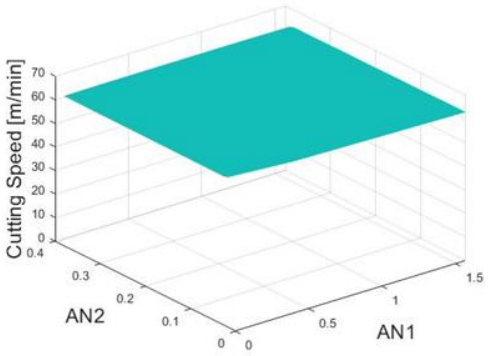


*Figure 7-18: Resulting cutting speed.*

## 7.4 Conclusion

In this chapter, the primary challenge encountered in manufacturing free-form surfaces using a three-axis ball end mill is the variation in the working diameter of the cutter. This variation leads to fluctuations in cutting speed, subsequently affecting cutting parameters and surface quality.

The chapter presents an algorithm designed to address this issue by controlling spindle speed to achieve a constant cutting speed. Unlike other approaches, this algorithm does not require pre-processing and operates independently from any CAD or CAM system. It introduces a novel method for obtaining the normal vector at each surface point by parsing STL format files and APT language NC files, establishing a connection between cutter locations and STL file triangles.

A simulation demonstrates the algorithm's functionality, illustrating changes in working diameter and cutting speed during milling processes due to variations in surface slope angles. Additionally, it showcases how spindle speed and feed rate adjustments ensure a constant cutting speed throughout milling.

The next chapter presents the results obtained from applying the described algorithm. It will include a detailed comparison of the surface quality achieved with adjusted spindle speed versus constant spindle speed. This comparison aims to highlight the effectiveness of the algorithm in enhancing surface finish and overall machining performance.

# 8 The effect of the spindle speed control when milling free-from surfaces

## 8.1 Objective

The primary objective of this chapter is to thoroughly investigate and validate the algorithm introduced in the preceding chapter. Through systematic experimentation and analysis, this study aims to assess the algorithm's effectiveness and reliability. By conducting rigorous validation tests, the chapter seeks to provide robust evidence of the algorithm's capability to optimize machining processes and achieve superior outcomes compared to traditional methods.

This chapter presents results from milling tests conducted on a free-form surface using ball-end milling with five different feed directions. Two test series were executed: one with constant spindle speed and the other with controlled spindle speed. The surface roughness of these parts is then compared to assess the effectiveness of the proposed adaptive spindle speed control method within the context of 3-axis milling.

## 8.2 Materials and methods

The workpiece material used for the present work was C45 (1.0503) medium-carbon unalloyed steel. C45 steel is commonly utilized in the manufacturing of parts with high strength requirements, such as gears, shafts, and piston pins, as well as less stressed components like machined parts, forgings, stampings, bolts, nuts, and pipe joints. It possesses a tensile strength range Rm=650-800 MPa. Table 8-1 presents the chemical composition of C45 steel

*Table 8-1: Chemical composition of C45 steel (analysis in %)*

| C | Si | Mn | P | S | Cr | Mo | Ni |
|---|---|---|---|---|---|---|---|
| 0.42-0.5 | <0.4 | 0.5-0.8 | <0.045 | <0.045 | <0.4 | <0.1 | <0.4 |

The size of the test part was 50x50 mm, it contains a sphere (R=106.25 mm), a toroid (R=25 mm) sections, and a horizontal plane surface (Figure 8-1). The height of the 3D surface is 10 mm.

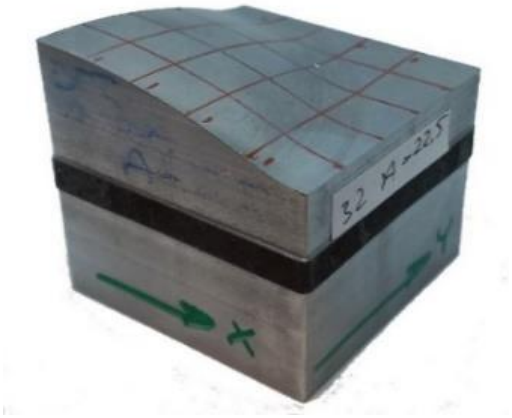

*Figure 8-1: The test part.*

After the milling, the surface roughness was measured by a Mahr-Perten GD130 instrument. The Rz parameter was measured in 25 zones, 3 times on the surface, in

perpendicular direction to the feed and the presented values calculated with the averages of three measures. The value of the cut-off was 0.8 mm, the speed of probe was 0.5 mm/s.

The test parts were machined by a Mazak 410-AII CNC machining center with a YG NC-Mill G9F44100N ball-end milling cutter with 10 mm diameter ($D_c$) and 2 teeth (z). The cutting parameters were the following: nominal cutting speed was $v_c$ = 63 m/min, and the feed per tooth $f_z$ = 0.125 mm. In case of the determining of the cutting parameters, the recommendation of the tool catalogue, the properties of the machine tool and the possible changing and the maximum value of the spindle speed were considered. The depth of cut was $a_p$ = 0.3 mm and the width of cut $a_e$ = 0.25 mm. In order to constant depth of cut, the pre-finishing 3D ball-end milling was performed.

The test surfaces were machined by zig-zag 3D surface milling method with five different feed directions comparing to the x axis. The feed directions were $A_f$ = 0°, 22°, 45°, 67.5°, 90°.

In case of the first test set the constant spindle speed was applied, the spindle speed was n = 2000 1/min, and the feedrate was $v_f$ = 500 mm/min. In the case of the second test set, the spindle speed and the feedrate were modified along the tool path considering the actual cutting diameter.

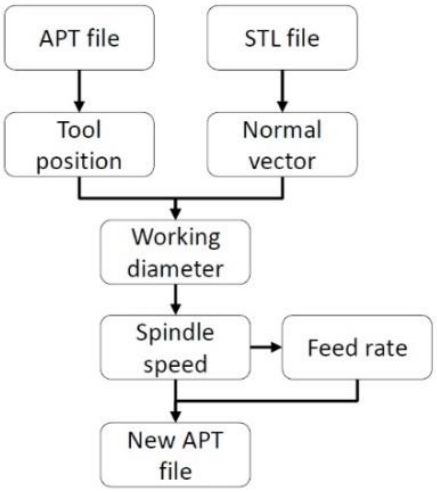


*Figure 8-2: The processing workflow.*

The developed algorithm (which was presented in the previous chapter) changes only the values of the spindle speed and the feedrate, the points of the milling tool path are not changed, so the accuracy of the CNC program is unchanged.

Figure 8-3 shows how the spindle speed changes during the milling process to keep the cutting speed constant. The diagrams show the spindle speed in the case of five different milling feed directions (0°, 22.5°, 45°, 67.5°, 90°).

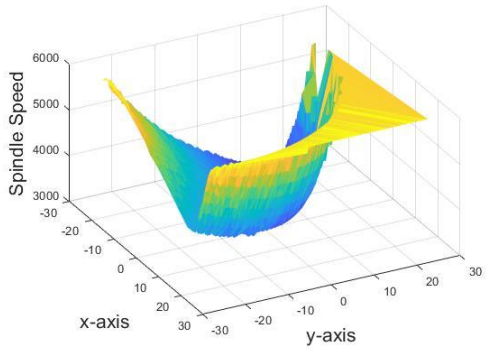


*a) $A_f$ = 0°*

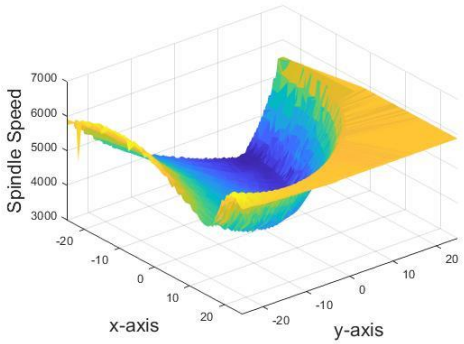


*b) $A_f$ = 22.5°*

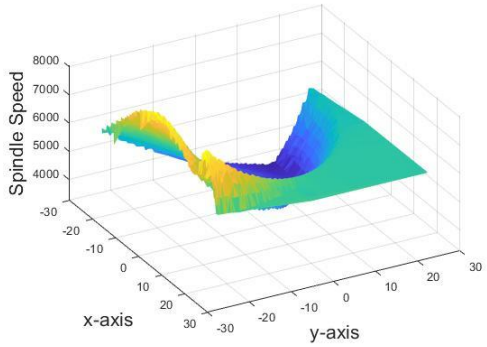


*c) $A_f$ = 45°*

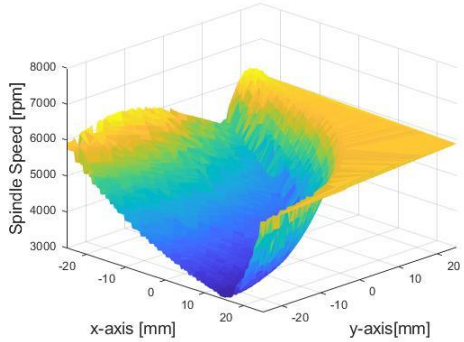


*d) $A_f$ = 67.5°*

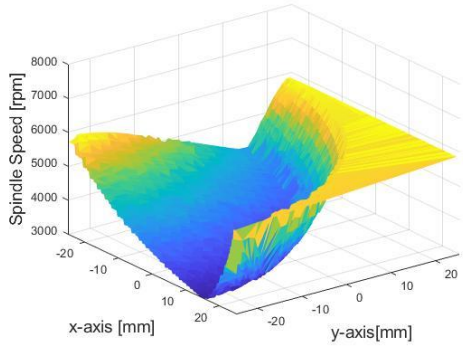


*e) $A_f$ = 90°*

*Figure 8-3: The controlled spindle speed in case of the five feed directions.*

As can see in the above figures, as the surface inclination changes, the effective diameter changes. To make up for the decrease in cutting speed, the spindle speed must be increased. It is evident that the effective diameter and cutting speed decrease to their lowest values at the points where the tool is perpendicular to the surface. In these points, the algorithm calculates the highest speed for the spindle. When the surface inclination changes fast (at the small radius), the spindle speed changes fast also

The minimum and the maximum values of the spindle speed depend on the feed direction. The minimum values are 3002, 3066, 3251, 3062 and 3002 1/min and the maximum values are 5877, 6308, 8066, 6308, 5877 1/min. Because of the symmetric surface (the diagonal plane is a symmetric plane too), the minimum and the maximum values of the spindle speed show symmetricity also.

The spindle speed changed point by point, and however the diagrams look similar (Figure 8-3), because of the different length and the different number of the points of the toolpaths, there are some differences. These differences can be presented by the integral value of the

spindle speed by path (the area under the function of spindle speed). This integral characterizes the dynamic load of the spindle.

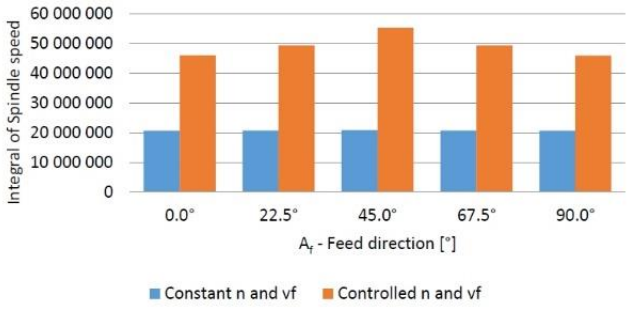


*Figure 8-4: The integral of the spindle speed by the path.*

As Figure 8-4 shows, in case of constant spindle speed, the value of the integral is virtually the same. The maximum difference in tool path length is 100 mm ($A_f$ = 0°: 10286 mm and $A_f$ = 45°: 10383 mm), so it has a little effect on it. In case of the controlled spindle speed, the larger spindle speeds because higher integral values and the effect of the different ways of the changing can shows in the integral. The largest value there is at the feed direction 45°, and the smallest at 0° and 90°. The difference is 17%.

## 8.3 Results

The investigation focused on the Rz parameter of surface roughness and its comparison. The average Rz value of all measured data (5 feed directions x 25 sections x 3 repetitions) with constant spindle speed was found to be 4.1 µm, with a standard deviation of 1.3 µm. Conversely, with controlled (compensated) spindle speed, the average Rz value was 1.7 µm, with a standard deviation of 0.4 µm.

If the actual cutting speed had no effect on surface roughness, the Rz values should have been consistent across the five different feed directions. However, the results indicated that controlled spindle speed and constant feed per tooth resulted in a more homogeneous surface roughness, with smaller average Rz values and standard deviations.

Figure 8-5 and Figure 8-6 illustrate the surface roughness for milling processes with constant spindle speed and controlled cutting speed, respectively. The figures reveal that surface roughness values are smaller and exhibit less variation along the surface in the case of controlled spindle speed.

Based on the diagrams, the values of the surface roughness in case of controlled spindle speed are smaller, and the changing along the surface is smaller in every case.

Higher surface roughness values for uncontrolled milling were observed in horizontal surface sections (Figure 8-5), where the working diameter and thus cutting speed were decreased. In contrast, controlled parameters led to smoother surface maps (Figure 8 6), with smaller differences.

The comparison of statistical data on surface roughness confirms the significant effect of controlled spindle speed on surface roughness variation.

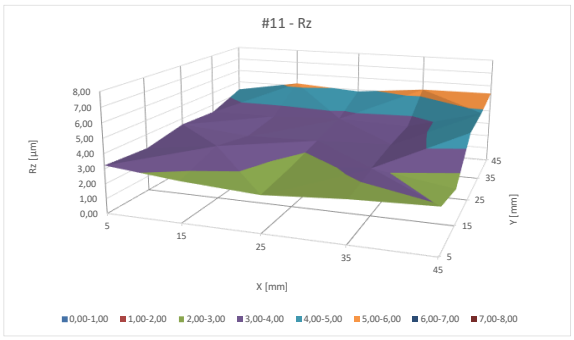


*a) $A_f$ = 0°*

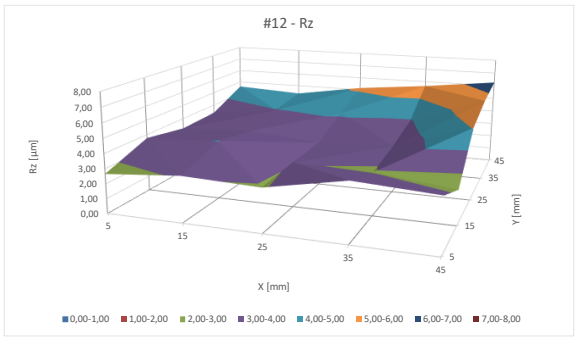


*b) $A_f$ = 22.5°*

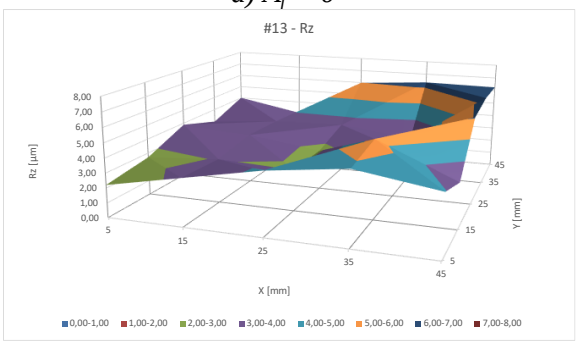


*c) $A_f$ = 45°*

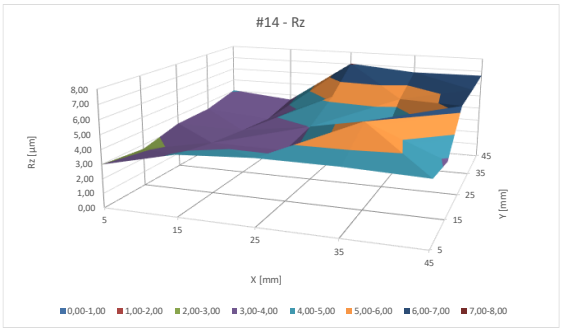


*d) $A_f$ = 67.5°*

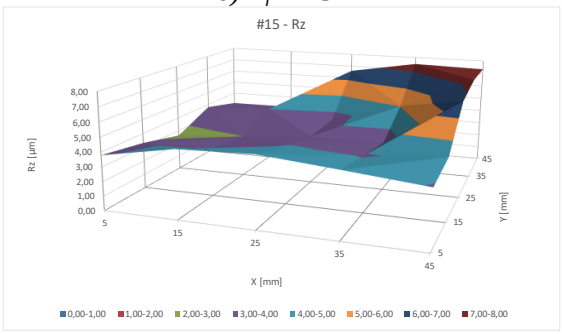


*e) $A_f$ = 90°*

*Figure 8-5: The maps of surface roughness Rz – constant spindle speed.*

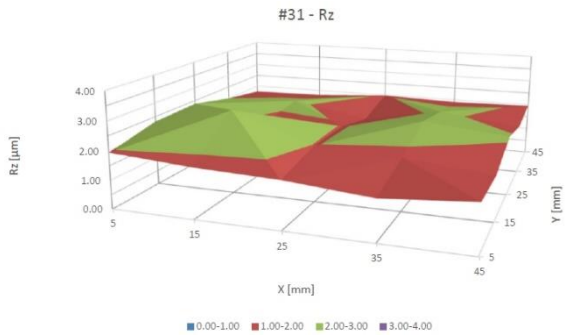


*a) $A_f$ = 0°*

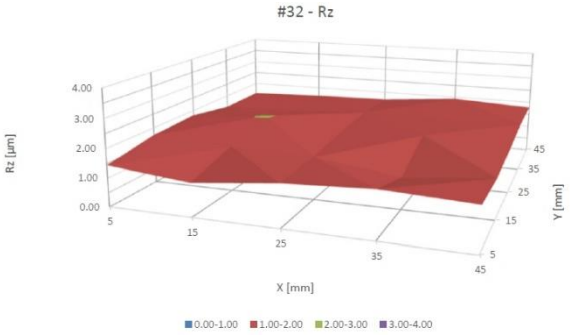


*b) $A_f$ = 22.5°*

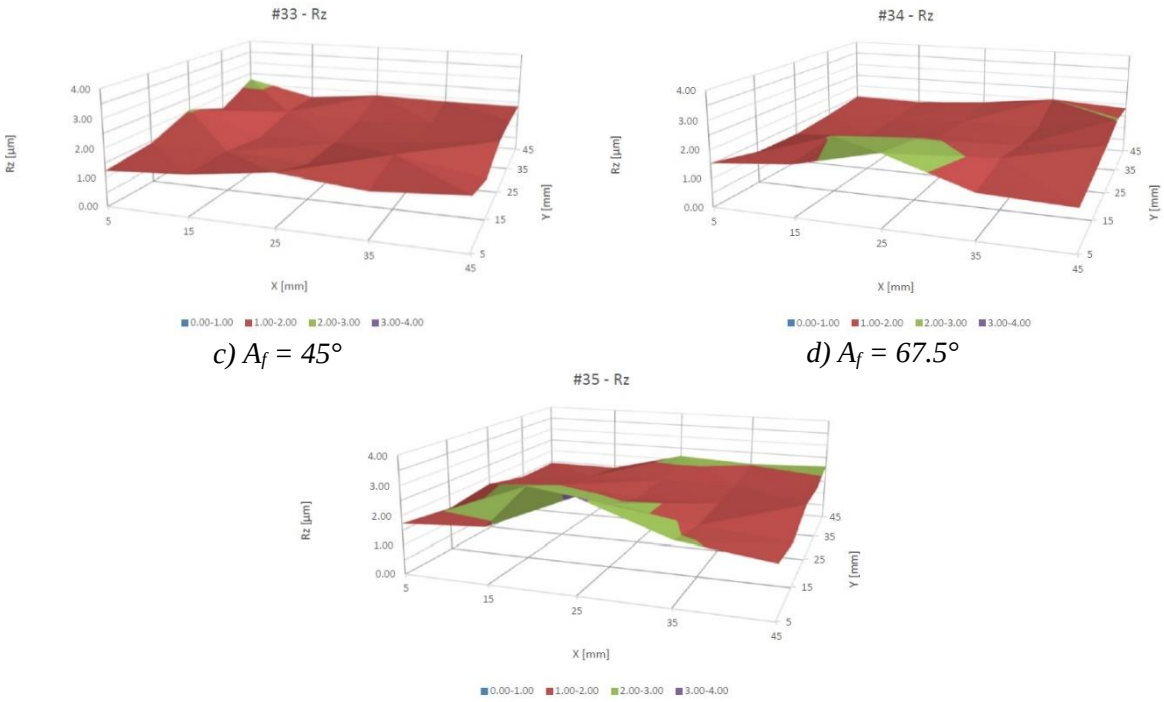


*c) $A_f$ = 45°* *d) $A_f$ = 67.5°*

*e) $A_f$ = 90°*

*Figure 8-6: The maps of surface roughness Rz – controlled spindle speed.*

Figure 8-7 compares the average values of surface roughness Rz for each milling direction. The difference between the Rz surface roughness values after modification is small (2.0 µm in the case of milling direction 0° and 1.6 µm in the case of 45°) compared to milling under a constant spindle speed (ranging from 4.5 µm in the case of feed direction 67.5° to 3.7 µm in the case of milling direction 0°). Maintaining a constant cutting speed reduces the effect of milling direction on surface quality, ensuring similar surface roughness under different milling directions and a more homogeneous surface regardless of surface inclination.

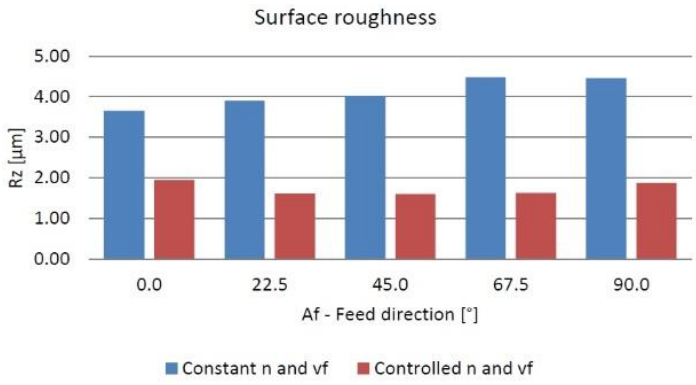


*Figure 8-7: Average values of the surface roughness (Rz).*

As depicted in Figure 8-8, the Rz parameter ranges (defined as the difference between the maximum and minimum values) from 1 µm to about 2 µm in the case of controlled surface, varying based on feed direction. In contrast, with conventional milling methods (constant spindle speed), the ranges are between 3.7 µm and 5.3 µm in each direction. The smaller range in controlled milling indicates a more homogeneous surface quality.

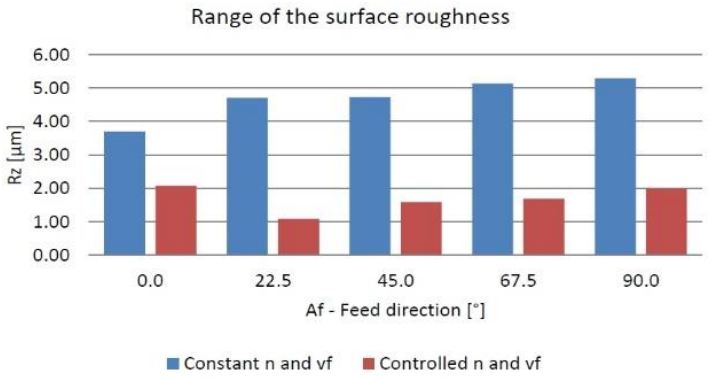


*Figure 8-8: The ranges of the surface roughness (Rz).*

In Figure 8-9 the standard deviation of the Rz surface roughness is depicted for each milling direction, comparing constant and controlled spindle speed conditions. The standard deviations of workpieces machined with controlled spindle speed are smaller (less than 0.5 µm) compared to those machined without optimization, which range from 1 to 1.5 µm. This minimal standard deviation implies that the surface maintains consistent roughness after the machining process, regardless of milling direction. Conversely, similar values of standard deviation across different milling directions underscore the effectiveness of the suggested method in mitigating the impact of milling direction on surface quality.

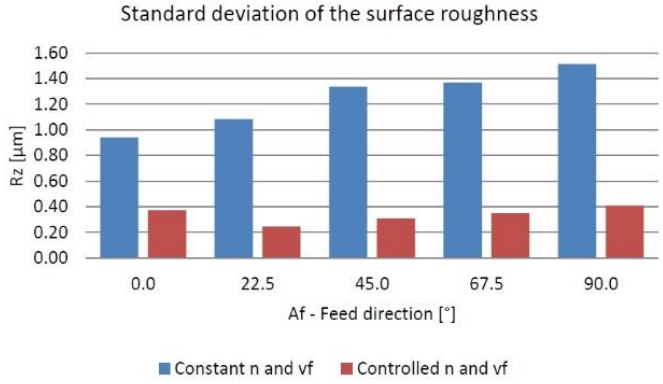


*Figure 8-9: Standard deviation of Rz surface roughness.*

The visual comparison indeed confirms these differences, which are evident in the data. Below are examples illustrating these disparities, with each picture representing a 4.5 x 3.75 mm area.

Figure 8-10 illustrates differences in various locations on the surface, with four examples provided for a feed direction of 45°. Each pair of pictures displays the surface machined with constant spindle speed on the left and the result of the proposed method on the right.

The four surface sections exhibit distinct characteristics:

1. Section 1.1 is positioned at the top of the test surface on a large radius section and is nearly horizontal.
2. Sections 2.4 and 4.2 are situated at the bottom of the high radius, with a greater surface slope in mirrored positions.
3. Section 4.4 is positioned at the transition between the small radius and the horizontal surface section.

In section 1.1, the visible difference is minimal despite the significant difference in roughness values. Conversely, the visual disparity is more noticeable for sections 2.4 and 4.2.

In transition zone 4.4, while the flat section appears similar, the radial section exhibits significant differences.

In horizontal sections where the working diameter is markedly reduced, the increased speed fails to correct the unfavorable cutting conditions. However, on steeper sections, surface aesthetics are also improved alongside roughness values.

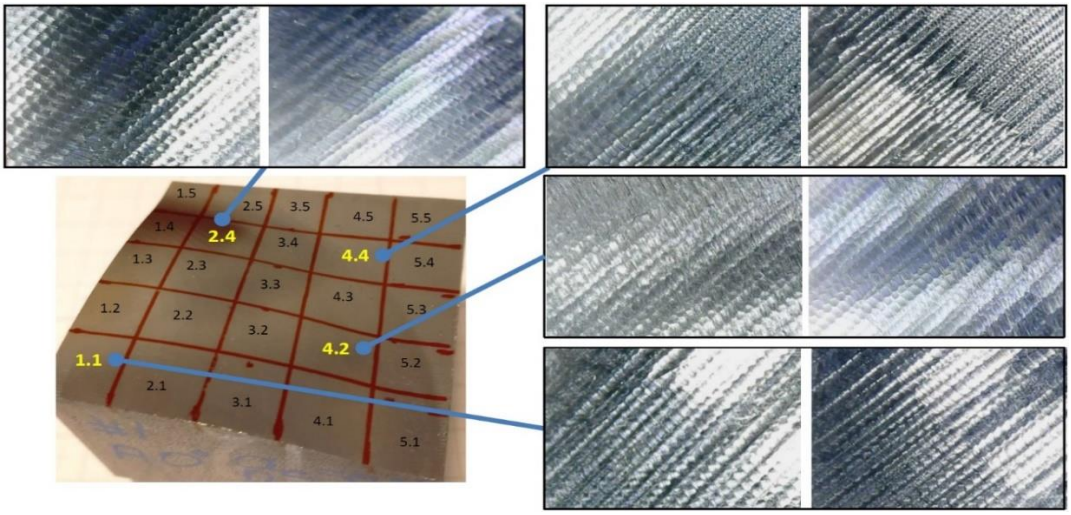


*Figure 8-10: Pictures of the surface zones in case of constant (left) and controlled (right) spindle speed (Af = 45°).*

Figure 8-11 displays images of surface zone 3.4 for five different feed directions. The left side depicts the result of milling at constant spindle speed, while the right side shows the result of milling at controlled spindle speed.

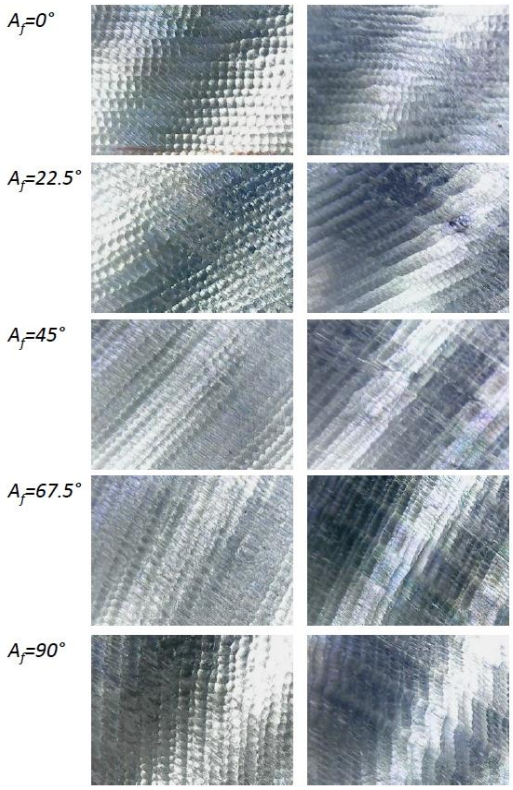


*Figure 8-11: 3.4 surface zone in case of different feed directions (left: constant spindle speed; right: controlled spindle speed).*

The differences in the surface roughness values (Figure 8-12) are also reflected in the visual properties of the surface. The more advantageous chip removal conditions resulting from the controlled machining parameters led to changes in the surface appearance.

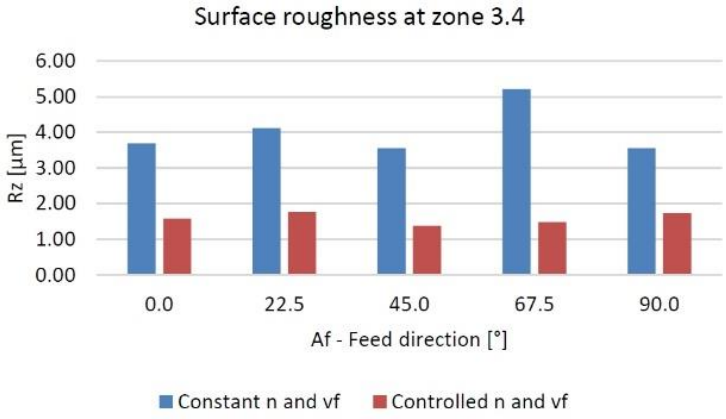


*Figure 8-12: Rz surface roughness at the 3.4 surface zone.*

## 8.4 Conclusion

In this chapter, the effectiveness of the method (which has been presented in the previous chapter) is demonstrated through cutting experiments conducted on C45 steel test pieces using a 10 mm diameter ball-end milling cutter, with different feed directions, constant and controlled spindle speed, and feed rate. Surface roughness (Rz) measurements were taken at various points on the surface with different characteristics.

Key findings and focuses of this chapter include:

1. Improvement in surface roughness observed when milling under a constant cutting speed, with decreased average value and standard deviation of surface roughness.
2. Reduced dependency of surface roughness on milling direction when milling with controlled spindle speed.
3. Implementation of controlled spindle speed resulting in greater dynamic stress on the machine tool, with the integral value of spindle speed along the path indicating dynamic spindle load, aiding in selecting the most efficient milling direction.
4. The presented method is suitable for post-processing a free-form surface finishing CNC milling program to compensate for cutting speed variations, thereby enhancing surface quality and visual appearance.
5. Further research is warranted to explore the integral value in detail, potentially aiding in identifying the most favorable milling strategy considering surface changes and dynamic spindle loading.

Overall, this chapter sets the groundwork for enhancing free-form surface milling processes. It also proposes future research directions aimed at optimizing milling strategies and improving surface quality, as detailed in the subsequent chapter, which focuses on introducing a novel method to address changes in working diameter through optimized tool path planning.

# 9 Tool path planning of ball-end milling of free-form surfaces as a search algorithm

## 9.1 Objective

The aim of this chapter is to optimize the milling tool path of the ball end milling based on the calculation of the working (effective, $D_{eff}$) diameter. In the case of free-form milling, the working diameter is changed because of the changing of the surface inclination. The changing working diameter has an effect on the cutting speed and the surface roughness. During the previous research stage, these effects were investigated, and an optimization algorithm was developed, which modified the spindle speed and the feed in order to compensate the negative effect of the working diameter. The algorithm requires the tool position data and the surface inclination. The APT file format is used for tool path and the STL format for surface description. The modified NC code contains the variable cutting parameters. The acceleration and the dynamic load of the spindle can be high depending on the surface inclination [151].

In this chapter, a new concept is introduced that focuses on modifying the tool path based on changes in the working diameter of the ball-end tool. The goal is to minimize variations in working diameter, thereby reducing the required spindle speed adjustments needed to mitigate changes in cutting speed when applying the previous algorithm.

## 9.2 The tool path planning as a search algorithm

The algorithm has been developed with a specific focus: generating an optimal tool path for milling free-form surfaces. The primary objective is to minimize variations in the working diameter of the ball-end tool during the machining process. By achieving minimal changes in the working diameter, the resulting reduction in cutting speed fluctuations ensures a more uniform and homogeneous machined surface.

The core objective of the algorithm is to perform path planning for CNC machining. This involves determining the sequence of points (toolpath) that the CNC machine should follow while milling the freeform surfaces. The developed algorithm solves the tool path re-planning as a search algorithm. The algorithm uses the pre-generated NC code in APT form. The code contains the points of the toolpath. The search algorithm reorders the points in order to equalize the value of the working diameter and reduce the dynamic load of the spindle. The algorithm implements a path planning that takes into account the difference in the effective diameter between the current point and its neighbor points. Once a point is processed, it is marked as visited (tabu) to prevent the algorithm from revisiting it. The overarching goal is to ensure that the algorithm systematically covers all points without duplication while minimizing fluctuations in the working diameter.

The algorithm begins by reading and processing data from an STL file, which represents 3D models using triangular facets and contains vital geometry information. Subsequently, it extracts tool position coordinates from an APT file, a format used in CNC machining. To enhance precision, the code generates additional tool positions as needed and calculates normal vectors at each position based on facet data from the STL file. It also determines neighbor points and computes the working diameter using an established mathematical model. Finally, the code's core objective is path planning for CNC machining, aiming to optimize toolpaths by considering variations in the effective diameter while efficiently covering all points on the surface.

Figure 9-1 shows the pre-processing of the tool path and the surface data. The algorithm can be summarized in the following sequential steps:

The developed algorithm uses APT file to determine the tool position coordinates at each point of the surface. An APT (Automatically Programmed Tool) file is a file format used in computer-aided manufacturing (CAM) and computer numerical control (CNC) machining. APT is a high-level programming language specifically designed for defining toolpaths and machining operations for CNC machines. By reading the file, the algorithm extracts tool position coordinates.

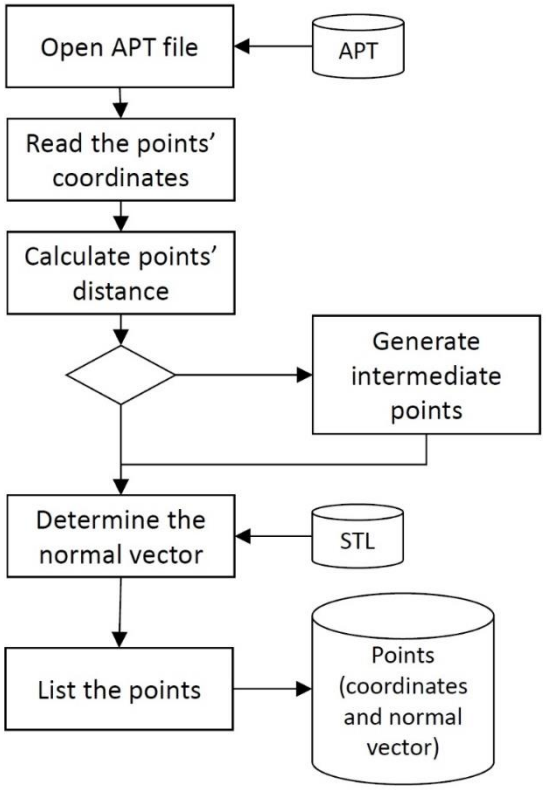


*Figure 9-1 Pre-processing of the tool position and surface data.*

The original CNC code contains the points of the tool path. The distance of the consecutive points depends on the surface inclination. In the case of plane surface segments, which can be horizontal or inclined, the distances can be large. But where the curvature of the surface is greater, the distance between the points is smaller. In order to reconfigure the tool path, quasi-equal density of the points is required. If the distance of points is larger than the defined limit ($d_{lim}$), new points are added. The suggested limit is the value of the width of cut parameter ($a_e$), which is the distance between two parallel paths. The procedure divides the line between two points into pieces, where the distance is smaller than the defined limit. It has no effect on the accuracy of the machining because the original tool path follows the same linear segment.

The distance between two points is:

$$d_i = \sqrt{(x_i - x_{i+1})^2 + (y_i - y_{i+1})^2 + (z_i - z_{i+1})^2} \qquad (9\text{-}1)$$

$$I = Roundup\left(\frac{d_i}{d_{lim}}\right) \qquad (9\text{-}2)$$

If $I > 1$, additional points must be added, the number of new points is ($I$-1). The coordinates of the new points can be calculated by the next equation:

$$\underline{P}_{new\_j} = \underline{P}_i + \frac{j}{I} \cdot \left(\underline{P}_{i+1} - \underline{P}_i\right) = \begin{bmatrix} x_i + \frac{j}{I} \cdot (x_{i+1} - x_i) \\ y_i + \frac{j}{I} \cdot (y_{i+1} - y_i) \\ z_i + \frac{j}{I} \cdot (z_{i+1} - z_i) \end{bmatrix}; j = 1 \dots (I-1) \qquad (9\text{-}3)$$

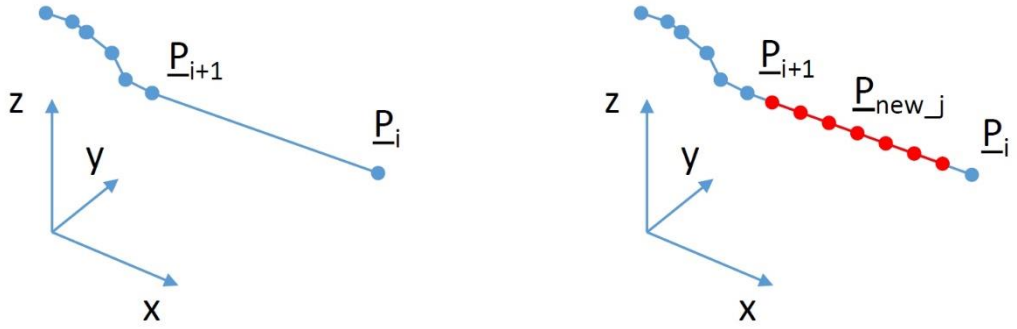


*Figure 9-2 Intermediate points.*

The algorithm proceeds by processing data from the STL file, which is commonly used for representing 3D models with triangular facets. STL file contains information that characterizes the surface's geometry. This file format presents the surface as a collection of triangles along with their associated normal vectors within a three-dimensional coordinate system. It's important to note that the STL file does not contain any additional surface details, such as color or texture information. As the algorithm reads the STL file, it accumulates a list of the normal vectors, and calculates the incentre point of each triangle. The resolution of the STL file can be adjusted. The STL file describes the free-form surface with some deviation, but this has no effect on the accuracy of the method, because the normal vector of the machined area is required only, and in case of technical free-form surfaces, the changing is limited.

The algorithm calculates the normal vectors at each tool position using the facet normal obtained from the STL file. These normal vectors are associated with the corresponding tool positions by identifying the nearest incentre point. Essentially, this process ensures that at each position, the tool aligns with a specific triangle and adopts the same normal vector as that triangle.

The search algorithm of the reordering the points of the tool path is started by the selection of the starting point (Figure 9-3). It must be on the border of the machined surface. The point can be defined by rules, like the lowest or the highest point of the contour or it can be a random point.

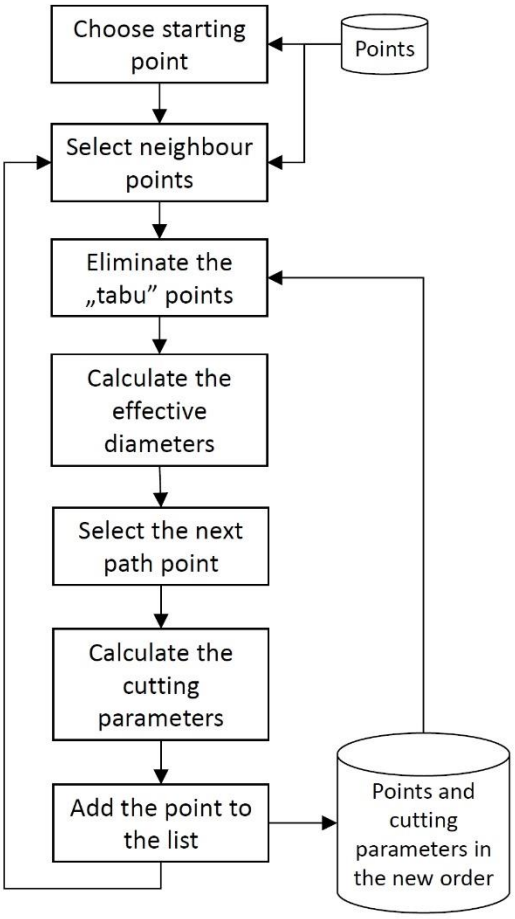


*Figure 9-3 Search algorithm.*

The next step is finding the neighbor points. Because of the non-uniform and non-regular distribution of the tool points, an adaptive method must be used. This code then performs some neighbor point calculations based on a distance threshold R. It iterates over tool position elements and checks for nearby points. If the count of nearby points is less than a specific number, it incrementally increases the distance threshold R until it reaches or exceeds a specific number of points. The resulting points are stored in a list. If a point was chosen previously, it is deleted from the neighbor set, as a taboo point.

The algorithm calculates the milling direction for each tool position based on the slopes between the tool position and its neighbor points. Then it calculates the working diameter of each neighbor point using a mathematical model presented by Mikó and Zentay [77].

At the last step, the point is selected, which has the smallest difference value in the working diameter. If there is no difference in the working diameter because the surface is horizontal, the next point is selected in the feed direction.

The modified cutting parameters (cutting speed and feed) are calculated and added to the list of the points of the new tool path. The algorithm starts again by the selection of the neighbor points. The reordering of the points of the tool path ends when all points are selected.

## 9.3 Results

The algorithm was tested on a free-form surface (Figure 9-4), the size of the part is 50x50 mm, and the height of the profile is 10 mm. The machining parameter in the simulation is shown in Table 9-1. The tool diameter was 10 mm, the nominal cutting speed was 63 m/min,

the feed was 500 mm/min, the depth of cut was 0.3 mm, the width of cut was 0.5 mm, and the feed direction was 90°.

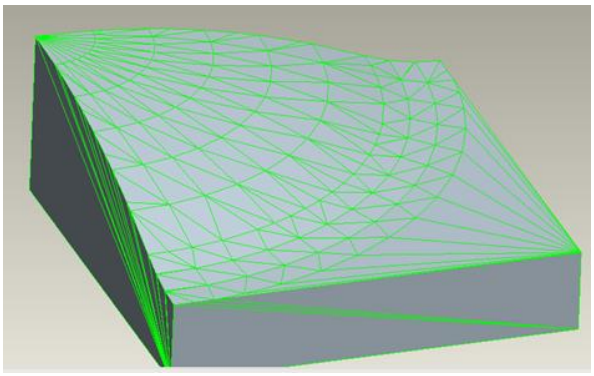

*Figure 9-4 Test part geometry*

*Table 9-1 Parameters of the simulation.*

| | |
|---|---|
| Tool diameter (D) | 10 mm |
| Cutting speed ($v_c$) | 63 m/min |
| Feed ($v_f$) | 500 mm/min |
| Depth of cut ($a_p$) | 0.3 mm |
| Width of cut ($a_e$) | 0.5 mm |
| Feed direction ($A_f$) | 90° |

Figure 9-5 illustrates the outcome of point processing. The first image displays the original distribution of path points, while the second reveals the extended point cloud. This extension of the point cloud provides valuable data for optimizing tool paths. Algorithms can leverage this data to determine the most efficient and safe routes for the cutting tool. To maintain relatively uniform point spacing, the width of cut ($a_e$) was used as a standard distance between points. This approach ensures reasonably consistent inter-point distances. Moreover, extending the original point cloud allows for a faithful representation of the complex free-form surface geometry, thereby enhancing the precision of tool path planning and reducing the risk of errors or defects in the final product.

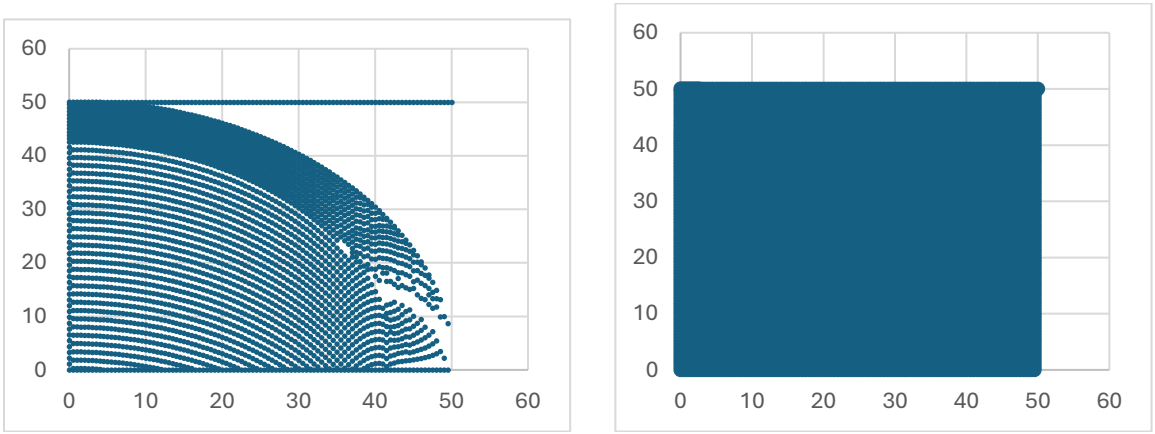


*a) Original distribution of the points* *b) Extended point cloud*

*Figure 9-5 Original and extended distribution of the points.*

In Figure 9-6 and Figure 9-7 a tool path comparison between the original and improved versions is presented. The improved tool path originates from two positions: the point with index 0, coordinates 50, 50, 10 (located in the top right corner of the workpiece), and the point with index 4269, coordinates 28.500, 43.919, 10.00 (situated in the middle of the workpiece). The improvement considers both 4 and 8 neighbor points.

It is important to note that the generated path contains jump points. These occur when all adjacent points to the current position are marked as visited. In such instances, the algorithm seeks the closest unvisited point in the tool-position list. However, this strategy involves a trade-off; the tool may traverse a greater distance in the proposed path compared to the original path.

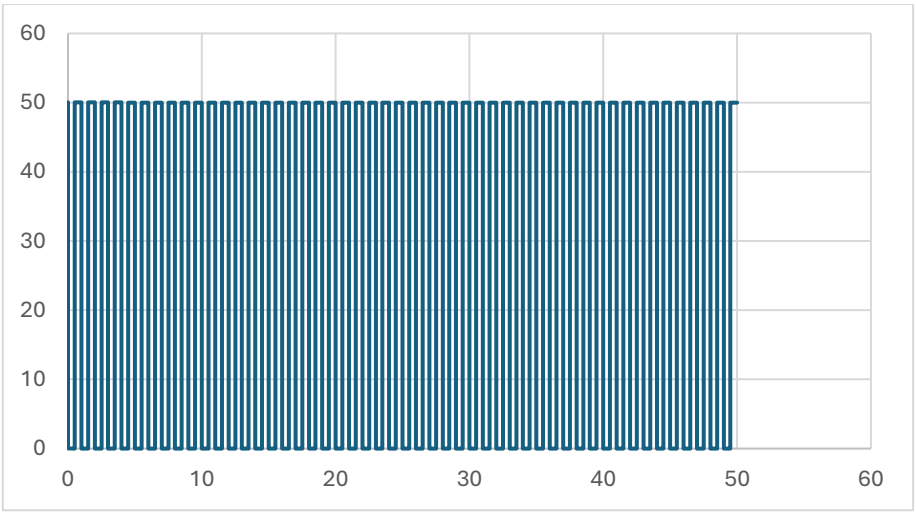


*Figure 9-6 Original tool path*

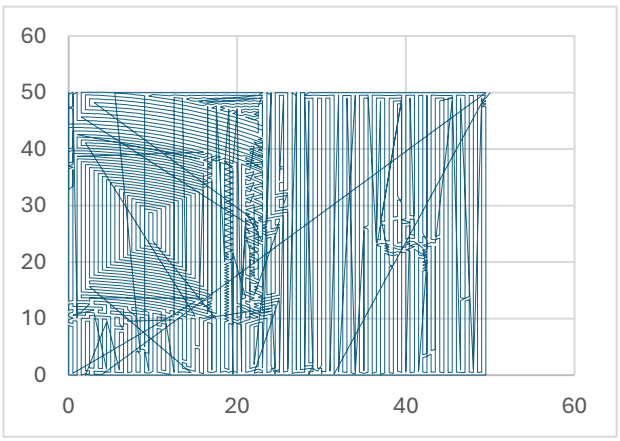


*a) Start point 0, 4 neighbor points*

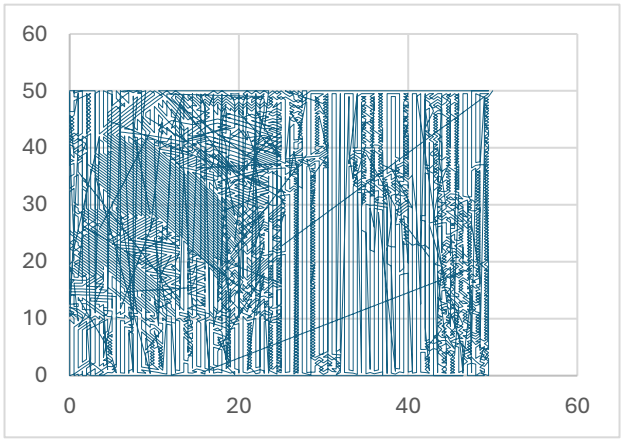


*b) Start point 0, 8 neighbor points*

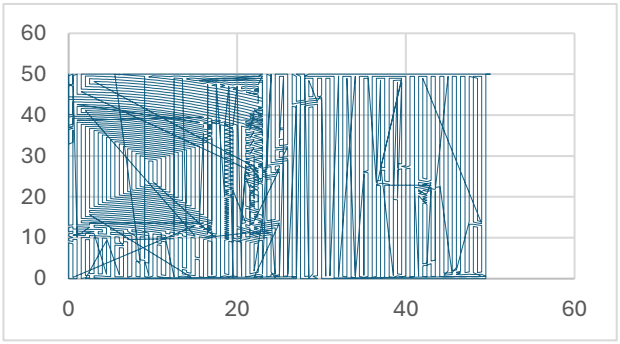


*c) Start point 4269, 4 neighbor points*

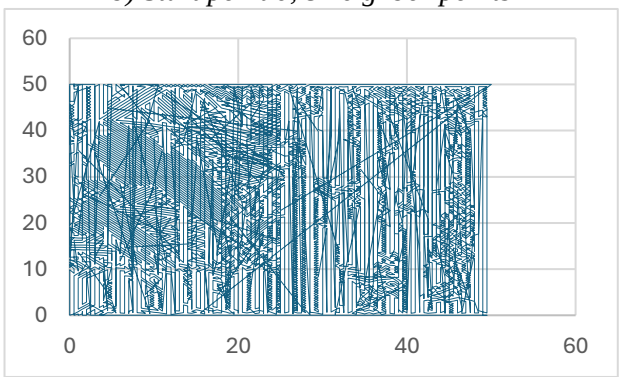


*d) Start point 4269, 8 neighbor points*

*Figure 9-7 Optimized tool path.*

The resulting toolpath depends on the position of the starting point, and the number of the investigated neighbor points. Therefore, four cases were studied as presented in Table 9-2.

*Table 9-2 Comparative Analysis of Tool Path Optimization: Four Distinct Cases Investigated*

| Case | Starting point | Number of the neighbor points |
|---|---|---|
| 1 | 0 | 4 |
| 2 | 4948 | 4 |
| 3 | 0 | 8 |
| 4 | 4948 | 8 |

The comparison of the four tool path planning cases unveils distinct trends influenced by the selected starting points and the number of neighboring points. Figure 9-8 a) illustrates the traveling distance in the four cases. Cases 1 and 3, both originating from the top right corner but differing in neighboring points, demonstrate that an increase in neighboring points leads to a longer tool path (6183) for Case 1 with four neighbors and 8805 for Case 3 with eight neighbors. Similarly, Cases 2 and 4, both starting from the middle but varying in neighboring points, follow a similar pattern, with Case 4 (10645) having a longer tool path compared to Case 2 (7097). Conversely, Figure 9-8 b) highlights the impact of starting points and neighboring points on jumping points. Initially comparing Cases 1 and 2, both starting from distinct locations but with four neighboring points, reveals a minimal difference in jumping points (181 in Case 1 and 180 in Case 2). This suggests that the starting point's influence on jumping points is relatively limited when the number of neighboring points remains constant. A parallel trend is observed in Cases 3 and 4, where starting from the middle but with different neighboring points results in comparable jumping points (426 in Case 3 and 432 in Case 4). This underscores that the number of neighboring points plays a more significant role than the starting point in determining the number of jumping points.

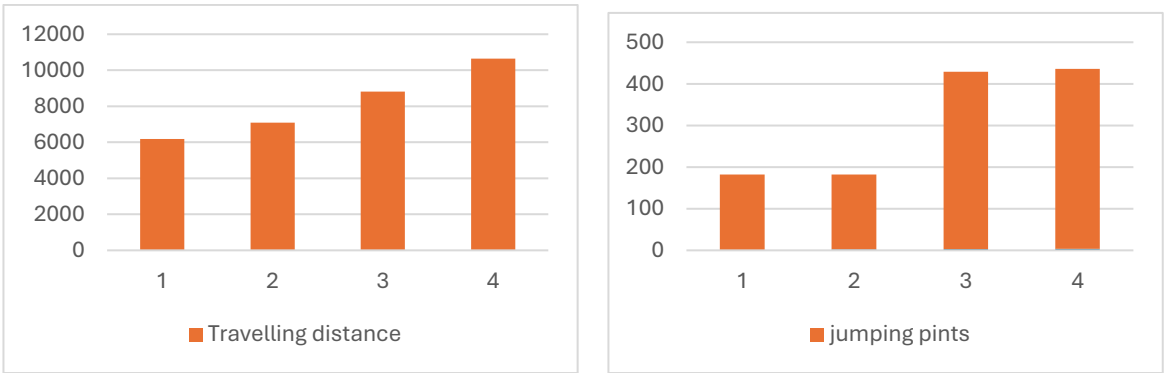


*Figure 9-8 Number of jumping points and travelling distance at each case.*

On the other hand, the main objective of the proposed algorithm is to minimize changes in effective diameter and regulate the spindle's dynamic load. This assessment involves two key comparisons. Firstly, it examines the absolute change in effective diameter in two specific scenarios: the original toolpath and the modified tool path in case 1. Secondly, the algorithm calculates the spindle speed at each point to ensure a constant cutting speed, and it compares the absolute change in spindle speed between these same two cases.

Figure 9-9 and Figure 9-10 provide a visual representation of the change in the working diameter when employing two different milling strategies: the traditional down milling tool path and an optimized tool path. The working diameter, a critical parameter in machining operations, is analyzed to understand its variation and impact on the machining process.

In the case of the traditional down milling tool path, Figure 9-9 illustrates a significant range of change in the working diameter, spanning from 0 to 0.9155. This wide variation suggests that the machining process under traditional down milling conditions results in a less consistent effective diameter throughout the operation.

On the other hand, Figure 9-10 highlights the working diameter variation when utilizing a modified tool path. In this scenario, the effective diameter fluctuates within a narrower range, specifically between 0 and 0.6. This narrower range indicates that the proposed tool path leads to a more controlled and predictable working diameter during the milling process.

The observed difference in the effective diameter range between the two milling strategies has noteworthy implications, particularly in terms of surface homogeneity. A smaller variation in the working diameter, as achieved with the modified tool path, contributes to enhanced surface homogeneity.

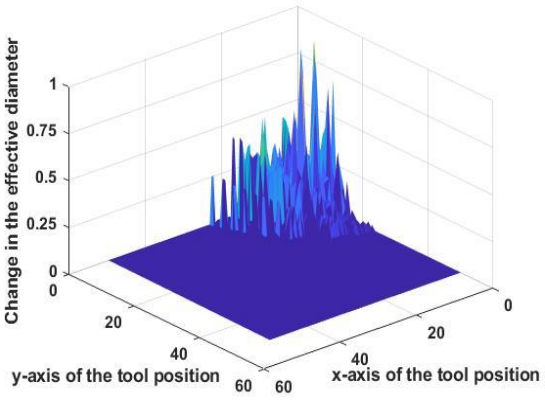


*Figure 9-9 The change in the working diameter in the case of original tool path*

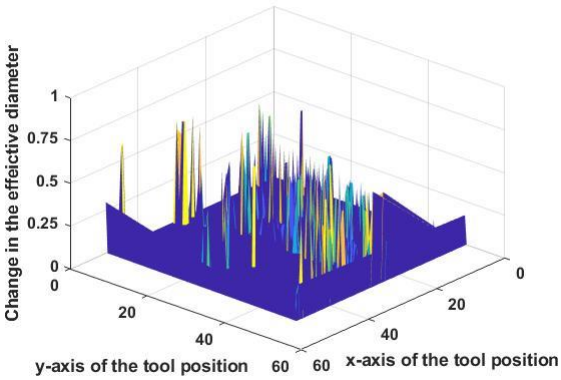


*Figure 9-10 The change in the working diameter in the case of optimized tool path*

Figure 9-11 illustrates the spindle speed change in the case of the traditional down milling approach, showcasing a wide range from 0 to 622. This broad variation implies that under traditional down milling conditions, the spindle speed undergoes significant changes throughout the machining process. Such fluctuations may introduce challenges such as tool wear, vibration, and inconsistent cutting conditions, potentially impacting the overall quality of the machined surface.

Conversely, Figure 9-12 represents the spindle speed variation for the optimized tool path. In this case, the spindle speed changes within a smaller range, specifically from 0 to 128. The narrower variation indicates that the proposed tool path leads to a more controlled and stable adjustment of spindle speed during machining.

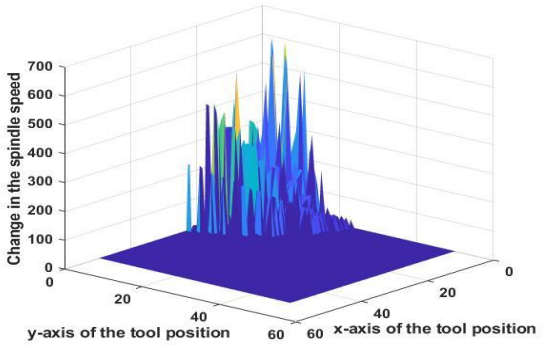


*Figure 9-11 The change in the spindle speed in the case of original tool path*

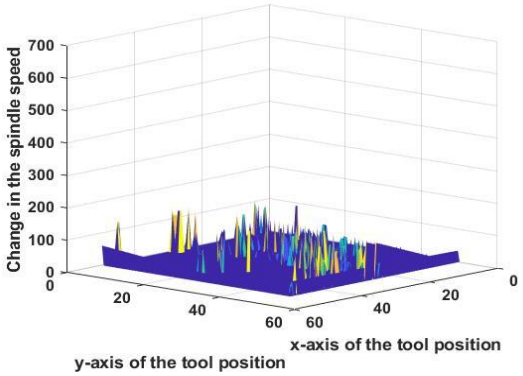


*Figure 9-12 The change in the spindle speed in the case of optimized tool path*

## 9.4 Conclusion

The presented algorithm was developed for improving toolpaths in CNC machining, with a primary focus on minimizing variations in the working diameter of the ball-end tool during milling of free-form surfaces. The algorithm reorders the tool points of the CNC program and functions as a search algorithm. It systematically calculates the working diameter of neighboring points and directs tool movement to points with minimal diameter differences, ensuring minimal changes in the working diameter and the adjustment of the spindle speed to maintain a constant cutting speed.

Key steps involve reading and processing data from an STL file to extract surface geometry and tool position data from an APT file. Normal vectors are calculated and associated with tool positions, aligning the tool with specific triangles of the STL file.

Neighboring point calculations consider a distance threshold, and working diameters are determined for each point. The core path planning algorithm minimizes working diameter fluctuations, preventing point revisits for efficiency.

The comparative analysis between the original and improved tool paths highlighted the nuanced impact of starting points and neighboring points on the resultant tool path. Successfully achieving the primary optimization goal - reducing the change in effective diameter and moderating spindle dynamic loads - was evidenced in the controlled working diameter variation observed in the improved tool path, contributing to enhanced surface.

# 10 Summary of new scientific results

The dissertation findings are summarized in seven thesis points. In square brackets are the author's works in which the actual thesis points were published:

**Thesis 1**

I have created a simulation model to compute the working diameter of the ball-end milling tool in a broader context. This simulation approach has allowed for a more comprehensive examination of each tool and cutting parameters. I have found that the working diameter and therefore the cutting speed varies during the chip removal. This variation is larger for larger nominal tool diameters and down milling technology. Based on the simulation, I have found that the feed direction has a significant effect on the value of the working diameter, therefore this parameter is suitable for controlling the milling process from the point of view of the working diameter.

The parameters of the simulation were: Tool diameter: $D_c$ = 6-8-10 mm; Depth of cut: $a_p$ = 0.1 – 1.0 mm; Width of cut: $a_e$ = 1 mm; Feed direction: $A_f$ = 0-180°.

Related publications: [1]

**Thesis 2**

I have made a regression model for the calculation of the working diameter of free form ball-end milling. I have demonstrated that to create an accurate regression model, it is essential to include the first, third, and fifth powers of both the surface inclination and the relative feed direction. I suggest a separated regression model based on tool diameter, which results in higher accuracy. The general form of the proposed regression model is:

$$D_{eff} = \sum f_i(D) \cdot C_i$$

where: the $f_i(D)$ is a linear function of the tool diameter, and the $C_i$ is the influential parameter.

Related publications: [4]

**Thesis 3**

I have designed a method for maintaining a constant cutting speed by regulating the spindle speed, independent of any CAD or CAM system by using standard STL file for surface representation and APT file for toolpath description. The algorithm utilizes the standard STL file format to calculate the normal vector at each surface point considering the tool position from the APT file. It establishes a connection between cutter positions and triangles within the STL file, subsequently computing the working diameter at each point. Following the desired cutting speed, the spindle speed is determined for each point. The algorithm then produces a new NC file with adjusted spindle speed values.

I have verified that implementing controlled spindle speed introduces greater dynamic stress to the machine tool. The integral value of spindle speed along the tool path serves as an indicator of dynamic load, making it a useful parameter for selecting the most efficient milling

direction. It allows for the compensation of cutting speed, leading to improved surface quality and visual appearance.

Related publications: [2]

**Thesis 4**

By milling experiments, I have demonstrated that at a controlled variable spindle speed, taking into account a constant cutting speed, the surface roughness is significantly improved in the case of ball-end milling of a free-form surface compared to constant speed milling. Depending on feed direction, the average values of Rz surface roughness parameters are 36-56% of the original values, in the case of controlled spindle speed. The surfaces are more homogenous, which is indicated by the values of the range and standard deviation of the surface roughness. The ranges of the Rz values are 23-56% and the standard deviation are 23-39% of the original values.

The parameters of the experiments were the next: workpiece material: C45 steel; Nominal cutting speed: $v_c$ = 63 m/min; Feed per tooth: $f_z$ = 0.125 mm; Depth of cut: $a_p$ = 0.3 mm; Width of cut: $a_e$ = 0.25 mm; Feed direction: $A_f$ = 0 - 90°; Spindle speed: $n_{constant}$ = 1845 1/min; $n_{controlled}$ = 3002-8066 1/min.

Related publications: [3][7]

**Thesis 5**

I have developed a novel approach to plan a milling toolpath for free form ball-end milling, focusing on variations in the effective diameter. The developed approach solved the tool path-planning problem as a searching algorithm. The algorithm aims to find an optimal solution, ensuring minimal changes in the working diameter. It reorders the points of the milling toolpath considering the changing of the working diameter of the tool. Therefore, it minimizes the spindle speed compensation in order to reduce the dynamic load of the spindle. The results show that by adjusting the spindle speed, the optimized toolpath notably reduces the range of spindle speed values. The implementation of this method involves developing an algorithm that utilizes standard STL files and APT.

Related publications: [8]

# 11 Publication list

**Journal articles with impact factor**

1. Mgherony Abdulwahab; Mikó Balázs (2022) *Simulation of the working diameter in 3-axis ball-end milling of free form surface.* Tehnički vjesnik 29(4):1164-1170 (**IF 0.9**) https://doi.org/10.17559/TV-20210719181212
2. Mgherony Abdulwahab; Mikó Balázs (2023) *Controlling the spindle speed when milling free-form surfaces using ball-end milling cutter*. Acta Polytechnica Hungarica 20(6):135-149 ISSN 1785-8860 (**IF 1.7**) https://doi.org/10.12700/APH.20.6.2023.6.8
3. Mgherony Abdulwahab; Mikó Balázs (2024) *The effect of the spindle speed control when milling free-form surfaces.* The International Journal of Advanced Manufacturing Technology; 130(3-4):1439-1449 (**IF 3.4**) https://doi.org/10.1007/s00170-023-12811-1
4. Mgherony Abdulwahab; Mikó Balázs (2024) *Regression analysis and neural network model of working diameter of ball-end mill.* Acta Polytechnica Hungarica xx(x):xxx-xxx ISSN 1785-8860 (**IF 1.7**) 10.12700/APH.xxxxxx (***under review***)

**Journal articles whithout impact factor**

5. Mgherony Abdulwahab; Mikó Balázs; Drégelyi-Kiss Ágota (2020) *Design of experiment in investigation regarding milling machinery.* Cutting & Tooling in Technological Systems (Rezanie i instrumenty v tekhnologicheskih sistemah) 92:68-84 https://doi.org/10.20998/2078–7405.2020.92.09
6. Mgherony Abdulwahab; Mikó Balázs; Farkas Gabriella (2021) *Comparison of surface roughness when turning and milling.* Periodica Polytechnica - Mechanical engineering 65(4):337-344 https://doi.org/10.3311/PPme.17898
7. Mgherony Abdulwahab; Mikó Balázs (2021) *The effect of the cutting speed on the surface roughness when ball-end milling.* Hungarian Journal of Industry and Chemistry 49(2):9-13 https://doi.org/10.33927/hjic-2021-14 hjic.mk.uni-pannon.hu
8. Mgherony Abdulwahab; Mikó Balázs (2024) *Tool path planning of ball-end milling of free-form surfaces as a search algorithm.* Acta Technica Jaurinensis, 17(2):75-83, 2024 https://doi.org/10.14513/actatechjaur.00736

**Conference proceedings**

9. Mgherony Abdulwahab; Nagy János; Mikó Balázs (2022) *Application of the regression method in case of the free-form surface error.* Proceedings of Development in Machining Conference - DiM 2022; Crakow, Poland 18-19.05.2022. Development in machining technology 10:63-73 Ed.: W. Zebala, I. Manková; Cracow University of Technology, Cracow 2022 ISBN 978-80-553-4133-0

**Citation information (03-07-2024):**

| No | Independent | Self | Total |
|---|---|---|---|
| **[1]** | | 1 | 1 |
| **[2]** | 1 | 2 | 3 |
| **[3]** | 1 | | 1 |
| **[4]** | | | |
| **[5]** | 2 | 1 | 3 |
| **[6]** | 6 | | 6 |
| **[7]** | 1 | | 1 |
| **[8]** | | | |
| **[9]** | | | |
| **Sum** | **11** | **4** | **15** |

**List of Figures:**

**List of Tables:**

**References:**


[1] D. A. Stephenson and J. S. Agapiou, *Metal Cutting Theory and Practice*. CRC Press, 2018. [Online]. Available: https://books.google.hu/books?id=WouADwAAQBAJ

[2] L. Norberto López de Lacalle, F. J. Campa, and A. Lamikiz, "Milling," in *Modern Machining Technology*, J. Paulo Davim, Ed., Elsevier, 2011, pp. 213–303. doi: 10.1533/9780857094940.213.

[3] G. Schneider, *Cutting tool applications*. Nelson Pub., 2002.

[4] W. A. Knight and G. Boothroyd, *Fundamentals of Metal Machining and Machine Tools*. CRC Press, 2019. [Online]. Available: https://books.google.hu/books?id=xqYGEAAAQBAJ

[5] M. Mattson, *CNC programming: principles and applications*. Cengage Learning, 2009.

[6] C. X. Yue, F. G. Yan, L. Bin Li, H. Y. You, and Q. J. Yu, "Parametric Design of Ball-End Milling Tools for High Speed Milling," *Materials Science Forum*, vol. 800–801, pp. 484–488, Jul. 2014, doi: 10.4028/www.scientific.net/MSF.800-801.484.

[7] L. Blunt and X. Jiang, *Advanced Techniques for Assessment Surface Topography: Development of a Basis for 3D Surface Texture Standards "Surfstand."* Elsevier Science, 2003. [Online]. Available: https://books.google.hu/books?id=H4-dIu4IbscC

[8] N. Hatem, Y. Yusof, A. Z. A. Kadir, K. Latif, and M. A. Mohammed, "A novel integrating between tool path optimization using an ACO algorithm and interpreter for open architecture CNC system," *Expert Syst Appl*, vol. 178, p. 114988, Sep. 2021, doi: 10.1016/j.eswa.2021.114988.

[9] M. Uzun, Ü. A. Usca, M. Kuntoğlu, and M. K. Gupta, "Influence of tool path strategies on machining time, tool wear, and surface roughness during milling of AISI X210Cr12 steel," *The International Journal of Advanced Manufacturing Technology*, vol. 119, no. 3–4, pp. 2709–2720, Mar. 2022, doi: 10.1007/s00170-021-08365-9.

[10] M. Luo, H. Luo, D. Zhang, and K. Tang, "Improving tool life in multi-axis milling of Ni-based superalloy with ball-end cutter based on the active cutting edge shift strategy," *J Mater Process Technol*, vol. 252, pp. 105–115, Feb. 2018, doi: 10.1016/j.jmatprotec.2017.09.010.

[11] L. T. Tunc, "Smart tool path generation for 5-axis ball-end milling of sculptured surfaces using process models," *Robot Comput Integr Manuf*, vol. 56, pp. 212–221, Apr. 2019, doi: 10.1016/j.rcim.2018.10.002.

[12] M. Sadílek, Z. Poruba, L. Čepová, and M. Šajgalík, "Increasing the Accuracy of Free-Form Surface Multiaxis Milling," *Materials*, vol. 14, no. 1, p. 25, Dec. 2020, doi: 10.3390/ma14010025.

[13] R. A. Mali, T. V. K. Gupta, and J. Ramkumar, "A comprehensive review of free-form surface milling– Advances over a decade," *J Manuf Process*, vol. 62, pp. 132–167, Feb. 2021, doi: 10.1016/j.jmapro.2020.12.014.

[14] S. Lotfi, B. Rami, B. Maher, D. Gilles, and B. Wassila, "Cutter-workpiece engagement calculation in 3-axis ball end milling considering cutter runout," *J Manuf Process*, vol. 41, pp. 74–82, May 2019, doi: 10.1016/j.jmapro.2019.03.025.

[15] T. R. Thomas and T. R. Thomas, "FRONT MATTER," in *Rough Surfaces*, vol. 278, PUBLISHED BY IMPERIAL COLLEGE PRESS AND DISTRIBUTED BY WORLD

SCIENTIFIC PUBLISHING CO., 1998, pp. i–xvi. doi: 10.1142/9781860943805_fmatter.

[16] L. Blunt and X. Jiang, *Advanced Techniques for Assessment Surface Topography*. Elsevier, 2003. doi: 10.1016/B978-1-903996-11-9.X5000-2.

[17] L. De Chiffre *et al.*, "Quantitative Characterisation of Surface Texture," *CIRP Annals*, vol. 49, no. 2, pp. 635–652, 2000, doi: 10.1016/S0007-8506(07)63458-1.

[18] K. J. Stout and L. Blunt, *Three Dimensional Surface Topography*. Elsevier, 2000. doi: 10.1016/B978-1-85718-026-8.X5112-1.

[19] P. G. Benardos and G.-C. Vosniakos, "Predicting surface roughness in machining: a review," *Int J Mach Tools Manuf*, vol. 43, no. 8, pp. 833–844, Jun. 2003, doi: 10.1016/S0890-6955(03)00059-2.

[20] A. Antoniadis, C. Savakis, N. Bilalis, and A. Balouktsis, "Prediction of Surface Topomorphy and Roughness in Ball-End Milling," *The International Journal of Advanced Manufacturing Technology*, vol. 21, no. 12, pp. 965–971, Sep. 2003, doi: 10.1007/s00170-002-1418-8.

[21] I. Buj-Corral, J.-A. Ortiz-Marzo, L. Costa-Herrero, J. Vivancos-Calvet, and C. Luis-Pérez, "Optimal Machining Strategy Selection in Ball-End Milling of Hardened Steels for Injection Molds," *Materials*, vol. 12, no. 6, p. 860, Mar. 2019, doi: 10.3390/ma12060860.

[22] M. F. Batista, A. R. Rodrigues, and R. T. Coelho, "Modeling and characterisation of roughness of moulds produced by high-speed machining with ball-nose end mill," *Proc Inst Mech Eng B J Eng Manuf*, vol. 231, no. 6, pp. 933–944, May 2017, doi: 10.1177/0954405415584898.

[23] B. Mikó, "Surface Quality Prediction in Case of Steep Free Form Surface Milling," *Key Eng Mater*, vol. 686, pp. 119–124, Feb. 2016, doi: 10.4028/www.scientific.net/KEM.686.119.

[24] S. Wojciechowski, P. Twardowski, and M. Wieczorowski, "SURFACE TEXTURE ANALYSIS AFTER BALL END MILLING WITH VARIOUS SURFACE INCLINATION OF HARDENED STEEL," *Metrology and Measurement Systems*, vol. 21, no. 1, pp. 145–156, Mar. 2014, doi: 10.2478/mms-2014-0014.

[25] P. Kovač, B. Savković, M. Gostimirovic, D. Jesic, and I. Mankova, "Modeling of the machining surface roughness parameters for steel difficult to machining," *Analele Universitatii Eftimie Murgu Resita*, vol. 24, no. 1, pp. 175–193, 2017.

[26] I. Tlhabadira, I. A. Daniyan, R. Machaka, C. Machio, L. Masu, and L. R. VanStaden, "Modeling and optimization of surface roughness during AISI P20 milling process using Taguchi method," *The International Journal of Advanced Manufacturing Technology*, vol. 102, no. 9–12, pp. 3707–3718, Jun. 2019, doi: 10.1007/s00170-019-03452-4.

[27] A. Sharma and V. K. Dwivedi, "Effect of milling parameters on surface roughness: An experimental investigation," *Mater Today Proc*, vol. 25, pp. 868–871, 2020, doi: 10.1016/j.matpr.2019.11.256.

[28] A. W. Mgherony, B. Mikó, and Á. Drégelyi-Kiss, "Design of experiment in investigation regarding milling machinery," 2020, doi: 10.20998/2078–7405.2020.92.09.

[29] S. Tiryaki, Ş. Özşahin, and A. Aydın, "Employing artificial neural networks for minimizing surface roughness and power consumption in abrasive machining of wood," *European Journal of Wood and Wood Products*, vol. 75, no. 3, pp. 347–358, May 2017, doi: 10.1007/s00107-016-1050-1.

[30] Y. V. Deshpande, A. B. Andhare, and P. M. Padole, "Application of ANN to estimate surface roughness using cutting parameters, force, sound and vibration in turning of Inconel 718," *SN Appl Sci*, vol. 1, no. 1, p. 104, Jan. 2019, doi: 10.1007/s42452-018-0098-4.

[31] X. A. Vasanth, P. S. Paul, and A. S. Varadarajan, "A neural network model to predict surface roughness during turning of hardened SS410 steel," *International Journal of System Assurance Engineering and Management*, vol. 11, no. 3, pp. 704–715, Jun. 2020, doi: 10.1007/s13198-020-00986-9.

[32] S. P. Leo Kumar, "Experimental investigations and empirical modeling for optimization of surface roughness and machining time parameters in micro end milling using Genetic Algorithm," *Measurement*, vol. 124, pp. 386–394, Aug. 2018, doi: 10.1016/j.measurement.2018.04.056.

[33] L. Li, M. Wu, X. Liu, Y. Cheng, and Y. Yu, "The prediction of surface roughness of PCBN turning GH4169 based on adaptive genetic algorithm," *Integrated Ferroelectrics*, vol. 180, no. 1, pp. 118–132, May 2017, doi: 10.1080/10584587.2017.1338881.

[34] T. Zhou, L. He, J. Wu, F. Du, and Z. Zou, "Prediction of Surface Roughness of 304 Stainless Steel and Multi-Objective Optimization of Cutting Parameters Based on GA-GBRT," *Applied Sciences*, vol. 9, no. 18, p. 3684, Sep. 2019, doi: 10.3390/app9183684.

[35] B. Savkovic, P. Kovac, D. Rodic, B. Strbac, and S. Klancnik, "Comparison of artificial neural network, fuzzy logic and genetic algorithm for cutting temperature and surface roughness prediction during the face milling process," *Advances in Production Engineering & Management*, vol. 15, no. 2, pp. 137–150, Jun. 2020, doi: 10.14743/apem2020.2.354.

[36] J. Kundrák and C. Felhő, "Investigation of the Topography of Face Milled Surfaces," *Materials Science Forum*, vol. 919, pp. 78–83, Apr. 2018, doi: 10.4028/www.scientific.net/MSF.919.78.

[37] C. Felhő and J. Kundrák, "Effects of Setting Errors (Insert Run-Outs) on Surface Roughness in Face Milling When Using Circular Inserts," *Machines*, vol. 6, no. 2, p. 14, Apr. 2018, doi: 10.3390/machines6020014.

[38] A. Meijer, J. A. Bergmann, E. Krebs, D. Biermann, and P. Wiederkehr, "Analytical and Simulation-Based Prediction of Surface Roughness for Micromilling Hardened HSS," *Journal of Manufacturing and Materials Processing*, vol. 3, no. 3, p. 70, Aug. 2019, doi: 10.3390/jmmp3030070.

[39] A. Lasemi, D. Xue, and P. Gu, "Recent development in CNC machining of freeform surfaces: A state-of-the-art review," *Computer-Aided Design*, vol. 42, no. 7, pp. 641–654, Jul. 2010, doi: 10.1016/j.cad.2010.04.002.

[40] X. J. Jiang and P. J. Scott, "Fundaments for free-form surfaces," in *Advanced Metrology*, Elsevier, 2020, pp. 11–34. doi: 10.1016/B978-0-12-821815-0.00002-2.

[41] J. Beňo, I. Maňková, P. Ižol, and M. Vrabel', "An approach to the evaluation of multivariate data during ball end milling free-form surface fragments," *Measurement*, vol. 84, pp. 7–20, Apr. 2016, doi: 10.1016/j.measurement.2016.01.043.

[42] R. A. Mali, T. V. K. Gupta, and J. Ramkumar, “A comprehensive review of free-form surface milling– Advances over a decade,” *J Manuf Process*, vol. 62, pp. 132–167, Feb. 2021, doi: 10.1016/j.jmapro.2020.12.014.

[43] B. Varga and B. Mikó, “Investigation of geometric accuracy of free-form surface profile,” in *The publications of the MultiScience - XXXII. MicroCAD International Scientific Conference*, University of Miskolc, 2018, pp. 6–9. doi: 10.26649/musci.2018.040.

[44] L. Chang, *A Parametric Design of Ball End Mill and Simulating Process*. Concordia University, 2016. [Online]. Available: https://books.google.hu/books?id=yEUsyQEACAAJ

[45] L. Chang, “A parametric design of ball end mill and simulating process,” Concordia University, 2016.

[46] L. Yang and M. L. Zheng, “Simulation and Analysis of Ball-End Milling of Panel Moulds Based on Deform 3D,” *International Journal of Simulation Modeling*, vol. 16, no. 2, pp. 343–356, Jun. 2017, doi: 10.2507/IJSIMM16(2)CO9.

[47] M. Sekulic, V. Pejic, M. Brezocnik, M. Gostimirovic, and M. Hadzistevic, “Prediction of surface roughness in the ball-end milling process using response surface methodology, genetic algorithms, and grey wolf optimizer algorithm,” *Advances in Production Engineering & Management*, vol. 13, no. 1, pp. 18–30, Mar. 2018, doi: 10.14743/apem2018.1.270.

[48] H. Radhwan, S. Sharif, Z. Shayfull, M. A. Suhaimi, M. T. M. Khushairi, and M. R. M. Najmi, “Optimization of cutting parameters for surface roughness in ball end milling of aluminium epoxy using Taguchi method,” in *AIP Conference Proceedings*, 2019, p. 020156. doi: 10.1063/1.5118164.

[49] A. F. de Souza, A. E. Diniz, A. R. Rodrigues, and R. T. Coelho, “Investigating the cutting phenomena in free-form milling using a ball-end cutting tool for die and mold manufacturing,” *The International Journal of Advanced Manufacturing Technology*, vol. 71, no. 9–12, pp. 1565–1577, Apr. 2014, doi: 10.1007/s00170-013-5579-4.

[50] B. Mikó and J. Beňo, “Effect of the Working Diameter to the Surface Quality in Free-Form Surface Milling,” *Key Eng Mater*, vol. 581, pp. 372–377, Oct. 2013, doi: 10.4028/www.scientific.net/KEM.581.372.

[51] A. H. Seikh, B. B. Mandal, A. Sarkar, M. Baig, N. Alharthi, and B. Alzahrani, “Application of response surface methodology for prediction and modeling of surface roughness in ball end milling of OFHC copper,” *International Journal of Mechanical and Materials Engineering*, vol. 14, no. 1, p. 3, Dec. 2019, doi: 10.1186/s40712-019-0099-0.

[52] A. Zhang, X. Liu, C. Yue, R. Li, S. Y. Liang, and L. Wang, “Velocity effect sensitivity analysis of ball-end milling Ti-6Al-4 V,” *The International Journal of Advanced Manufacturing Technology*, vol. 118, no. 11–12, pp. 3963–3982, Feb. 2022, doi: 10.1007/s00170-021-08049-4.

[53] P. Vavruska, P. Zeman, and M. Stejskal, “Reducing Machining Time by Pre-Process Control of Spindle Speed and Feed-Rate in Milling Strategies,” *Procedia CIRP*, vol. 77, pp. 578–581, 2018, doi: 10.1016/j.procir.2018.08.216.

[54] R. B. Käsemodel, A. F. de Souza, R. Voigt, I. Basso, and A. R. Rodrigues, “CAD/CAM interfaced algorithm reduces cutting force, roughness, and machining time in free-form

milling," *The International Journal of Advanced Manufacturing Technology*, vol. 107, no. 3–4, pp. 1883–1900, Mar. 2020, doi: 10.1007/s00170-020-05143-x.

[55] R. A. Mali, R. Aiswaresh, and T. V. K. Gupta, "The influence of tool-path strategies and cutting parameters on cutting forces, tool wear and surface quality in finish milling of Aluminium 7075 curved surface," *The International Journal of Advanced Manufacturing Technology*, vol. 108, no. 1–2, pp. 589–601, May 2020, doi: 10.1007/s00170-020-05414-7.

[56] S. Wojciechowski, R. W. Maruda, S. Barrans, P. Nieslony, and G. M. Krolczyk, "Optimisation of machining parameters during ball end milling of hardened steel with various surface inclinations," *Measurement*, vol. 111, pp. 18–28, Dec. 2017, doi: 10.1016/j.measurement.2017.07.020.

[57] C. Yao, L. Tan, P. Yang, and D. Zhang, "Effects of tool orientation and surface curvature on surface integrity in ball end milling of TC17," *The International Journal of Advanced Manufacturing Technology*, vol. 94, no. 5–8, pp. 1699–1710, Feb. 2018, doi: 10.1007/s00170-017-0523-7.

[58] P. Gao *et al.*, "Effects of machining inclination angles on microgroove quality in micro ball end milling of Ti-6Al-4V," *The International Journal of Advanced Manufacturing Technology*, vol. 92, no. 5–8, pp. 2725–2734, Sep. 2017, doi: 10.1007/s00170-017-0305-2.

[59] A. Daymi, M. Boujelbene, J. M. Linares, E. Bayraktar, and A. Ben Amara, "Influence of workpiece inclination angle on the surface roughness in ball end milling of the titanium alloy Ti-6Al-4V," *Journal of Achievements in Materials and Manufacturing Engineering*, vol. 35, no. 1, pp. 79–86, 2009, [Online]. Available: http://jamme.acmsse.h2.pl/papers_vol35_1/35110.pdf

[60] M. Habibi, O. Tuysuz, and Y. Altintas, "Modification of Tool Orientation and Position to Compensate Tool and Part Deflections in Five-Axis Ball End Milling Operations," *J Manuf Sci Eng*, vol. 141, no. 3, p. 31004, Mar. 2019, doi: 10.1115/1.4042019.

[61] J. Burek, T. Rydzak, and A. Szajna, "The influence of the tool axis orientation changes and the direction of tool driving in free surface machining on surface roughness," *Mechanik*, vol. 91, no. 8–9, pp. 684–686, Sep. 2018, doi: 10.17814/mechanik.2018.8-9.107.

[62] R. Belguith, H. Khlifi, L. Sai, M. Baili, G. Dessein, and W. Bouzid, "Effects of the Tool Bending on the Cutting Force in Ball End Milling," in *Advances in Mechanical Engineering and Mechanics: Selected Papers from the 4th Tunisian Congress on Mechanics, CoTuMe 2018, Hammamet, Tunisia, October 13–15, 2018*, 2019, pp. 143–151. doi: 10.1007/978-3-030-19781-0_18.

[63] M. Sadílek, L. Kousal, N. Náprstková, T. Szotkowski, and J. Hajnyš, "The Analysis of Accuracy of Machined Surfaces and Surfaces Roughness after 3axis and 5axis Milling," *Manufacturing Technology*, vol. 18, no. 6, pp. 1015–1022, Dec. 2018, doi: 10.21062/ujep/217.2018/a/1213-2489/MT/18/6/1015.

[64] W. Mersni, M. Boujelbene, S. Ben Salem, and A.-S. Alghamdi, "Optimization of the surface roughness in ball end milling of titanium alloy Ti-6Al-4V using the Taguchi Method," *Procedia Manuf*, vol. 20, pp. 271–276, 2018, doi: 10.1016/j.promfg.2018.02.040.

[65] A. Matras and W. Zębala, “Optimization of Cutting Data and Tool Inclination Angles During Hard Milling with CBN Tools, Based on Force Predictions and Surface Roughness Measurements,” *Materials*, vol. 13, no. 5, p. 1109, Mar. 2020, doi: 10.3390/ma13051109.

[66] J. Fan, “Cutting speed modeling in ball nose milling applications,” *The International Journal of Advanced Manufacturing Technology*, vol. 73, no. 1–4, pp. 161–171, Jul. 2014, doi: 10.1007/s00170-014-5672-3.

[67] P. Krajnik and J. Kopač, “Modern machining of die and mold tools,” *J Mater Process Technol*, vol. 157–158, pp. 543–552, Dec. 2004, doi: 10.1016/j.jmatprotec.2004.07.146.

[68] A. V. Vyboishchik, “Modeling Topology of Freeform Surfaces with Ball-end Milling,” *Procedia Eng*, vol. 150, pp. 761–767, 2016, doi: 10.1016/j.proeng.2016.07.103.

[69] S. Lotfi, B. Rami, B. Maher, D. Gilles, and B. Wassila, “Cutter-workpiece engagement calculation in 3-axis ball end milling considering cutter runout,” May 01, 2019, *Elsevier Ltd*. doi: 10.1016/j.jmapro.2019.03.025.

[70] M. Forootan, J. Akbari, and M. Ghorbani, “A new geometric approach for real-time cutting force simulation in 3-axis ball-end milling compatible with graphical game engines,” *International Journal of Advanced Manufacturing Technology*, vol. 128, no. 9–10, pp. 4003–4022, Oct. 2023, doi: 10.1007/s00170-023-12025-5.

[71] H. Y. Feng and N. Su, “A mechanistic cutting force model for 3d ball-end milling,” *Journal of Manufacturing Science and Engineering, Transactions of the ASME*, vol. 123, no. 1, pp. 23–29, 2001, doi: 10.1115/1.1334864.

[72] J. H. Ko and D. W. Cho, “3D ball-end milling force model using instantaneous cutting force coefficients,” *J Manuf Sci Eng*, vol. 127, no. 1, pp. 1–12, 2005, doi: 10.1115/1.1826077.

[73] M. Ghorbani and M. R. Movahhedy, “An analytical model for cutter-workpiece engagement calculation in ball-end finish milling of doubly curved surfaces,” *International Journal of Advanced Manufacturing Technology*, vol. 102, no. 5–8, pp. 1635–1657, Jun. 2019, doi: 10.1007/s00170-018-3188-y.

[74] Z. C. Wei, M. J. Wang, J. N. Zhu, and L. Y. Gu, “Cutting force prediction in ball end milling of sculptured surface with Z-level contouring tool path,” *Int J Mach Tools Manuf*, vol. 51, no. 5, pp. 428–432, May 2011, doi: 10.1016/j.ijmachtools.2011.01.011.

[75] Z. C. Wei, M. J. Wang, Y. J. Cai, and S. F. Wang, “Prediction of cutting force in ball-end milling of sculptured surface using improved Z-map,” *International Journal of Advanced Manufacturing Technology*, vol. 68, no. 5–8, pp. 1167–1177, Sep. 2013, doi: 10.1007/s00170-013-4909-x.

[76] I. Nishida, R. Okumura, R. Sato, and K. Shirase, “Cutting Force Simulation in Minute Time Resolution for Ball End Milling under Various Tool Posture,” *Journal of Manufacturing Science and Engineering, Transactions of the ASME*, vol. 140, no. 2, Feb. 2018, doi: 10.1115/1.4038499.

[77] B. Mikó and P. Zentay, “A geometric approach of working tool diameter in 3-axis ball-end milling,” *The International Journal of Advanced Manufacturing Technology*, vol. 104, no. 1–4, pp. 1497–1507, Sep. 2019, doi: 10.1007/s00170-019-03968-9.

[78] A. W. Mgherony and B. Mikó, “aSimulation of the Working Diameter in 3-Axis Ball-end Milling of Free Form Surface,” *Tehnicki Vjesnik*, vol. 29, no. 4, pp. 1164–1170, Jun. 2022, doi: 10.17559/TV-20210719181212.

[79] M. Cheng *et al.*, “Prediction of surface residual stress in end milling with Gaussian process regression,” *Measurement (Lond)*, vol. 178, Jun. 2021, doi: 10.1016/j.measurement.2021.109333.

[80] J. Lu *et al.*, “Effect of machining parameters on surface roughness for compacted graphite cast iron by analyzing covariance function of Gaussian process regression,” *Measurement (Lond)*, vol. 157, Jun. 2020, doi: 10.1016/j.measurement.2020.107578.

[81] J. Xu, L. Xu, Z. Geng, Y. Sun, and K. Tang, “3D surface topography simulation and experiments for ball-end NC milling considering dynamic feedrate,” *CIRP J Manuf Sci Technol*, vol. 31, pp. 210–223, Nov. 2020, doi: 10.1016/j.cirpj.2020.05.011.

[82] B. Denkena, V. Böß, D. Nespor, P. Gilge, S. Hohenstein, and J. Seume, “Prediction of the 3D surface topography after ball end milling and its influence on aerodynamics,” in *Procedia CIRP*, Elsevier B.V., 2015, pp. 221–227. doi: 10.1016/j.procir.2015.03.049.

[83] S. Wojciechowski, “The estimation of cutting forces and specific force coefficients during finishing ball end milling of inclined surfaces,” *Int J Mach Tools Manuf*, vol. 89, pp. 110–123, 2015, doi: 10.1016/j.ijmachtools.2014.10.006.

[84] M. Baburaj, A. Ghosh, and M. S. Shunmugam, “Development and experimental validation of a mechanistic model of cutting forces in micro- ball end milling of full slots,” *Machining Science and Technology*, vol. 22, no. 5, pp. 787–810, Sep. 2018, doi: 10.1080/10910344.2017.1415932.

[85] J. Santhakumar and U. M. Iqbal, “Role of trochoidal machining process parameter and chip morphology studies during end milling of AISI D3 steel,” *J Intell Manuf*, vol. 32, no. 3, pp. 649–665, Mar. 2021, doi: 10.1007/s10845-019-01517-5.

[86] Y. C. Lin, K. Da Wu, W. C. Shih, P. K. Hsu, and J. P. Hung, “Prediction of surface roughness based on cutting parameters and machining vibration in end milling using regression method and artificial neural network,” *Applied Sciences (Switzerland)*, vol. 10, no. 11, Jun. 2020, doi: 10.3390/app10113941.

[87] J. Xie *et al.*, “Multi-objective feed rate optimization of three-axis rough milling based on artificial neural network”, doi: 10.1007/s00170-021-06902-0/Published.

[88] K. Kannadasan, D. R. Edla, M. H. Yadav, and A. Bablani, “Intelligent-ANFIS Model for Predicting Measurement of Surface Roughness and Geometric Tolerances in Three-Axis CNC Milling,” *IEEE Trans Instrum Meas*, vol. 69, no. 10, pp. 7683–7694, Oct. 2020, doi: 10.1109/TIM.2020.2980599.

[89] S. Shankar, T. Mohanraj, and R. Rajasekar, “Prediction of cutting tool wear during milling process using artificial intelligence techniques,” *Int J Comput Integr Manuf*, vol. 32, no. 2, pp. 174–182, Feb. 2019, doi: 10.1080/0951192X.2018.1550681.

[90] Q. Zou, J. Zhang, B. Deng, and J. Zhao, “Iso-level tool path planning for free-form surfaces,” *Computer-Aided Design*, vol. 53, pp. 117–125, Aug. 2014, doi: 10.1016/j.cad.2014.04.006.

[91] L. C. Magalhães and J. C. E. Ferreira, “Assessment of tool path strategies for milling complex surfaces in hardened H13 steel,” *Proc Inst Mech Eng B J Eng Manuf*, vol. 233, no. 3, pp. 834–849, Feb. 2019, doi: 10.1177/0954405418755824.

[92] X. Niu, T. Wang, B. Shen, T. Zhao, and Q. Huang, “Study on Tool Path Optimization in Multi-axis NC Machining,” *MATEC Web of Conferences*, vol. 34, p. 02012, Dec. 2015, doi: 10.1051/matecconf/20153402012.

[93] Y. SUN, J. JIA, J. XU, M. CHEN, and J. NIU, “Path, feedrate and trajectory planning for free-form surface machining: A state-of-the-art review,” *Chinese Journal of Aeronautics*, vol. 35, no. 8, pp. 12–29, Aug. 2022, doi: 10.1016/j.cja.2021.06.011.

[94] P. Ižol, M. Tomáš, and J. Beňo, “Milling strategies evaluation when simulating the forming dies’ functional surfaces production,” *Open Engineering*, vol. 6, no. 1, May 2016, doi: 10.1515/eng-2016-0013.

[95] J. Varga, T. Tóth, Ľ. Kaščák, and E. Spišák, “The Effect of the Machining Strategy on the Surface Accuracy When Milling with a Ball End Cutting Tool of the Aluminum Alloy AlCu4Mg,” *Applied Sciences*, vol. 12, no. 20, p. 10638, Oct. 2022, doi: 10.3390/app122010638.

[96] D.-D. Vu, F. Monies, and W. Rubio, “A new optimization tool path planning for 3-axis end milling of free-form surfaces based on efficient machining intervals,” in *AIP Conference Proceedings*, 2018, p. 070011. doi: 10.1063/1.5034907.

[97] G. Huo *et al.*, “CNC Tool Path Generation for Freeform Surface Machining Based on Preferred Feed Direction Field,” *International Journal of Precision Engineering and Manufacturing*, vol. 20, no. 5, pp. 777–790, May 2019, doi: 10.1007/s12541-019-00084-2.

[98] A. Kukreja and S. S. Pande, “Optimal toolpath planning strategy prediction using machine learning technique,” *Eng Appl Artif Intell*, vol. 123, p. 106464, Aug. 2023, doi: 10.1016/j.engappai.2023.106464.

[99] U. Župerl, K. Stepien, G. Munđar, and M. Kovačič, “A Cloud-Based System for the Optical Monitoring of Tool Conditions during Milling through the Detection of Chip Surface Size and Identification of Cutting Force Trends,” *Processes*, vol. 10, no. 4, p. 671, Mar. 2022, doi: 10.3390/pr10040671.

[100] J. Zhang, R. Mo, N. Wan, and C. Xia, “Tool path planning for five-axis flank milling of free-form surfaces,” *The International Journal of Advanced Manufacturing Technology*, vol. 108, no. 1–2, pp. 73–90, May 2020, doi: 10.1007/s00170-020-05283-0.

[101] A. Kukreja and S. S. Pande, “An Efficient Iso-Scallop Toolpath Planning Strategy Using Voxel-Based Computer Aided Design Model,” *J Comput Inf Sci Eng*, vol. 23, no. 3, Jun. 2023, doi: 10.1115/1.4055372.

[102] W. Liu, S.-M. Zhu, T. Huang, and C. Zhou, “An efficient iso-scallop tool path generation method for three-axis scattered point cloud machining,” *The International Journal of Advanced Manufacturing Technology*, vol. 107, no. 7–8, pp. 3471–3483, Apr. 2020, doi: 10.1007/s00170-020-05188-y.

[103] W. Liu, L. Zhou, and L. An, “Constant scallop-height tool path generation for three-axis discrete data points machining,” *The International Journal of Advanced Manufacturing Technology*, vol. 63, no. 1–4, pp. 137–146, Nov. 2012, doi: 10.1007/s00170-011-3892-3.

[104] B. Durakovic, “Design of experiments application, concepts, examples: State of the art,” *Periodicals of Engineering and Natural Sciences*, vol. 5, pp. 421–439, Oct. 2017, doi: 10.21533/pen.v5i3.145.

[105] A. Drégelyi-Kiss, R. Horváth, and B. Mikó, “Design of experiments (DOE) in investigation of cutting technologies,” *Development in Machining Technology/Scientific-Research Reports*, vol. 3, Oct. 2013.

[106] J. Antony, *Design of Experiments for Engineers and Scientists*. in Elsevier insights. Elsevier Science, 2014. [Online]. Available: https://books.google.hu/books?id=p7pCAgAAQBAJ

[107] R. Noorani, Y. Farooque, and T. Ioi, “Improving surface roughness of CNC milling machined aluminum samples due to process parameter variation,” *URL: http://ineer. org/Events/ICEEiCEER2009/full_pa- pers/full_paper_188. pdf*, 2009.

[108] M. S. Kasim *et al.*, “Analysis of Tool Performance during Ball-End Milling of Aluminium Alloy 6061-T6,” *Applied Mechanics and Materials*, vol. 761, pp. 318–323, May 2015, doi: 10.4028/www.scientific.net/AMM.761.318.

[109] D. S. S. R. Kiran and S. P. Kumar, “Multi Objective Optimization of Tool Life and Total Cost Using 3-Level Full Factorial Method in Cnc End Milling Process,” *Int. J. Mech. Eng. Robot. Res*, vol. 2, no. 3, pp. 255–270, 2013.

[110] V. V. K. Lakshmi and K. V. Subbaiah, “Modeling and optimization of process parameters during end milling of hardened steel,” *Int J Eng Res Appl*, vol. 2, no. 2, pp. 674–679, 2012.

[111] H. Shahrajabian and M. Farahnakian, “Multi-constrained optimization in ball-end machining of carbon fiber-reinforced epoxy composites by PSO,” *Cogent Eng*, vol. 2, no. 1, p. 993157, Dec. 2015, doi: 10.1080/23311916.2014.993157.

[112] A. T. Abbas, A. E. Ragab, E. A. Al Bahkali, and E. A. El Danaf, “Optimizing Cutting Conditions for Minimum Surface Roughness in Face Milling of High Strength Steel Using Carbide Inserts,” *Advances in Materials Science and Engineering*, vol. 2016, pp. 1–14, 2016, doi: 10.1155/2016/7372132.

[113] K. Vipindas, B. Kuriachen, and J. Mathew, “Investigations into the effect of process parameters on surface roughness and burr formation during micro end milling of TI-6AL-4V,” *The International Journal of Advanced Manufacturing Technology*, vol. 100, no. 5–8, pp. 1207–1222, Feb. 2019, doi: 10.1007/s00170-016-9210-3.

[114] D. R. T. R. Deshmukh and others, “Experimental Investigation of Factors Affecting Milling Operation,” *MAYFEB Journal of Mechanical Engineering*, vol. 2, 2017.

[115] G. Bolar, A. Das, and S. N. Joshi, “Measurement and analysis of cutting force and product surface quality during end-milling of thin-wall components,” *Measurement*, vol. 121, pp. 190–204, Jun. 2018, doi: 10.1016/j.measurement.2018.02.015.

[116] B. Mikó and J. Nagy, “Surface profile error of free form surface in Z-level milling,” *Development in Machining Technology/Scientific-Research Reports*, Oct. 2019.

[117] T. P. Ryan, *Statistical Methods for Quality Improvement*. in Wiley Series in Probability and Statistics. Wiley, 2011. [Online]. Available: https://books.google.hu/books?id=uxsN44uX0wgC

[118] S. K. Saini and S. K. Pradhan, “Optimization of Machining Parameters for CNC Turning of different Materials,” in *Applied Mechanics and Materials*, 2014, pp. 605–609.

[119] L. D. K. Catherine, R. Ma’arof, R. Aziz, and S. Suresh, “A Study on the Impact of the Milling Parameters on the Surface Roughness when using Polyurethane Board as a Base

Material in Manufacturing Automotive Checking Fixtures," in *Materials Science Forum*, 2015, pp. 449–454.

[120] T.-L. B. Tseng, U. Konada, and Y. J. Kwon, "A novel approach to predict surface roughness in machining operations using fuzzy set theory," *J Comput Des Eng*, vol. 3, no. 1, pp. 1–13, 2016.

[121] Y. El-Taybany, M. Hossam, and H. El-Hofy, "Experimental investigation of ultrasonic-assisted milling of soda glass using factorial design of experiments," *Procedia CIRP*, vol. 58, pp. 381–386, 2017.

[122] R. K. Roy, *A Primer on the Taguchi Method, Second Edition*. Society of Manufacturing Engineers, 2010. [Online]. Available: https://books.google.hu/books?id=k5VBsRZfzQsC

[123] D. P. Singh and R. N. Mall, "Optimization of Surface Roughness of Aluminum by ANOVA based Taguchi Method using Minitab15 Software," *International Journal For Technological Research In Engineering*, vol. 2, no. 11, pp. 2782–2787, 2015.

[124] K. Ramesh, "Optimization of Cutting Parameters for Minimizing Cycle Time in Machining of SS 310 using Taguchi Methodology and Anova.," *IOSR Journal of Mechanical and Civil Engineering*, vol. 12, no. 1, pp. 31–39, 2015.

[125] K. G. Malay, H. N. K. JaideepGangwar, A. M. Nitya Prakash Sharma, and R. G. Sudhir Kumar, "Optimization of process parameters of CNC milling," *International Journal of Advance Research and Innovation*, vol. 3, no. 4, pp. 59–63, 2016.

[126] S. Ghalme, A. Mankar, and Y. J. Bhalerao, "Parameter optimization in milling of glass fiber reinforced plastic (GFRP) using DOE-Taguchi method," *Springerplus*, vol. 5, no. 1, p. 1376, 2016.

[127] C. Ratnam, K. A. Vikram, B. S. Ben, and B. S. N. Murthy, "Process monitoring and effects of process parameters on responses in turn-milling operations based on SN ratio and ANOVA," *Measurement*, vol. 94, pp. 221–232, 2016.

[128] A. Gupta, C. M. Krishna, and S. Suresh, "Modeling and Analysis of CNC Milling Process Parameters on Aluminium Silicate Alloy," *International Journal of Engineering Technology Science and Research*, 2017.

[129] A. Kumar, N. Kumar, S. Kumar, and R. Garg, "Comparative study of Parametric Optimization of the End Milling of Al2024-SiC MMC on Surface Roughness using Taguchi Technique with Applied Statistical Plots," *International Journal of Applied Engineering Research*, vol. 12, no. 21, pp. 10816–10823, 2017.

[130] P. B. Sosa, R. D. Makwana, and G. D. Acharya, "Optimization of Machining Parameters on End Milling of EN 8 Back Shaft for Power Press," 2018.

[131] E. J. Kim and C. M. Lee, "A Study on the Optimal Machining Parameters of the Induction Assisted Milling with Inconel 718," *Materials*, vol. 12, no. 2, p. 233, 2019.

[132] S. U. Ahmed and R. Arora, "Quality characteristics optimization in CNC end milling of A36 K02600 using Taguchi's approach coupled with artificial neural network and genetic algorithm," *International Journal of System Assurance Engineering and Management*, vol. 10, no. 4, pp. 676–695, 2019.

[133] R. H. Myers, D. C. Montgomery, and C. M. Anderson-Cook, *Response surface methodology: process and product optimization using designed experiments*. John Wiley & Sons, 2016.

[134] M. Subramanian, M. Sakthivel, K. Sooryaprakash, and R. Sudhakaran, “Optimization of end mill tool geometry parameters for Al7075-T6 machining operations based on vibration amplitude by response surface methodology,” *Measurement*, vol. 46, no. 10, pp. 4005–4022, 2013.

[135] S. Jeyakumar, K. Marimuthu, and T. Ramachandran, “Prediction of cutting force, tool wear and surface roughness of Al6061/SiC composite for end milling operations using RSM,” *Journal of Mechanical Science and Technology*, vol. 27, no. 9, pp. 2813–2822, 2013.

[136] B. Patel, H. Nayak, K. Araniya, and G. Champaneri, “Parametric optimization of temperature during CNC end milling of mild steel using RSM,” *International Journal of Engineering Research & Technology*, vol. 3, no. 1, pp. 69–73, 2014.

[137] D. Kumar and G. Rajamohan, “OPTIMIZATION OF SURFACE ROUGHNESS AND FLATNESS IN END MILLING OF ALUMINIUM ALLOY AL 6063-T6,” *Int J Adv Eng Technol*, vol. 8, no. 6, p. 937, 2015.

[138] K. V. Rao and P. Murthy, “Modeling and optimization of tool vibration and surface roughness in boring of steel using RSM, ANN and SVM,” *J Intell Manuf*, vol. 29, no. 7, pp. 1533–1543, 2018.

[139] M. K. N. Khairusshima, B. M. H. Zakwan, M. Suhaily, I. S. S. Sharifah, N. M. Shaffiar, and M. A. N. Rashid, “The optimization study on the tool wear of carbide cutting tool during milling Carbon Fibre Reinforced (CFRP) using Response Surface Methodology (RSM),” *IOP Conf Ser Mater Sci Eng*, vol. 290, p. 12068, Jan. 2018, doi: 10.1088/1757-899x/290/1/012068.

[140] G. BAŞAR, F. KAHRAMAN, and G. T. ÖNDER, “Mathematical Modeling and Optimization of Milling Parameters in AA 5083 Aluminum Alloy,” *European Mechanical Science*, vol. 3, no. 4, pp. 159–163, Dec. 2019, doi: 10.26701/ems.537087.

[141] A. P. Singh, A. Samad, and A. K. Saraf, “Enhancement of Surface Finish by Optimization Technique Employed for Al 6061 Considering Different Parameters Using RSM,” *SSRN Electronic Journal*, 2019, doi: 10.2139/ssrn.3468726.

[142] N. Saha, A. Swetapadma, and M. Mondal, “A Brief Review on Artificial Neural Network: Network Structures and Applications,” in *2023 9th International Conference on Advanced Computing and Communication Systems, ICACCS 2023*, Institute of Electrical and Electronics Engineers Inc., 2023, pp. 1974–1979. doi: 10.1109/ICACCS57279.2023.10112753.

[143] J. E. Solís-Pérez, J. A. Hernández, A. Parrales, J. F. Gómez-Aguilar, and A. Huicochea, “Artificial neural networks with conformable transfer function for improving the performance in thermal and environmental processes,” *Neural Networks*, vol. 152, pp. 44–56, Aug. 2022, doi: 10.1016/j.neunet.2022.04.016.

[144] C. Iancu, “ABOUT 3D PRINTING FILE FORMATS.,” *Annals of’Constantin Brancusi’University of Targu-Jiu. Engineering Series*, no. 2, 2018.

[145] M. Szilvśi-Nagy and Gy. Mátyási, “Analysis of STL files,” *Math Comput Model*, vol. 38, no. 7–9, pp. 945–960, Oct. 2003, doi: 10.1016/S0895-7177(03)90079-3.

[146] Y. H. Chen, C. T. Ng, and Y. Z. Wang, “Generation of an STL File from 3D Measurement Data with User-Controlled Data Reduction,” *The International Journal of Advanced Manufacturing Technology*, vol. 15, no. 2, pp. 127–131, Feb. 1999, doi: 10.1007/s001700050049.

[147] S. A. Brown, C. E. Drayton, and B. Mittman, “A description of the APT language,” *Commun ACM*, vol. 6, no. 11, pp. 649–658, Nov. 1963, doi: 10.1145/368310.368322.

[148] H. Y. Cheng, J. P. Tsai, and Y. C. Kao, “The Development of an APT Program Interpreter for 5-Axis Machining,” *Adv Mat Res*, vol. 482–484, pp. 2247–2252, Feb. 2012, doi: 10.4028/www.scientific.net/AMR.482-484.2247.

[149] D. T. Ross, “The design and use of the APT language for automatic programming of numerically controlled machine tools,” in *Proc. 1959 Computer Applications Symposium, Chiergo*, 1959, pp. 80–99.

[150] D. T. Ross, “Origins of the APT language for automatically programmed tools,” in *History of programming languages*, New York, NY, USA: ACM, 1978, pp. 279–338. doi: 10.1145/800025.1198374.

[151] A. Mgherony and B. Mikó, “Controlling the Spindle Speed when Milling Free-Form Surfaces using Ball-End Milling Cutter,” *Acta Polytechnica Hungarica*, vol. 20, no. 6, pp. 135–149, 2023, doi: 10.12700/APH.20.6.2023.6.8.